Interplay between the amyloid precursor protein (APP) and α-secretases at the plasma membrane

Dissertation

zur

Erlangung des Doktorgrades (Dr. rer. nat)

der

Mathematisch-Naturwissenschaftlichen Fakultät

der

Rheinischen Friedrich-Wilhelms-Universität Bonn

vorgelegt von

Lisa Hitschler

aus

Landau in der Pfalz

Bonn 2022

Angefertigt mit Genehmigung der Mathematisch-Naturwissenschaftlichen Fakultät der
Rheinischen Friedrich-Wilhelms-Universität Bonn

1. Gutachter: Prof. Dr. Thorsten Lang

2. Gutachter: Prof. Dr. Jochen Walter

Tag der Promotion: 07.04.2022

Erscheinungsjahr: 2022

Anmerkung

Teile dieser Arbeit wurden bereits in folgender Publikation veröffentlicht:

Hitschler L, Lang T (submitted 2021) The APP transmembrane domain is required for anti-amyloidogenic processing by ADAM10. *(Manuscript submitted)*

Table of contents

List of Figures

List of Figures

List of Tables

Abbreviations

aa	amino acids
Aβ	amyloid β peptide
AD	Alzheimer’s disease
ADAM	a disintegrin and metalloprotease
APH	anterior pharynx defective
APP	amyloid precursor protein
APS	ammonium persulfate
a.u.	arbitrary units
BACE	β-site APP cleaving enzyme
BSA	bovine serum albumin
CBD	collagen binding domain
C-terminus	Carboxy-terminus
CuBD	copper binding domain
$_{dd}H_2O$	double distilled water
DMEM	Dulbecco's Modified Eagle Medium
DMSO	dimethyl sulfoxide
DNA	deoxyribonucleic acid
DPBS	Dulbecco's phosphate-buffered saline
E. coli	*Escherichia coli*
EDTA	Ethylenediaminetetraacetic acid
EGF	epidermal growth factor
EGFR	epidermal growth factor receptor
EGTA	ethylene glycol-bis-(beta-aminoethylether)-tetraacetic acid
ER	endoplasmatic reticulum
FAD	familial Alzheimer’s disease
FBS	fetal bovine serum
FRAP	fluoresecence recovery after photobleaching
FWHM	full width at half maximum
HBD	Heparin binding domain
HEPES	(4-(2-hydroxyethyl)-1-piperazineethanesulfonic acid)
IF	immunofluorescence
GFLD	Growth-factor like domain
GFP	green fluorescent protein
kb	kilobases
MEM	Minimum Essential Medium Eagle

NA	numerical aperture
nt	nucleotides
N-terminus	Amino-terminus
PBS	phosphate buffered saline
PBS-T	phosphate buffered saline with 0.1 % Tween-20
PCC	Pearson correlation coefficient
PCR	polymerase chain reaction
PEN	presenilin enhancer protein
PFA	paraformaldehyde
PHF	Paired helical filaments
PKC	protein kinase C
PLL	poly-L-lysine
PMA	Phorbol-12-myristate-13-acetate
PSEN	presenilin
ROI	region of interest
rSDM	relative standard deviation of the mean
RT	room temperature
SAD	sporadic Alzheimer's disease
SD	standard deviation
SDS	sodium dodecyl sulfate
SDS-PAGE	sodium dodecyl sulfate polyacrylamide gel electrophoresis
STED	stimulated emission depletion
TEMED	tetramethylethylenediamine
TMA-DPH	1-(4-tri-methyl-ammonium-phenyl)−6-phenyl-1,3,5-hexatriene p-toluene-sulfonate
TMD	transmembrane domain
TMS	transmembrane segment
WB	Western blot

1 Summary

Alzheimer's disease (AD) is the most common form of dementia. A principle pathological feature of AD are senile plaques consisting of extracellular aggregations of amyloid β peptides (Aβ). Aβ is derived from the amyloid precursor protein (APP) that forms tight clusters composed of 20 – 30 molecules in the plasma membrane. In the amyloidogenic cleavage pathway, Aβ is generated by sequential cleavages, involving first a β-secretase followed by a ɣ-secretase complex.

On the other hand, Aβ is precluded upon APP cleavage at the cell surface by α-secretases. Yet, it is unkown what are the limiting factors in α-processing. Enhancement of α-secretase activity may be possible by either increasing the accessibility of the substrate, presumably limited through APP clustering, or after having gained a deeper understanding of the substrate-secretase interaction. These strategies could be the basis for therapeutic approaches to reduce Aβ generation and as a result treat the progression of Alzheimer's disease.

We tested the hypothesis that pathogenic mutants are more prone to β-secretase cleavage because they are more tightly clustered and therefore less accessible to α-secretases. For clarification, epifluorescence microscopy and fluorescence recovery after photobleaching (FRAP) were utilized to examine the clustering degree and mobility of familial APP mutants. However, APP mutants behaved similarly as wild-type APP.

Next, we studied the proximity and physical interaction of APP and the α-secretases ADAM10 and ADAM17. Although ADAM10 is the predominant constitutive α-secretase, both secretases were found to be organized in individual nanodomains and located with equal frequency closer than 50 nm to their substrate APP. However, antibody-induced cross-linking of APP in the native membrane revealed a physical interaction of APP with ADAM10 but not with ADAM17, which might indicate a higher binding affinity of ADAM10 explaining its predominant role. More specifically, the transmembrane domain of APP was required for the physical interaction as well as for α-processing. The interaction with α-secretases was not enhanced when utilizing phorbol esters for stimulation of α-cleavage. The secretase interaction was also not altered with APP mutants carrying familial mutations in the Aβ region.

In conclusion, the substrate APP and the α-secretases ADAM10 and ADAM17 are organized in nanodomains close to each other. The here identified physical link between APP and ADAM10 might explain its predominat role as α-secretase. These results contribute to a more detailed understanding of the APP-enzyme interaction. Further research on the identification of parameters regulating this interaction could be

beneficial in the future for therapeutic approaches to stimulate APP processing by α-secretases and as a result decrease Aβ generation.

2 Introduction

2.1 Alzheimer's Disease (AD)

The term dementia comprises neurocognitive disorders, which are characterized by a decline in memory, problem-solving and other cognitive skills that impair the person's ability to perform everyday activities. The most common cause of dementia is Alzheimer's disease (AD), accounting for an estimated 60 % to 80 % of dementia cases (Alzheimer's Association, 2021; Barker *et al,* 2002; Kalaria *et al,* 2008). The global number of people affected by AD or other dementia was estimated to be 43.8 million patients in 2016 (Nichols *et al,* 2019) and increased to 50 million people until today (World Health Organization (WHO), 2021). Adults aged 65 years or older are at greatest risk for developing AD (Alzheimer's Association, 2021). With the number of older people expected to grow further due to increasing medical knowledge, quality of health care and aging of the baby-boom generation, the prevalence of AD is projected to double every 20 years to 131 million people affected worldwide in 2050 (Figure 1) (Prince *et al,* 2015). Especially in developing low and middle income countries a rapid growth in prevalence of dementia is predicted (Prince *et al,* 2015). These regional differences in trends are mainly caused by dissimilarities in population growth and demographic aging (Shaji, 2009; Prince *et al,* 2015).

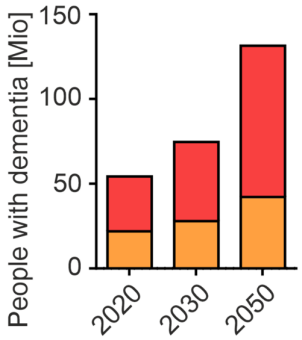

Figure 1. The prevalence of Alzheimer's disease and other dementia worldwide
The projected growth in numbers of people with dementia in high income (orange) and low and middle income countries (red). Graph based on Prince *et al* (2015).

2.1.1 Clinical symptoms and socio-economic burden of AD

Alzheimer's disease is a degenerative brain disease characterized by a progressive decline in memory, language, problem-solving and other cognitive functions that affect a person's ability to perform everyday activities (Alzheimer's Association, 2021). This

decline in cognitive abilities is caused by damage and eventually cell death of neurons in parts of the brain involved in cognitive functions (DeKosky *et al,* 1996; Terry *et al,* 1991) as well as a decrease in brain volume (Chan *et al,* 2003). In the late stage of illness, the severe dementia stage, almost all cognitive functions are severely impaired making the patient unable to express even the simplest of needs (Förstl & Kurz, 1999). The neuronal damage eventually affects parts of the brain that are responsible for basic bodily function such as walking or swallowing (Alzheimer's Association, 2021). People require extensive care and are bed-bound which makes them vulnerable to conditions such as swallowing disorders, lung as well as skin infections and sepsis resulting in body-wide inflammations and organ failure. Alzheimer's disease is ultimately fatal with an average duration of survival of 5 to 9 years after clinical diagnosis (Bracco *et al,* 1994; Walsh *et al,* 1990). The long duration of the illness before death and the amount of time spent in disability and dependence contributes significantly to the public health impact of Alzheimer's disease (Alzheimer's Association, 2021). The costs of health care and long-term care for patients affected by AD are substantial with dementia being one of the most expensive conditions to society in the United states (Hurd *et al,* 2013). Total costs of care for patients with AD or other dementia was estimated at 355 billion dollars for 2021 in the United States (Alzheimer's Association, 2021).

2.1.2 Histopathology of AD

In 1906, Alois Alzheimer was the first to describe the disease on his patient Auguste Deter, who showed an altered behaviour including paranoia and delusions as well as progressive memory impairment and decline in language function (Alzheimer, 1907; Maurer *et al,* 1997). After a post-mortem examination of the patient's brain Alzheimer described an extracellular deposition of senile plaques and intracellular accumulation of neurofibrillary tangles (Alzheimer, 1907; Maurer *et al,* 1997) (Figure 2) as the today known histopathological hallmarks of Alzheimer's disease.

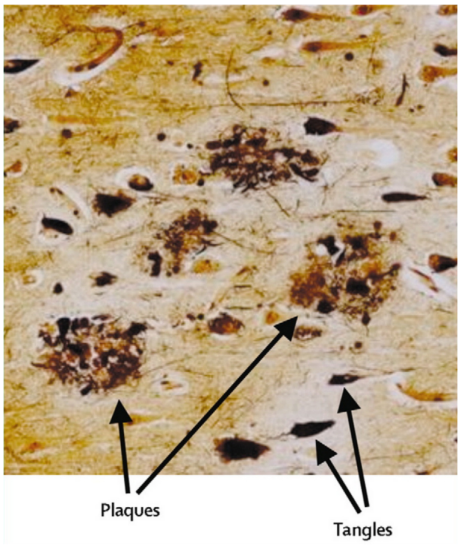

Figure 2. Histopathology of Alzheimer's disease
Senile plaques and neurofibrillary tangles (marked with arrows) in the cerebral cortex of an Alzheimer's disease patient. Plaques are extracellular deposits of Aβ surrounded by dystrophic neurites, reactive astrocytes and microglia. Tangles are intraneuronal aggregates composed of hyperphosphorylated tau protein. Figure taken from Blennow *et al* (2006).

One hallmark of AD are intraneuronal neurofibrillary tangles (Figure 2) which are filamentous inclusions composed of hyperphosphorylated tau proteins that assemble into paired helical filaments (PHF) (Grundke-Iqbal *et al,* 1986). Under physiological conditions, tau is a soluble, cytoplasmic protein which binds to tubulin and promotes assembly and stabilization of the microtubule-associated cytoskeleton (Brandt & Lee, 1993; Drechsel *et al,* 1992; Drubin & Kirschner, 1986; Gustke *et al,* 1994). Under pathological conditions, the protein shows altered solubility properties (Goedert *et al,* 1992) and an atypical hyperphosphorylation (Goedert *et al,* 1992; Grundke-Iqbal *et al,* 1986), which is probably caused by an imbalance of kinases and phosphatases regulating tau phosphorylation (Iqbal *et al,* 2009) and leads to destabilization of microtubules (Li *et al,* 2007; Alonso *et al,* 1994). Reduced axonal tranport, impaired impulse and finally degeneration of neurons are the consequence (Takashima *et al,* 2019). Neurofibrillary tau inclusions are also observed in other neurodegenerative disorders, such as frontal temporal dementia, Down's syndrome and Pick's disease (Lee *et al,* 2001). Therefore, tau abnormalities seem to be linked directly to the pathogenesis of neurodegenerative diseases.

A second hallmark of AD are extracellular plaques in the brain of patients (Figure 2). A distinction is made between neuritic (senile) plaques, which were first described as a characteristic of the disease by Alois Alzheimer, and diffuse plaques later identified using more sensitive immunostaining methods (Selkoe, 2001; Yamaguchi *et al,* 1988).

Senile plaques primarily consist of the amyloid β peptide (Aβ) (Glenner & Wong, 1984) and are usually found in brain regions such as hippocampus, amygdala and specific cortical and subcortical areas (LaFerla & Oddo, 2005; Selkoe, 2001). The Aβ peptide results from proteolytic processing of a larger membrane protein, the amyloid precursor protein (APP). Analysis of the plaques found in brains of AD patients revealed that they are mainly composed of Aβ peptides with a length of 42 amino acids (Aβ42) and only a smaller proportion of a 40 amino acid-long form (Aβ40) (Selkoe, 2001; Iwatsubo *et al,* 1994). The slightly longer Aβ42 peptide is more hydrophobic and thus more prone to aggregation (Jarrett *et al,* 1993). The diffuse or pre-amyloid plaques are an alternative form of Aβ deposits that occur in a finely granular, amorphous, non-fibrillar pattern (Selkoe, 2001). Diffuse plaques consist only of Aβ42 (Iwatsubo *et al,* 1994; Lemere *et al,* 1996; Lambert *et al,* 1998) and, in contrast to senile plaques, are not surrounded by activated microglia and astrocytes (Itagaki *et al,* 1989). They are found in brain regions not necessarily implicated in the symptomatology of Alzheimer's disease, such as cerebellum, striatum and thalamus and are also present in the brains of healthy people (Selkoe, 2001). It is assumed that diffuse plaques might represent precursor lesions of neuritic plaques as Aβ42 deposits were found in Down's syndrom patients decades before Aβ40 peptides were detected and neuritic plaques developed (Selkoe, 2001; Lemere *et al,* 1996).

Because of the senile plaques found in the brains of AD patients consisting of Aβ, the amyloid cascade hypothesis (Hardy & Higgins, 1992) has been postulated to explain the possible cause of the disease. This still prevailing hypothesis states that aggregation of the Aβ peptide is the causative agent of the disease and initiates the cascade of events that eventually causes neurofibrillary tangles, neurodegeneration and cognitive decline. The hypothesis is supported by findings that memory deficits could be rescued by decreasing Aβ levels in the brains of transgenic APP mouse models (Li *et al,* 2013; Morgan *et al,* 2000; Janus *et al,* 2000). However, several studies have shown that the number or size of plaques in the brain does not correlate well with the degree of dementia (Aizenstein *et al,* 2008; Katzman *et al,* 1988; Villemagne *et al,* 2011). This inconsistency has recently been explained by the identification of smaller soluble Aβ oligomers with neurotoxic properties, as the level of these soluble Aβ oligomers correlated better to disease severity (McDonald *et al,* 2012). These lower order Aβ oligomers rather than the highly aggregated insoluble Aβ were shown to induce cell death, hinder neuronal signaling and impair memory (Walsh *et al,* 2002; Lambert *et al,* 1998; Shankar *et al,* 2008). Additionally, those oligomers have been associated with changes in calcium homeostasis, oxidative stress, Tau hyperphosphorylation and other pathological effects (Sakono & Zako, 2010).

However, the failure of clinical trials aiming to reduce the Aβ load in the brain and hinder cognitive decline (Castellani *et al,* 2019) demonstrated that the pathogenesis of AD is much more complex. There is still a lot to learn on the physiological functions of APP and its cleavage products as well as on the interplay between the secretases involved in APP processing and the substrate APP.

2.2 The amyloid precursor protein (APP)

APP is part of an evolutionary highly conserved protein family that also includes the mammalian genes encoding APP-like proteins (APLP) APLP1 and APLP2 (Shariati & Strooper, 2013). Although APP and its homologues share a similar structural organisation and partially overlapping functions, only APP is processed to generate Aβ. Homologues in other species also include the APP-like proteins APPL (Rosen *et al,* 1989) in fruit fly (*Drosophila melanogaster*), APL-1 (Daigle & Li, 1993) in nematode (*Caenorhabditis elegans*), APP-A (Okado & Okamoto, 1992; van den Hurk *et al,* 2001) in African clawed frog (*Xenopus laevis*) as well as APPa and APPb (Musa *et al,* 2001) in zebrafish (*Danio rerio*).

2.2.1 Structure of APP

APP is a type I transmembrane protein with a signal peptide, a large N-terminal ectodomain, a transmembrane domain (TMD) and a short cytoplasmic domain (Figure 3A) (Dyrks *et al,* 1988).The human APP gene is located on chromosome 21 and consists of at least 18 exons coding for 3.3-3.5 kb mRNA transcripts (Robakis *et al,* 1987; Yoshikai *et al,* 1990). There are several splice variants of APP, but the 3 isoforms consisting of 695 (APP695), 751 (APP751) and 770 (APP770) amino acids are mainly expressed. Although APP is ubiquitously expressed in all tissues (Tanzi *et al,* 1987), APP695 is the main isoform expressed in neurons (LeBlanc *et al,* 1991; Goedert, 1987) and only found in small quantities in other cells.

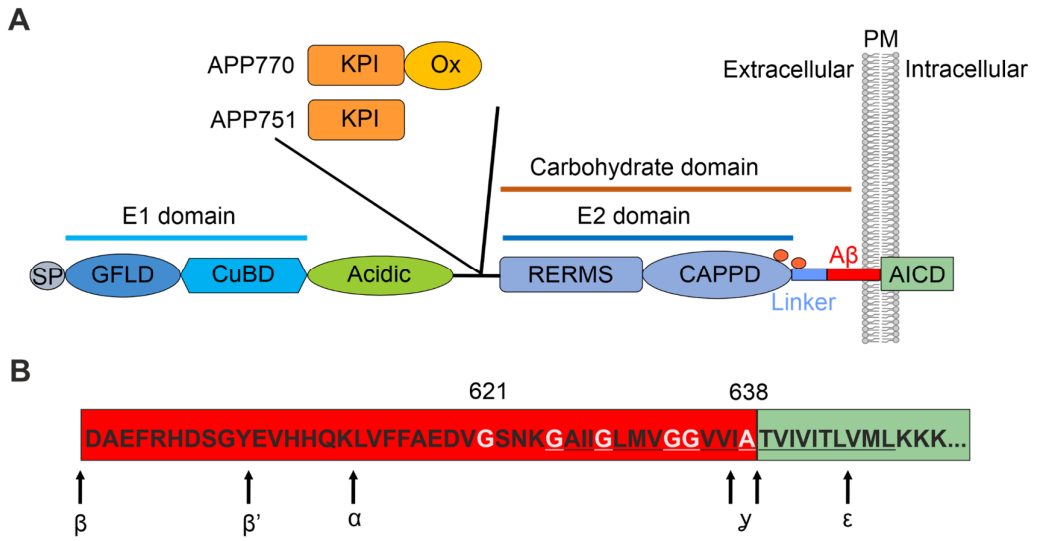

Figure 3. Schematic structure of APP and the Aβ region
(A) Domain organisation of APP: the N-terminal signal peptide (SP) is followed by the E1 domain consisting of a growth-factor-like domain (GFLD) and copper-binding domain (CuBD). The E1 region is linked via the acidic region to the carbohydrate domain. The carbohydrate domain contains an E2 domain with a RERMS sequence and central APP domain (CAPPD) as well as a linker which connects the E2 domain with the Aβ region (amino acids 597~638; APP695 numbering). APP751 and APP770 contain a Kunitz-type protease inhibitor domain (KPI) and APP770 additionally possesses an Ox2 sequence. Figure based on Reinhard *et al* (2005). (B) Schematic representation of the juxtamembrane and transmembrane region of APP. The amino acids of the Aβ region are represented in a red box. The α-, β-(β and β') and main γ-secretase (γ and ε) cleavage sites are indicated by arrows. Positions of the consecutive GxxxG/A motifs (621-625, 625-629, 629-633, 634-638; numbering according to APP695) are labelled white. The amino acids of the transmembrane domain are underlined. Figure based on Kienlen-Campard *et al* (2008) and Khalifa *et al* (2010).

The APP protein can be divided into multiple distinct domains (Figure 3A). The Aβ sequence begins at the putative β-cleavage site at amino acid 597 (of APP695) (Kandalepas & Vassar, 2012) (Figure 3B) and is the origin of the Aβ peptide after proteolytic cleavage of APP. Between amino acids 612 and 613 (of APP695) the α-secretase cleavage site is located (Lammich *et al,* 1999). The γ-cleavage site, located in the transmembrane region, marks the end of the Aβ region and the beginning of the APP intracellular domain (AICD) consisting of a highly conserved YENPTY motif for interaction with many adaptors and effector proteins (Borg *et al,* 1996; King & Scott Turner, 2004). There are several studies indicating that the APP family proteins are able to form homo- and heterodimers (Soba *et al,* 2005; Scheuermann *et al,* 2001), affecting their function and processing (Kaden *et al,* 2008; Soba *et al,* 2005; Scheuermann *et al,* 2001; Munter *et al,* 2007).Three regions have been implicated to be important for dimerization, namely the E1 (Kaden *et al,* 2008), E2 (Wang & Ha, 2004) and transmembrane domains (Munter *et al,* 2007; Marenchino *et al,* 2008). NMR

spectroscopy, biochemical purification, co-immunoprecicipation studies and FRET analysis revealed that homo-dimerization of APP was reduced or completely diminished in E1 deletion constructs (Kaden *et al,* 2009; Kaden *et al,* 2008; Soba *et al,* 2005) indicating that this domain is a major interaction interface for dimerization. X-ray spectroscopy implicated that the E2 domain is also able to dimerize (Wang & Ha, 2004) but homo-dimerization of APP was not influenced by deletion of the E2 domain (Soba *et al,* 2005). GxxxG or GxxxG-like motifs present in the extracellular juxtamembrane and transmembrane regions of APP (Khalifa *et al,* 2010) (Figure 3B) have been shown to mediate sequence-specific dimerization of α-helices in other transmembrane proteins (Lemmon *et al,* 1992; Russ & Engelman, 2000). Disruption of these motifs by familial Alzheimer's disease mutations destabilized the APP-transmembrane dimer and increased the proportion of monomers (Gorman *et al,* 2008). Additionally, substitutions of Glycine by isoleucine or alanine in the G625xxxG629-motif led to reduced dimerization and a higher ratio of shorter to longer Aβ peptides (Munter *et al,* 2007).

2.2.2 Physiological function of APP

Although the contribution of Aβ to AD pathogenesis is generally accepted, the incomplete understanding of AD pathophysiology makes a more detailed examination of the physiological and possibly pathophysiological roles of APP and its cleavage products necessary.

2.2.2.1 APP

Most of the studies on APP focus on its role as precursor of the pathogenic Aβ peptide in Alzheimer's disease. However, the physiological functions of APP are not completely elucidated. A function as a cell surface receptor was postulated for APP due to its domain structure and the similarity of proteolytic processing of APP to the Notch receptor (Selkoe & Kopan, 2003; Kang *et al,* 1987). Although several possible ligands such as glycoprotein F-spondin, heparin, netrin-1 or the Aβ peptide itself have been identified (Lorenzo *et al,* 2000; Lourenço *et al,* 2009; Ho & Südhof, 2004; Shaked *et al,* 2006; Deyts *et al,* 2016), evidence for the receptor function of APP has not been provided until today. Additionally, knockout of APP and its homologs in animal models revealed that APP and its family members are important for early development of the central nervous system, such as mediating cell adhesion, migration and synaptogenesis (Aydin *et al,* 2012; Herms *et al,* 2004; Guo *et al,* 2012; Müller & Zheng, 2012). Interestingly, the phenotypes of single knockout mice of APP or its homologues were relatively mild as the mice were viable and fertile (Koch *et al,* 1997; Heber *et al,* 2000; Müller, 1994). However, combined knockout of APP and its homologues resulted

in early postnatal lethality (Heber *et al,* 2000; Koch *et al,* 1997). Apart from neuronal development, neurite growth, synaptogenesis as well as plasticity, APP may also be involved in metal ion homeostasis (Maynard *et al,* 2005). APP may bind Cu^{2+} ions via its copper binding domain and reduce them to Cu^{+} ions (Hesse *et al,* 1994; Valensin *et al,* 2004).

2.2.2.2 Cleavage products

In addition to full-length APP, its cleavage products seem to also have physiological functions. The Aβ peptide derived from APP by sequential cleavage is mainly known for its central role in the pathophysiology of Alzheimer's disease. However, the Aβ peptide has also been associated with zinc and iron homeostasis as changes of the ion balance have been related to progression of AD (Maynard *et al,* 2005). Addionally, Aβ might convey protection against oxidative stress (Baruch-Suchodolsky & Fischer, 2009; Zou *et al,* 2002). Aβ may also function as a signaling molecule, transcriptional factor or cholesterol transport regulator (Nhan *et al,* 2015).

In contrast to the neurotoxic properties of Aβ, the α-secretase cleavage product sAPPα derived from the ectodomain of APP has been implicated with neuroprotective properties. Pre-treatment of sAPPα prevented neuronal death in human cortical cell cultures deprived of glucose or exposed to excitotoxins (Mattson *et al,* 1993). Several *in vitro* and *in vivo* studies have shown that sAPPα contributes to memory functions and neuronal survival (Saitoh *et al,* 1989; Roch *et al,* 1994; Meziane *et al,* 1998; Araki *et al,* 1991). Additionally, a protective effect against Aβ toxicity was demonstrated for sAPPα (Goodman & Mattson, 1994).

2.3 Mechanisms of APP processing

After biosynthesis in the endoplasmatic reticulum, APP is sorted to the Golgi complex and modified post-translationally by N- and O-glycosylation, phosphorylation as well as tyrosine sulfation (Weidemann *et al,* 1989; Oltersdorf *et al,* 1990). Part of APP is transported to the cell surface via the trans-Golgi network. At the plasma membrane α-secretase mediated processing of APP occurs because this protease is primarily present at the cell surface (Parvathy *et al,* 1999). The α-secretase cleaves between the amino acids leucine and lysine at positions 612 and 613 (APP695 numbering) within the Aβ region (Esch *et al,* 1990; Wang *et al,* 1991) (Figure 3B). Because α-processing thus prevents generation of Aβ it is also called the non-amyloidogenic pathway. α-Secretase cleavage releases the soluble N-terminal extracellular domain sAPPα into the extracellular space (Figure 4). An 83 amino acid long C-terminal fragment (α-CTF

or C83) remains in the membrane and is subsequently cleaved by the γ-secretase complex. γ-Secretase processing is not precise and sequential cleavage in the transmembrane domain generates fragments of varying lengths (Sastre *et al,* 2001; Qi-Takahara *et al,* 2005; Weidemann *et al,* 2002; Takami *et al,* 2009). The N-terminal cleavage product called p3 is secreted into the lumen, while a larger C-terminal AICD (APP intracellular domain) fragment is released into the cytosol (Figure 4).

Apart from non-amyloidogenic processing at the plasma membrane, APP can also be internalized together with β- and γ-secretases via clathrin-dependent endocytosis into early endosomal compartments (Nordstedt *et al,* 1993; Kinoshita *et al,* 2003). Because the β-secretase BACE1 is primarily active in the endosomal system due to a low pH optimum (He *et al,* 2007; Rajendran *et al,* 2008), sorting of APP into endosomes is a requirement for amyloidogenic processing and Aβ release (Koo & Squazzo, 1994). In addition to endocytosis from the cell surface, APP can be directly transported into endosomal compartments from the trans-Golgi network (O'Brien & Wong, 2011). APP is cleaved by the β-secretase prior to the Aβ sequence between methionine and aspartate at positions 596 and 597 (APP695 numbering) resulting in sAPPβ released into the endosomal vesicle lumen and a β-C-terminal fragment (β-CTF or C99) remaining in the membrane. Sequential cleavage of β-CTF by the γ-secretase results in the amyloidogenic Aβ peptide, which is contained in the vesicle lumen, and the AICD fragment, which is released into the cytosol (Figure 4). Because of the inaccurate sequential processing of the γ-secretase, Aβ peptides of 37 to 49 amino acid length are generated (Sastre *et al,* 2001; Qi-Takahara *et al,* 2005; Weidemann *et al,* 2002; Takami *et al,* 2009). Additionally, it has been shown that a 50 amino acid short AICD fragment can be generated by proteolytic cleavage between amino acids 645 and 646 (APP695 numbering) near the cytoplasmic membrane boundary, which is called ε-cleavage, rather than proteolytic cleavage at the γ-site (amino acids 636-638) (Gu *et al,* 2001; Sastre *et al,* 2001; Weidemann *et al,* 2002). The β-secretase has also one alternative cleavage site, referred to as β' (Figure 3B), which lies between tyrosine and glutamate at positions 606 and 607 (APP695 numbering) (Kimura *et al,* 2016) and results in an Aβ peptide which lacks the first 10 amino acids of the Aβ domain. Following amyloidogenic processing, the products sAPPβ as well as Aβ are either recycled back to the cell surface and released to the extracellular space (Koo & Squazzo, 1994) or a small fraction can be degraded by transport to the lysosomes (Haass *et al,* 1992).

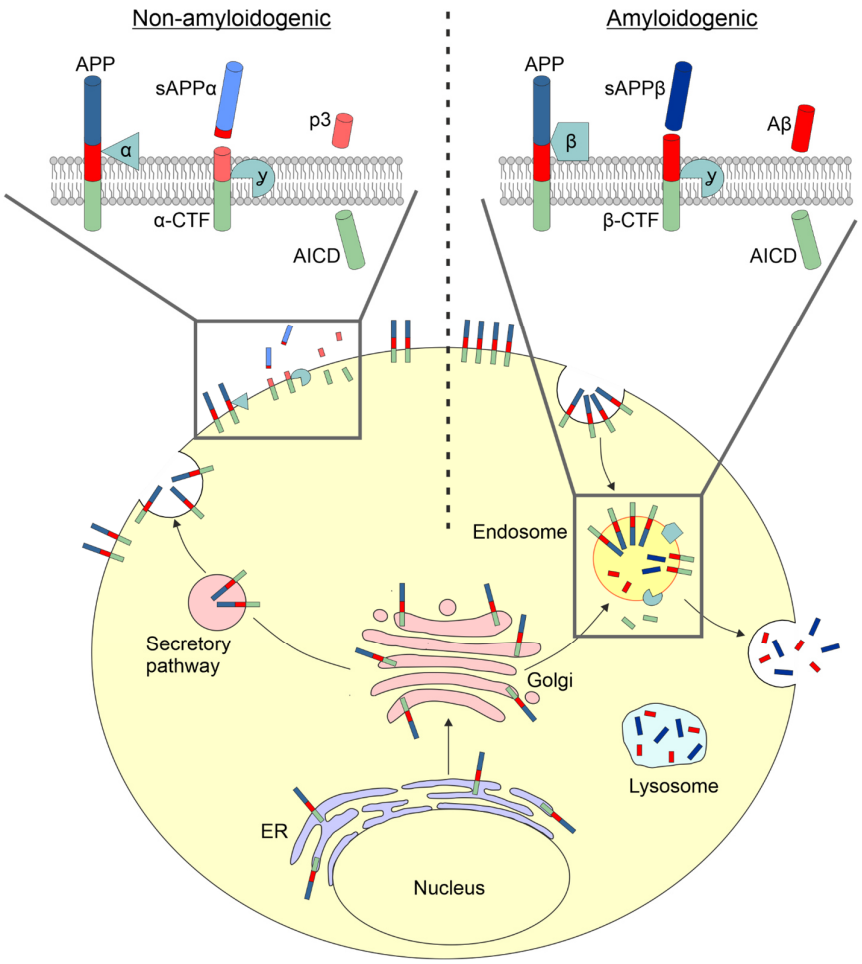

Figure 4. Cellular trafficking and processing of APP
APP molecules (colored bars) are trafficked from the endoplasmatic reticulum (ER) to the Golgi apparatus (Golgi) and reach the cell surface via the constitutive secretory pathway. At the plasma membrane some APP is processed by sequential α- and γ-secretase cleavage (non-amyloidogenic pathway; for cleavage sites see Figure 3B). Remaining APP is rapidly internalized via Clathrin-mediated endocytosis into endosomes. Alternatively, nascent APP can be sent directly to endosomal compartments from the trans-Golgi network. In this compartment the amyloidogenic pathway takes place with β- and γ-secretase cleavage leading to Aβ production. The products are either recycled back to the cell surface or degraded in lysosomes. Figure based on Haass *et al* (2012) and O'Brien & Wong (2011).

2.3.1 Genetic risk factors

Most forms of AD are sporadic (SAD) with symptoms generally beginning to show after 65-70 years of age. The APP gene was the first gene identified in which autosomal-dominant, inheritable mutations caused early-onset Alzheimer's disease (Goate *et al,* 1991). Most of these missense mutations causing familial AD (FAD) are located close to the APP cleavage sites within or flanking the Aβ encoding sequence. These mutations result in overproduction of the total Aβ cleavage product or a shift in the Aβ42 to Aβ40 ratio towards the more toxic and aggregation-prone Aβ42 (Citron *et al,* 1992;

de Jonghe *et al,* 2001; Di Fede *et al,* 2009; Kwok *et al,* 2000; Scheuner *et al,* 1996; Suzuki *et al,* 1994). As Aβ generation is altered, it is thought that mutations close to the cleavage sites influence recognition or cleavage by secretases. Other mutations are located within the Aβ sequence and affect the propensity of the Aβ peptide for aggregation (Nilsberth *et al,* 2001; Ono *et al,* 2010; Tomiyama *et al,* 2008) or its proteolytic degradation (Tsubuki *et al,* 2003; Betts *et al,* 2008). Additionally, there are several pathological mutations located close to the 5 N-terminal amino acids of the Aβ region associated with APP aggregation (Schreiber *et al,* 2012), such as the A2V mutation at position 2 of the Aβ region and the point mutations H6R, D7N, D7H as well as E11K (Lan *et al,* 2014; Wakutani *et al,* 2004; Zhou *et al,* 2011; Di Fede *et al,* 2009). Mutations in this region may influence the clustering behaviour of APP and thereby affect the accessibility of the substrate for cleavage. Only one mutation at position 2 of the Aβ region (A673T or A2T) has been identified that protects against Alzheimer's disease (Jonsson *et al,* 2012). This amino acid substitution reduced β-cleavage and Aβ generation significantly (Jonsson *et al,* 2012) and impaired the propensity of Aβ peptides to aggregate (Benilova *et al,* 2014). A reduced propensity for aggregate formation might therefore also be important for protection against AD in addition to reduced Aβ generation.

Apart from mutations within APP, FAD is also caused by the inheritance of fully penetrant mutations in the presenilin 1 (PSEN1) and presenilin 2 (PSEN2) genes, which are associated with APP processing. Presenilins have been shown to be the catalytic component of the multiprotein γ-secretase enzyme complex (Iwatsubo, 2004; Strooper, 2003; Wolfe, 2006). Almost all FAD mutations in PSEN1 and PSEN2 affect processing of APP and usually lead to an increase in the ratio of Aβ42 to Aβ40 (Kumar-Singh *et al,* 2006; Li *et al,* 2016; Scheuner *et al,* 1996). The relative increase in the more toxic and aggregation-prone Aβ42 promotes peptide aggregation to oligomers (Jarrett *et al,* 1993) and consequently accumulation of amyloid plaques (Oakley *et al,* 2006).

Sporadic AD is also influenced to ~60-80 % by genetic risk factors (Gatz *et al,* 2006). The gene variant established as the strongest genetic risk factor for late-onset AD is the ε4 allele of the apolipoprotein E gene (APOE), which is associated with increased Aβ deposition into amyloid plaques (Kim *et al,* 2009a). Another gene variant shown to convey moderate to large risk for sporadic AD are mutations in the α-secretase ADAM10 (a disintegrin and metalloproteinase 10) involved in APP proteolysis (Kim *et al,* 2009b; Suh *et al,* 2013). In genome-wide association studies (GWAS) several other genes have been identified as potential genetic risk factors with moderate risk effects but only modest statistical support exists (Tanzi, 2012; Bertram *et al,* 2010; Karch & Goate, 2015).

In conclusion, the major genetic risk factors for late on-set as well as early-onset AD are all associated with APP metabolism, such as APOE, PSEN1 and PSEN2, ADAM10 and APP itself. Therefore, it seems logical that APP and its cleavage products play a key role in the pathogenesis of AD. However, there is still a lot to learn on the physiology and interplay of the enzymes involved in the amyloidogenic and non-amyloidogenic pathways for a better understanding of the processing mechanism.

2.3.2 β-Secretase

A β-secretase is an aspartyl protease that cleaves APP between Met596 and Asp597 (APP695 numbering), which constitutes the first step towards Aβ production. Aβ primarily begins at Asp597 (Roher *et al,* 1993) and less often at Glu607 (Gouras *et al,* 1998), where another cleavage site of the β-secretase is located. A β-secretase is highly sequence specific as amino acid substitutions near the APP cleavage site decrease β-secretase processing of APP (Citron *et al,* 1995). Additionally, a β-secretase specifically targets membrane-incorporated substrates, as APP constructs lacking the transmembrane domain are not cleaved (Citron *et al,* 1995). For optimal activity the β-secretase requires a low pH (Haass *et al,* 1993; Haass *et al,* 1995a; Knops *et al,* 1995) and is primarily active in acidic intracellular compartments such as endosomes and the Golgi apparatus (Koo & Squazzo, 1994; Haass *et al,* 1995b; Thinakaran *et al,* 1996). Although β-secretase activity is detected in many cell and tissue types, the highest activity is observed in the brain and especially in neurons (Zhao *et al,* 1996; Seubert *et al,* 1993). Consistent with these observed properties, the β-site APP cleaving enzyme BACE1 has been precisely validated and identified by several research groups as the β-secretase essential for Aβ formation (Lin *et al,* 2000; Hussain *et al,* 1999; Sinha *et al,* 1999; Vassar *et al,* 1999; Yan *et al,* 1999). The strongest evidence for BACE1 as the β-secretase *in vivo* came from BACE1 knockout mice. In BACE1-deficient mice no Aβ peptides or any of the direct β-secretase cleavage products, C99 and sAPPβ, could be detected (Luo *et al,* 2001; Roberds *et al,* 2001; Dominguez *et al,* 2005). BACE1 is a 501 amino acids long integral type 1 transmembrane aspartyl protease with an N-terminal signal peptide, a prodomain, a large catalytic domain, a transmembrane domain and a small cytoplasmic domain (Hussain *et al,* 1999; Sinha *et al,* 1999; Vassar *et al,* 1999; Yan *et al,* 1999; Lin *et al,* 2000). While the majority of studies focus on BACE1 proteolysis of APP, many other transmembrane proteins have been identified as substrates, such as neuregulin-1 (Hu *et al,* 2006; Willem *et al,* 2006), neuregulin-3 (Hu *et al,* 2008), interleukin-1 type II receptor (Kuhn *et al,* 2007) and P-selectin glycoprotein ligand-1 (Lichtenthaler *et al,* 2003). The substrates of BACE1 hint toward potential roles in immunological and

inflammatory responses as well as regulation of nerve myelination (Kandalepas & Vassar, 2012).

2.3.3 γ-Secretase

The γ-secretase is a multi-protein complex comprising four subunits: either presenilin 1 or its homologue presenilin 2 (PSEN1/2), anterior pharynx defective 1a or 1b (APH1a/b), nicastrin and presenilin enhancer protein 2 (PEN2) (Strooper, 2010). Presenilin 1 was identified as the major catalytically active protein responsible for cleavage of APP in the transmembrane domain and release of the Aβ peptide (Strooper *et al,* 1998). Loss of PSEN1 in neurons led to an almost complete loss of Aβ generation (Strooper *et al,* 1998). The remaining γ-secretase activity is mediated by PSEN2 as no Aβ was detected anymore in knockout mice of both presenilins (Herreman *et al,* 2000; Zhang *et al,* 2000). Interestingly, all four subunits are required for an active γ-secretase complex (Kimberly *et al,* 2003; Takasugi *et al,* 2003; Francis *et al,* 2002; Edbauer *et al,* 2003). Nicastrin is a glycosylated type 1 transmembrane protein (Yu *et al,* 2000; Yang *et al,* 2002) and has been proposed to bind to the free N-terminus of ectodomain-shed substrates and act as the substrate receptor of the γ-secretase complex (Shah *et al,* 2005; Dries *et al,* 2009). APH1 has seven TMDs and might be important for assembly of the complex (Fortna *et al,* 2004; Strooper, 2010). Not much is known about the function of PEN2. The incorporation of this small hairpin like protein is associated with a major conformational change and likely auto-proteolytic cleavage of the PSEN1/2 into N- and C-terminal fragments, resulting in a proteolytically active complex (Strooper, 2010).

The complex is active in the plasma membrane as well as endosomal compartments (Vetrivel *et al,* 2004; Frykman *et al,* 2010; Chyung *et al,* 2005). Over 90 different substrates for the γ-secretase complex have been identified that do not share obvious common features (Haapasalo & Kovacs, 2011; Beel & Sanders, 2008). How substrate specificity is mediated is mostly unknown, except that the ectodomain of the substrate has to be shed and its length is inhibitory for recognition and cleavage by γ-secretase (Funamoto *et al,* 2013; Lichtenthaler *et al,* 2003). For APP, a fragment spanning from E22 to K55 in the C99 fragment seems to be sufficient and required for cleavage by γ-secretase (Yan *et al,* 2017) indicating that at least a few remaining amino acids N- and C-terminal to the transmembrane domain are necessary for substrate recognition. The generation of Aβ or p3 is probably achieved by a series of sequential cleavages resulting in first longer fragments which are subsequently shortened to fragments of varying lengths (Zhao *et al,* 2005; Qi-Takahara *et al,* 2005; Munter *et al,* 2007; Weidemann *et al,* 2002; Takami *et al,* 2009; Sastre *et al,* 2001). This difference in the

length of the final cleavage product due to unprecise cleavage of the γ-secretase is of greatest importance for AD pathology, because the longer Aβ42 species is more aggregation prone (Jarrett *et al,* 1993).

2.3.4 α-Secretase

The α-secretase cleaves APP between amino acids Leu16 and Lys17 within the Aβ region (Esch *et al,* 1990; Sisodia *et al,* 1990; Wang *et al,* 1991). α-Processing leads to secretion of most of the ectodomain as sAPPα and prevents Aβ generation because APP is cleaved within the Aβ region (Sisodia, 1992; Esch *et al,* 1990). It was shown that cleavage requires membrane association of APP, an α-helical conformation and a distance of the cleavage site of 12 to 13 amino acids from the membrane (Sisodia, 1992). The cleavage specificity is largely independent of the primary sequence of the substrate (Sisodia, 1992). Processing of APP by the α-secretase was determined to occur at the cell surface (Sisodia, 1992; Parvathy *et al,* 1999), suggesting that the α-secretase was a plasma membrane-associated protease. Although α-secretase cleavage occurs constitutively in almost all cells, sAPPα secretion can be stimulated by activation of protein kinase C (PKC), tyrosine kinases or extracellular signal-regulated kinases in response to receptor activation, such as muscarinic acetylcholine receptor or epidermal growth factor receptor (EGFR) (Refolo *et al,* 1989; Buxbaum *et al,* 1992; Nitsch *et al,* 1992; Mills & Reiner, 1999). α-Secretase activity can also be stimulated directly by activation of the PKC by phorbol ester (Buxbaum *et al,* 1993; Caporaso *et al,* 1992).

The α-secretase was early considered to be a metalloprotease due to the fact that APP α-secretase cleavage could be inhibited by certain metalloprotease inhibitors (Arribas *et al,* 1996; Buxbaum *et al,* 1998; Koike *et al,* 1999; Lammich *et al,* 1999; Lopez-Perez *et al,* 2001; Parvathy *et al,* 1998). Three members of the ADAM (a disintegrin and metalloproteinase) family, ADAM9, ADAM10 and ADAM17, have been proposed as possible candidates for the α-secretase because they exhibited α-secretase acitivity in different cell lines (Buxbaum *et al,* 1998; Lammich *et al,* 1999; Koike *et al,* 1999; Fahrenholz *et al,* 2000). ADAMs are type I integral membrane glycoproteins with multiple domains, including a signal peptide, a pro domain, a catalytic metalloprotease domain, followed by disintegrin- and cysteine-rich domains involved in substrate interaction, as well as a transmembrane and a short cytoplasmic domain (Figure 5) (Smith *et al,* 2002; White, 2003; Howard *et al,* 1996).

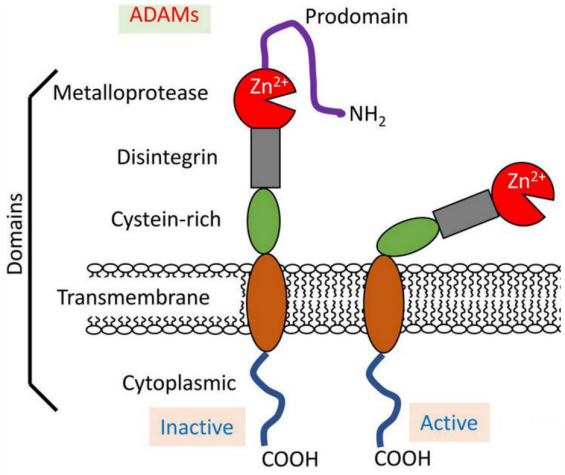

Figure 5. ADAM domain structure
A disintegrin and metalloprotease (ADAM) protein is divided into an extracellular domain comprising a prodomain, metalloprotease domain, disintegrin domain and a cysteine-rich region as well as a transmembrane domain followed by a short cytoplasmic tail. ADAMs also contain a N-terminal signal peptide, which is not shown. The activity is regulated by the presence (inactive) or absence (active) of the prodomain. Figure taken and modified from Kato *et al* (2018).

ADAM17 has previously been suggested as a candidate α-secretase, because overexpression of the protease in cells increased constitutive sAPPα shedding (Slack *et al,* 2001). In HEK293 cells but not neuronal SH-SY5Y cells, knockdown of ADAM17 resulted in a slight decrease of constitutive sAPPα generation (Kuhn *et al,* 2010). These results indicated that ADAM17 is capable of catalyzing constitutive α-secretase cleavage of APP but various studies suggest that ADAM17 is responsible mainly for regulated α-secretase cleavage (Buxbaum *et al,* 1998; Blacker *et al,* 2002; Merlos-Suárez *et al,* 2001). Similarly, when ADAM9 was activated by phorbol ester, sAPPα generation was improved (Koike *et al,* 1999), but knockdown of ADAM9 had no effect on sAPPα production (Kuhn *et al,* 2010). This implies that ADAM9 is only involved in stimulated α-secretase cleavage. Furthermore, it has been shown that ADAM9 regulates APP processing indirectly by modulation of ADAM10 activity (Cissé *et al,* 2005; Moss *et al,* 2011). Overexpression of ADAM10 in mice expressing human APP increased sAPPα levels and reduced the formation of Aβ peptides and plaques (Postina *et al,* 2004) which was the first *in vivo* evidence for a proteinase of the ADAM family displaying α-secretase activity. Knock-down of ADAM10 *in vitro* in neuronal cell lines and in primary cortical neurons as well as conditional knock-down in mice *in vivo* resulted in 79-90 % sAPPα reduction (Kuhn *et al,* 2010; Xu *et al,* 2009; Jorissen *et al,* 2010) and consolidated the enzyme's role in APP processing further. Together, these functional studies regarding APP processing point to ADAM10 as the major constitutive, physiological α-secretase. The reason for ADAM10's predominant role remains unclear

to date. Possible explanations may be found in different substrate specifities of the ADAM proteases or in the nature of the protease-substrate interaction that is not yet characterized.

Like all members of the ADAM family, ADAM10 as well as ADAM17 have a broad substrate range with overlapping substrates, such as APP, Notch and epidermal growth factor, but also substrates specific for ADAM10 like neuronal cadherin, ephrins, vascular endothelial cadherin and other ADAM17-specific substrates, such as amphiregulin, transforming growth factor alphas well as tumor necrosis factor receptor (Pruessmeyer & Ludwig, 2009). Because of the variety of substrates, ADAMs are thought to regulate many different functions, like development processes, inflammatory immune responses, leukocyte recruitment, cell migration and membrane fusion (Pruessmeyer & Ludwig, 2009; Seals & Courtneidge, 2003). Although there is no consensus cleavage motif to determine substrate specificity, immediately downstream of the cleavage site ADAM17 has been shown to be selective for smaller aliphatic residues, whereas ADAM10 can accommodate aromatic amino acids (Caescu *et al,* 2009). Substrate specificity of ADAMs may also rely on non-catalytic interactions between the substrate and the cysteine-rich domain (Reddy *et al,* 2000; Smith *et al,* 2002; White, 2003). For ADAM10, an acidic negatively-charged surface pocket has been identified to be important for substrate recognition (Janes *et al,* 2005). Additionally, the secondary structure of substrates has also been demonstrated to regulate its interaction with non-catalytic domains of ADAM10 as well as ADAM17 and consequently influence the protease activity (Stawikowska *et al,* 2013).

2.3.5 Relationship between secretases and therapeutic potential

As Aβ is accepted as one of the key molecules for AD pathogenesis therapeutic strategies mainly focus on decreasing Aβ generation. The abolishment of Aβ generation as well as the mild phenotype of BACE1 knockout mice (Luo *et al,* 2001; Luo *et al,* 2003) led to the conclusion that lowering of Aβ formation by β-secretase inhibition might be an attractive therapeutic approach for treatment of Alzheimer's disease. This therapeutic strategy has been followed for many years (Rajendran *et al,* 2008; Sankaranarayanan *et al,* 2009; Silvestri, 2009), but in the meantime therapeutic agents for β-secretase inhibition are considered to have failed because cognitive decline worsened with treatment in phase 3 trials (Knopman, 2019). The results of the studies suggested that BACE1 may be critical for synaptic functions and that lowering of Aβ generation needs to be accomplished by another approach.

Alternatively, a modulation or inhibition of the γ-secretase activity was proposed as a therapeutic approach to reduce Aβ generation. However, the complete inhibition of the

γ-secretase is problematic due to its broad substrate range. A clinical trial of the γ-secretase inhibitor semagacestat was discontinued because patients developed skin and gastrointenstinal side effects characteristic for the inhibition of γ-secretase processing of Notch (Selkoe, 2011; Imbimbo *et al,* 2011; Tate *et al,* 2012). Therefore modulators of γ-secretase activity are proposed as a better option by shifting the production of the more toxic Aβ42 peptide to shorter fragments and preserving the γ-secretase activity for other substrates. The clinical trials of one modulator failed due to a weak effect and poor distribution into the central nervous system (Green *et al,* 2009; Imbimbo, 2009) and the development of some modulators has been discontinued due to toxicities (Bulic *et al,* 2011). If second and third generation gamma secretase modulators proceeding toward clinical trials will be successful in therapeutic treatment remains to be seen.

Meanwhile, several studies demonstrated that activation of α-secretase by phorbol esters and muscarinic agonists increased sAPPα generation and reduced β-secretase cleavage and Aβ generation (Amtul *et al,* 2010; Caccamo *et al,* 2006; Fu *et al,* 2009; Hung *et al,* 1993; Nitsch *et al,* 1992; Skovronsky *et al,* 2000), indicating that α- and β-secretase may compete for APP as a substrate. Additionally, overexpression of ADAM10 in mice expressing human APP increased sAPPα levels and reduced the formation of Aβ peptides and plaques (Postina *et al,* 2004), while overexpression of BACE1 in cell lines or mice reduced α-secretase cleavage (Kuhn *et al,* 2010; Vassar *et al,* 1999). Together, these findings led to the concept that α- and β-secretase are inversely active and compete for APP as substrate. The localization of α- and β-secretase activities to different cellular compartments may be responsible for this effect. α-Secretase processing occurs almost exclusively at the cell-surface (Parvathy *et al,* 1999; Sisodia, 1992), while BACE-1 is primarily active in the endosomal system (He *et al,* 2007; Kinoshita *et al,* 2003; Rajendran *et al,* 2006). Therefore, α-secretase cleavage usually precludes endocytosis and subsequent cleavage of APP by β-secretase.

It remains unclear whether a competition between α- and β-secretase cleavage also occurs under constitutive cleavage conditions. Knock-down of ADAM10 in primary neurons mildly increased β-secretase cleavage and Aβ generation (Kuhn *et al,* 2010), indicating that there is a competition between α- and β-secretase for substrate. However, in conditional ADAM10 knock-out mice not only a reduction in sAPPα levels was observed, but also sAPPβ and Aβ production was decreased (Jorissen *et al,* 2010). The reasons for the discrepancies in the previous studies are not clear, but knock-out of ADAM10 may be better analysed in adult neurons where differentiation of neurons has been completed for better comparison with other studies. Interestingly, knockdown of ADAM10 in HEK293 and SH-SY5Y cells did not result in increased sAPPβ and Aβ

levels (Kuhn *et al,* 2010), indicating that competition between the secretases under constitutive conditions may depend on the cell type.

Although a competition between α- and β-secretase has not been established securely for constitutive cleavage, it was demonstrated that regulated activation of α-secretase can compete with β-secretase cleavage and consequently reduce Aβ generation. Therefore, a promising therapeutic approach would be an increase of α-secretase activity, especially of ADAM10, prior to endocytosis and processing by β-secretase (Fahrenholz, 2007). Since α-secretases cleave within the Aβ peptide domain, they combine several beneficial effects as a therapeutic target, as they not only preclude the neurotoxic Aβ peptide formation but also generate the putatively neuroprotective sAPPα (Mattson *et al,* 1993; Goodman & Mattson, 1994). As it has been difficult to find safe and selective β- and γ-secretase inhibitors, shifting APP processing towards the non-amyloidogenic pathway by α-secretase activation may be a better approach. A few α-secretase enhancers have already been shown to stimulate α-secretase activity and increase the production of potentially neuroprotective sAPPα and have already been tested in phase II clinical trials (Kumar *et al,* 2018). However, the impact of chronic upregulation in the processing of other substrates mediated by the α-secretase still needs to be evaluated. Additionally, for this approach to be effective and secure, the mechanisms responsible for regulation and substrate interaction of the physiological α-secretase need to be better understood.

2.4 Plasmalemmal organisation of APP and secretases

For many membrane proteins a heterogeneous distribution across the membrane and segregation into nano- and microdomains is a common occurence (Jacobson *et al,* 1995; Jacobson *et al,* 2007; Lang & Rizzoli, 2010). For APP it was demonstrated that at least a subpopulation of APP is organized in plasmalemmal protein clusters (Schneider *et al,* 2008). The majority of plasmalemmal APP was found in those multi-protein clusters which consisted of 20 to 30 molecules in neuronal SH-SY5Y cells (de Coninck *et al,* 2018). Protein-protein interactions seem to be important for APP oligomerization. For example, flotillin-2 has been shown to promote clustering of APP and knockdown of flotillin-2 reduced cluster sizes (Schneider *et al,* 2008). Recently, the first 5 amino acids of the Aβ region have been reported to mediate clustering of APP (Schreiber, 2012). Additionally, the E1 and transmembrane domain could also promote APP aggregation, as these domains are already associated with dimerization of APP (Marenchino *et al,* 2008; Munter *et al,* 2007; Kaden *et al,* 2008; Kaden *et al,* 2009; Soba *et al,* 2005).

The function of the cluster formation of APP remains unclear to date. For other transmembrane proteins it has been proposed that oligomerization may improve cellular signaling by increasing local protein concentrations and accelerating reaction kinetics (Cebecauer *et al,* 2010; Lang & Rizzoli, 2010; Kornberg *et al,* 1991). Another possible function may be a mechanism to maintain a reservoir of biochemical inactive membrane proteins and to block protein activity and interaction by steric hindrance, as already described for some membrane proteins (Bethani *et al,* 2007; Bethani *et al,* 2009; Bar-On *et al,* 2009). Oligomerization may also be a mechanism employed to protect against degradation and denaturation of proteins due to a reduced surface area (Goodsell & Olson, 2000; Ali & Imperiali, 2005). Furthermore, clustering has also been shown to induce or enhance internalization (Hofman *et al,* 2010; Cureton *et al,* 2012; Galmes *et al,* 2013; Yu *et al,* 2015). Previously, it has been demonstrated that APP clustering is a prerequisite for Clathrin-dependent endocytosis (Schreiber *et al,* 2012). The resulting endocytosis into the early endosomal compartment leads to amyloidogenic processing of APP and generation of the Aβ peptide, as the β-secretase mainly functions in early endosomes (Rajendran *et al,* 2006; Kinoshita *et al,* 2003; He *et al,* 2007). Furthermore, tight clustering might also reduce the accessibility for α-secretases significantly. APP clustering might therefore also regulate APP processing by preventing α-secretase cleavage. Interestingly, several pathological mutations (Lan *et al,* 2014; Wakutani *et al,* 2004; Zhou *et al,* 2011; Di Fede *et al,* 2009) and the only APP mutation known to protect against AD (Jonsson *et al,* 2012) are located close to the 5 N-terminal amino acids of the Aβ region associated with APP aggregation (Schreiber *et al,* 2012). Mutations in this region may influence the clustering behaviour of APP and thereby affect the accessibility of the substrate for α-cleavage. However, at present it remains to be demonstrated if these mutations affect clustering, processing or trafficking of APP.

Additionally, cholesterol seems to be required for clathrin-dependent endocytosis and subsequent amyloidogenic processing of APP and generation of the pathogenic Aβ peptide (Schneider *et al,* 2008; Cossec *et al,* 2010; Ehehalt *et al,* 2003). A small subpopulation of APP is partitioned in cholesterol- and sphingolipid microdomains (Ehehalt *et al,* 2003; Rushworth & Hooper, 2010), possibly due to direct binding of cholesterol (Beel *et al,* 2010; Barrett *et al,* 2012). In those microdomains, APP can form functional complexes with β- and ɣ-secretases as they are also targeted there, while the α-secretases competing for APP processing reside in regions of the plasma membrane with less cholesterol (Ehehalt *et al,* 2003; Kojro *et al,* 2001). In addition to the exclusion of α-secretases from cholesterol-rich microdomains, cholesterol is

expected to promote amyloidogenic processing by increasing substrate binding or catalysis of β- and ɣ-secretases (Beel *et al,* 2010).

In conclusion, the organisation and interaction of the substrate and the secretases in the plasma membrane affects the amyloidogenic and non-amyloidogenic processing of APP. However, a better understanding of the interplay of the involved proteins is necessary for future therapeutic approaches aiming to stimulate non-amyloidogenic processing by α-secretases.

3 Aim of the study

APP plays a central role in the pathophysiology of Alzheimer's disease due to the sequential cleavages by β- and γ-secretases that result in the generation of neurotoxic Aβ peptides. Aβ accumulation could be precluded by increasing non-amyloidogenic processing of APP mediated by α-secretases at the plasma membrane. However, a deeper understanding of the mechanisms regulating organisation, processing and interaction of the substrate APP with α-secretases is necessary to successfully exploit this processing pathway for therapeutic purposes.

Clustering of APP requires the first 5 amino acids of the Aβ region (Schreiber *et al,* 2012). Several familial mutations close or within the clustering region have been associated with altered α- and β-processing (Di Fede *et al,* 2009; Jonsson *et al,* 2012; Zhou *et al,* 2011). Therefore, it is tempting to speculate that these mutations affect clustering and by this regulate processing of APP. More efficient clustering may preclude access of the α-secretases to the cleavage site or tight clusters may be internalized more quickly and by this escape α-processing at the plasma membrane. To clarify, if a change in APP clustering correlates with altered APP processing, the clustering degree, plasmalemmal dynamics and processing of different familial APP mutants was examined in this study.

Furthermore, the physical interaction between APP and the α-secretases is not understood yet and it remains unclear why ADAM10 is the physiologically relevant, constitutive α-secretase from the several known candidates. Therefore, this work aimed to characterize the organisation and interaction of APP and the secretases in the native plasma membrane. For this purpose, the plasmalemmal distribution, abundance and lateral association of APP and the α-secretases ADAM10 and ADAM17 at the cell surface was studied employing super-resolution STED microscopy. Additionally, the APP-ADAM interaction was probed directly in native membranes by antibody-induced co-aggregation. Finally, it was examined if the interaction could be modulated by phorbol esters that stimulate α-secretases, or by exchanging certain amino acids in the Aβ region of APP.

4 Materials and Methods

4.1 Materials

If not stated otherwise, standard chemicals, reagents and consumables used in this study were purchased from Bio-Rad (Hercules, CA), Carl Roth (Karlsruhe, Germany), Invitrogen (Carlsbad, CA), Merck (Darmstadt, Germany), NEB (Ipswich, USA), PAN Biotech (Aidenbach, Germany), Paul Marienfeld (Lauda-Koenigshofen, Germany), Sarstedt (Nümbrecht, Germany), Sigma-Aldrich (Hamburg, Germany), Thermo Fisher Scientific (Waltham, USA) or VWR (Darmstadt, Germany).

4.1.1 Appliances

Table 1. Appliances

Name	Supplier	Application
Inverted microscope ECLIPSE TS100, CFI60 Infinity Optical System	Nikon, Tokyo, Japan	Brightfield microscope for cell culture purposes
Olympus IX81-ZDC fluorescence microscope, MT20E illumination system	Olympus, Tokyo, Japan	Epifluorescence microscopy
Zeiss Axio Observer D1	Carl Zeiss, Jena, Germany	Epifluorescence microscopy
Zeiss LSM 880 with Airyscan	Carl Zeiss, Jena, Germany	Confocal microscope for FRAP measurements
easy3D STED module coupled to Olympus IX83 confocal microscope	Abberior Instruments, Göttingen, Germany / Olympus, Tokyo, Japan	STED and confocal microscopy
Mini-PROTEAN Tetra Cell with Mini Trans-Blot Module	Bio-Rad, Hercules, USA	SDS-PAGE and protein transfer
Odyssey® CLx Imaging System	Li-Cor, Lincoln, USA	Western blot imaging
Neon™ Transfection system	Thermo Fisher Scientific, Waltham, USA	Transfection of eukaryotic cells by electroporation

Sonopuls HD 2070	Bandelin, Berlin, Germany	Sonification for membrane sheet generation
TPersonal/TProfessional basic gradient	Biometra, Goettingen, Germany	Polymerase chain reaction (PCR)
NanoDrop2000	Thermo Fisher Scientific, Waltham, USA	DNA concentration measurement

4.1.2 Buffers and solutions

All buffers and solutions were prepared using double distilled water ($_{dd}H_2O$) and autoclaved or sterile filtered if necessary.

Table 2. Buffers and solutions

Name	Composition/Preparation
Phosphate buffered saline (PBS)	137 mM NaCl, 2.7 mM KCl, 1.76 mM KH_2PO_4, 10mM Na_2HPO_4, pH 7.4
PBS-T	0.1 % Tween-20 (v/v) in PBS
Tris-acetate-EDTA (TAE) buffer	40 mM Tris, 1 mM EDTA, 0.11 % (v/v) acetic acid
Sonication buffer	120 mM potassium glutamate, 20 mM potassium acetate, 10 mM EGTA, 20 mM HEPES, pH 7.2
Ringer solution	130 mM NaCl, 4 mM KCl, 1 mM $CaCl_2$, 1 mM $MgCl_2$, 48 mM D-(+)-glucose, 10 mM HEPES-NaOH, pH 7.4
Lysis buffer for immunoprecipitation	10 mM Tris-HCl, 150 mM NaCl, 0.5 mM EDTA, 0.5 % (v/v) Nonidet® P40 Substitute (cat# 492016, Merck, Darmstadt, Germany), pH 7.5
Wash buffer for immunoprecipitation	10 mM Tris-HCl, 150 mM NaCl, 0.5 mM EDTA, pH 7.5
8 % SDS running gel	4.7 mL $_{dd}H_2O$, 2.7 mL 30 % (v/v) 1:37.5 bis:acrylamide, 2.5 mL 1.5 M Tris (pH 8.8), 100 µL 10 % (w/v) SDS, 100 µL 10 % (w/v) APS, 10 µL TEMED
4 % SDS stacking gel	3.05 mL $_{dd}H_2O$, 0.65 mL 1:37.5 bis:acrylamide, 1.25 mL 0.5 M Tris (pH

	6.8), 50 µL 10 % (w/v) SDS, 50 µL 10 % (w/v) APS, 10 µL TEMED
4x SDS sample buffer	250 mM Tris-HCl, 8% (w/v) SDS, 40% (w/v) Glycerol, 0.008 % (w/v) bromophenol blue, pH 6.8; shortly before usage 5 % (v/v) β-mercaptoethanol (working concentration) were added
SDS running buffer	25 mM Tris, 0.1% (w/v) SDS, 192 mM glycine, pH 8.3
Towbin buffer	25 mM Tris, 192 mM glycine, 20% (v/v) methanol, pH 8.3
Blocking/dilution buffer for Western blot	50 % (v/v) Odyssey blocking buffer (cat# 927-40000,Li-Cor, Lincoln, USA) in PBS; 0.1 % (v/v) Tween-20 were added for antibody dilution
Poly-L-lysine (PLL) stock solution (20x)	2 mg/mL PLL in $_{dd}H_2O$
Paraformaldehyde (PFA) stock solution	16 % (w/v) PFA in $_{dd}H_2O$
PFA fixative solution	PFA stock solution was adjusted with 10x PBS and $_{dd}H_2O$ to get fixative solution (4 % PFA in 1x PBS, pH 7.4)
Quenching buffer	50 mM NH_4Cl in PBS
Permeabilization buffer	0.2 % (v/v) Triton X-100 in PBS
Blocking buffer for immunostaining	4 % (w/v) BSA in PBS
Dilution buffer for immunostaining	1 % (w/v) BSA in PBS
Washing buffer for immunostaining	0.5 % (w/v) BSA in PBS

4.1.3 Kits

Kits were used according to the manufacturer's instructions unless specified otherwise.

Table 3: Kits

Name	Supplier
Neon™ Transfection System 100 µL Kit	cat# MPK10096, Thermo Fisher Scientific
NucleoBond Xtra Midi®	cat# 740410, Macherey-Nagel, Dueren, Germany

NucleoSpin Plasmid®	cat# 740588, Macherey-Nagel, Dueren, Germany
NucleoSpin Gel and PCR clean-up®	cat# 740609, Macherey-Nagel, Dueren, Germany
In-Fusion® HD Cloning Kit	cat# 639642, Takara Bio, Saint-Germain-en-Laye, France

4.1.4 Culture media and reagents

Table 4. Culture media and reagents

Medium/Reagent	Composition/Supplier
HepG2 growth medium	MEM Eagle (cat# P04-08509, PAN Biotech), supplemented with 10 % (v/v) fetal bovine serum (FBS, cat# P30-3031, PAN Biotech), 2 mM stable glutamine (cat# P04-82100, PAN Biotech) and 1 % (v/v) penicillin/streptomycin (cat# P06-07100, PAN Biotech)
SH-SY5Y growth medium	DMEM:F12 (cat# P04-41500, PAN Biotech), supplemented with 10 % (v/v) FBS (cat# P30-3031, PAN Biotech) and 1 % (v/v) penicillin/streptomycin (cat# P06-07100, PAN Biotech)
Trypsin solution	cat# P10-0231SP, PAN Biotech
Dulbecco's PBS (DPBS)	cat# P04-36500, PAN-Biotech
LB medium	2 % (w/v) LB (cat# X964, Carl Roth, Karlsruhe, Germany); for agar plates medium was supplemented with 2 % (w/v) agar

4.1.5 Cell lines

HepG2 cells: HepG2 cells are human liver hepatocellular cells isolated from a hepatoblastoma. For this study, they were acquired at passage 19 from Cell Line Services, Eppelheim, Germany (cat# 300198).

SH-SY5Y cells: SH-SY5Y cells are a thrice cloned subline of the human neuroblastoma cell line SK-N-SH derived from a bone marrow metastatic site. The cells resemble a neuroblast-like cell population. SH-SY5Y cells were purchased at passage 26 from LGC Standards, Wesel, Germany (cat# ATCC-CRL-2266).

Escherichia (*E.*) *coli* XL10-Gold Ultracompetent cells: *E. coli* XL10-Gold cells were used for all cloning purposes and purchased from Agilent Technologies, Waldbronn, Germany (cat# 200314).

4.1.6 Plasmids

Table 5. Plasmids
Plasmids based on pcDNA™6.2/C-emGFP-DEST confer an Ampicillin resistance; plasmids with pEGFP-C1 origin carry a Neomycin/Kanamycin resistance cassette

Construct	Source	Description
pcDNA™6.2/C-emGFP-DEST	cat# V35520, Thermo Fisher Scientific, Waltham, USA	Mammalian expression vector carrying a C-terminal monomeric emerald GFP
pEGFP-C1 (modified)	provided by Yahya Homsi (based on cat# 6084-1, Clontech, Mountain View, USA)	Mammalian expression vector carrying a C-terminal monomeric enhanced GFP (mEGFP)
pEGFP-C1-EGFR-mEGFP	provided by Jan-Gero Schloetel (former co-worker AG Membrane Biochemistry)	human EGFR (NM_005228.5) fused to C-terminal mEGFP
pCDNA6.2_mCherry-APP-emGFP	provided by Dennis de Coninck (de Coninck, 2020)	mCherry inserted between aa 18 and 19 of human APP695 (NM_201414), fused C-terminally to emGFP
pcDNA6.2-APP-emGFP	provided by Arne Schreiber (Schreiber *et al,* 2012)	human APP695 (NM_201414) fused to C-terminal emGFP
pcDNA6.2-APP-A2T-emGFP	provided by Dennis de Coninck (de Coninck, 2020)	pcDNA6.2-APP-emGFP carrying a A to T point mutation at postion 2 of the Aβ region
pcDNA6.2-APP-A2V-emGFP	provided by Dennis de Coninck (de Coninck, 2020)	pcDNA6.2-APP-emGFP carrying a A to V point mutation at postion 2 of the Aβ region

pcDNA6.2-APP-E11K-emGFP	provided by Vivien Averesch (former co-worker AG Membrane Biochemistry)	pcDNA6.2-APP-emGFP carrying a E to K point mutation at postion 11 of the Aβ region
pcDNA6.2_APP∆C-emGFP	provided by Arne Schreiber (Schreiber *et al,* 2012)	pcDNA6.2-APP-emGFP with C-terminal amino acids 649-695 deleted
pEGFP-C1-APP-mEGFP	see section 4.2.1	human APP695 (NM_201414) fused C-terminally to mEGFP
pEGFP-C1-mCh-APP-mEGFP	see section 4.2.1	human APP695 (NM_201414) fused N-terminally to mcherry and C-terminally to mEGFP
pEGFP-C1-mCh-APP-A2T-mEGFP	see section 4.2.1	pEGFP-C1-mCh-APP-mEGFP carrying a A to T point mutation at postion 2 of the Aβ region
pEGFP-C1-mCh-APP-A2V-mEGFP	see section 4.2.1	pEGFP-C1-mCh-APP-mEGFP carrying a A to V point mutation at postion 2 of the Aβ region
pEGFP-C1-APP∆N-mEGFP	see section 4.2.1	pEGFP-C1-APP-mEGFP with amino acids 22-626 deleted
pEGFP-C1-APP-TMS-mEGFP	see section 4.2.1	pEGFP-C1-APP-mEGFP with the transmembrane segment (TMS) amino acids 627-647 substituted by the TMS amino acids 646-668 of EGFR (NM_005228.5)
pEGFP-C1-APP(↔ 628-630)-mEGFP	see section 4.2.1	pEGFP-C1-APP-mEGFP carrying point mutations to exchange at amino acids 628 I to A,629 G to T and 630 L toG
pEGFP-C1-APP(↔ 634-639)-mEGFP	see section 4.2.1	pEGFP-C1-APP-mEGFP carrying point mutations to exchange at amino acids 634-639 GVVIAT to ALLLLL

pEGFP-C1-APP(↔ 641-644_646)-mEGFP	see section 4.2.1	pEGFP-C1-APP-mEGFP carrying point mutations to exchange at amino acids 641-644 IVIT to VALG and 646 V to F

4.1.7 Primary antibodies and nanobodies

Table 6. Primary antibodies and nanobodies
IF: immunofluorescence; WB: Western blot

Target / name	Origin / Clone	Supplier	Application / dilution
APP (C-Terminus), C1/6.1	Mouse, monoclonal	cat# 802801, Biolegend, San Diego, USA	IF, 1:200 WB, 1:2000
β-Amyloid 1-16, 6E10	Mouse, monoclonal	cat# SIG-39320, Biolegend, San Diego, USA	WB, 1:2000
ADAM10	Rabbit, polyclonal	cat# ab1997, Abcam, Cambridge, UK	IF, 1:1000 WB, 1:1000
ADAM17	Rabbit, polyclonal	cat# AB19027, Merck, Darmstadt, Germany	IF, 1:500
GFP, 9F9.F9	Mouse, monoclonal	cat# ab1218, Abcam, Cambridge, UK	IF, 1:200
β-Actin, 13E5	Rabbit, monoclonal	cat# 4970S; Cell Signaling Technology, Danvers, USA	WB, 1:5000
GFP, GFP-Booster Atto647N	Alpaca recombinant nanobody, monoclonal, conjugated to Atto647N	cat#gba647n-100, Chromotek, Planegg-Martinsried, Germany	IF, 1:200

4.1.8 Secondary antibodies

Table 7. Secondary antibodies
IF: immunofluorescence; WB: Western blot

Target species	Origin	Fluorophore	Supplier	Application / dilution
mouse	goat	STAR RED	cat# STRED-1001, Abberior Instruments, Bethesda, USA	IF, 1:200

rabbit	goat	STAR RED	cat# STRED-1002, Abberior Instruments, Bethesda, USA	IF, 1:200
rabbit	donkey	AlexaFluor594	cat#ab150064, Abcam, Cambridge, UK	IF, 1:200
mouse	goat	IRDye® 800CW	cat#925-32210, Li-Cor, Lincoln, USA	IF, 1:500 WB, 1:10000
rabbit	goat	IRDye® 680RD	cat# 926-68071, Li-Cor, Lincoln, USA	WB, 1:10000

4.1.9 Software

Appliances listed in Table 1 were operated by the software provided by the manufacturer. Other software used is listed in Table 8.

Table 8. Software

Software	Source	Application
ImageJ (MBF and Fiji bundle)	Wayne Rasband, National Institute of Health, USA	Image analysis
Microsoft Office 2016/365	Microsoft Corporation, Redmond, USA	Writing, data analysis and organisation
Graphpad Prism 6	GraphPad Software Inc., San Diego, USA	Data plotting
CorelDraw 2019	Corel Corporation, Ottawa, Canada	Preparation and editing of figures
Métamorphose 2	Ianaré Sévi	Sorting and renaming of files
SnapGene Viewer 1.1.3	GSL Biotech, Chicago, USA	DNA sequence editor

4.2 Methods

4.2.1 Cloning

Cloning was performed following the standard methods described previously (Sambrook & Russell, 2006). Primers used for DNA amplification and sequencing were designed manually and ordered from Eurofins Genomics (Ebersberg, Germany). DNA amplification was achieved by polymerase chain reaction (PCR) using a Q5® High-Fidelity DNA polymerase (cat# M0491S, NEB, Ipswich, USA). Plasmids used as templates for PCR or

as target vectors after amplification as well as constructed plasmids are listed in Table 5. PCR products were routinely separated by electrophoresis using TAE buffer and agarose gels. PCR products were extracted from agarose gels and purified using the NucleoSpin Gel and PCR clean-up® kit (see Table 3). For plasmid amplification, *Escherichia* (*E.*) *coli* XL10-Gold Ultracompetent cells (cat# 200314, Agilent Technologies, Waldbronn, Germany) were transformed and selectively grown in LB medium as well as on LB-agar plates containing the antibiotics carbenicillin (100 µg/mL) or kanamycin (30 µg/mL), depending on the antibiotic resistance encoded by the inserted plasmid. Plasmids were isolated using either the NucleoSpin Plasmid® kit for culture volumes up to 5 mL or the NucleoBond Xtra Midi® kit (see Table 3) for larger volumes. All constructs were verified by sequencing of the target region in one direction (Eurofins Genomics, Ebersberg, Germany).

For cloning of pEGFP-C1-APP-mEGFP, the DNA sequence of human APP695 (NCBI reference sequence NM_201414) without the Stop codon was amplified using pCDNA6.2-APP-emGFP as a template and 15 nt overhang primers. Sequences of those two primers are GTCAGATCCGCTAGCATGCTGCCCGGTTTGGCA (forward_APP) and GCCCTTGCTCACCATGTTCTGCATCTGCTCAAA (reverse_APP). The target vector pEGFP-C1 was amplified with primers carrying 15 nt overhangs for APP and the sequences GAGCAGATGCAGAACATGGTGAGCAAGGGCGAG (pEGFP_forward) and CAAACCGGGCAGCATGCTAGCGGATCTGACGGT (pEGFP_reverse). The APP PCR product was inserted directly upstream of the sequence coding for GFP into the target vector pEGFP-C1 via homologous recombination utilizing the In-Fusion® HD Cloning Kit (see Table 3), according to manufacturer's instructions.

For pEGFP-C1-mCh-APP-mEGFP, the DNA sequence of APP with a mCherry-tag inserted between amino acids 18 and 19 was amplified using pCDNA6.2_mCherry-APP-emGFP (de Coninck, 2020) as a template and the primers described above (forward_APP; reverse_APP). The target vector pEGFP-C1 was amplified with the primers pEGFP_forward and pEGFP_reverse (described above) and the insert was inserted directly upstream of the sequence coding for mEGFP into the target vector pEGFP-C1 via homologous recombination utilizing the In-Fusion® HD Cloning Kit (see Table 3), according to manufacturer's instructions.

For pEGFP-C1-mCh-APP-A2T-mEGFP and pEGFP-C1-mCh-APP-A2V-mEGFP, non-overlapping primers that introduce base pair substitutions and create blunt ends were used. pEGFP-C1-mCh-APP-mEGFP served as template for amplification. For both mutations the reverse primer AGAGATCTCCTCCGTCTTGATATTTGTCAACCCAG was used that anneals back-to-back to the forward primer for the A2T mutation GAAGTGAAGATGGATACAGAATTCCGACATGAC (A2T_forward) or for the A2V mutation GAAGTGAAGATGGATGTAGAATTCCGACATGAC (A2V_forward). PCR amplification was followed by *Dpn*I digestion, phosphorylation (cat# M0201S, NEB, Cambridge, UK) and ligation (cat# M0202S, NEB, Cambridge, UK) of the blunt ends.

From the pEGFP-C1-APP-mEGFP plasmid, the deletion construct pEGFP-C1-APPΔN-mEGFP (see Table 5) was produced by amplification of the whole plasmid excluding the nucleotides coding for amino acids (aa) 22-626 of the APP protein. Primers used were ATCATTGGACTCATGGTGGGCGGTGTT (forward) and GGGTACCTCCAGCGCCCGAG (reverse). PCR amplification was followed by *Dpn*I digestion, phosphorylation and ligation of the PCR product.

For pEGFP-C1-APP-TMS-mEGFP, the transmembrane domain of APP (aa 627-647) was exchanged for the transmembrane domain of the epidermal growth factor receptor (EGFR, NM_005228.5; aa 646-668). For this purpose, the pEGFP-C1-APP-mEGFP vector was amplified excluding the aa 627-647 of APP but carrying 15 nt overhangs to the EGFR transmembrane domain. Sequences of the primers used are ATCGGCCTCTTCATGCTGAAGAAGAAACAGTACAC (forward) and CATCCCAGTGGCGATTGCACCTTTGTTTGAACC (reverse). The EGFR transmembrane domain (aa 646-668 of EGFR) was amplified in another PCR using pEGFP-C1-EGFR-GFP as a template and primers TCAAACAAAGGTGCAATCGCCACTGGGATGGTGGG (forward) and CTGTTTCTTCTTCAGCATGAAGAGGCCGATCCCCA (reverse) carrying 15 nt overhangs for APP. Both PCR products were fused using the In-Fusion® HD Cloning Kit (see Table 3).

The APP-mutants pEGFP-C1-APP(↔ 628-630)-mEGFP, pEGFP-C1-APP(↔ 634-639)-mEGFP and pEGFP-C1-APP(↔ 641-644_646)-mEGFP were created by mutagenesis PCR with pEGFP-C1-APP-mEGFP serving as template. Specifically, forward and reverse primers that anneal back-to-back and introduce nucleotide substitutions in the

transmembrane domain of APP were employed. Primer pairs used were CAGGCATGGTGGGCGGTGTTGTCA (628-630_forward; nucleotide substitutions are underlined) and TAGCGATTGCACCTTTGTTTGAACCCACAT (628-630_reverse), CCTACTGCTAGTGATCGTCATCACCTTGGT (634-639_forward) and AGAAGAGCGCCCACCATGAGTCCAATGATT (634-639_reverse) as well as GGCTTGTTCATGCTGAAGAAGAAACAGTACACATC (641-644_646_forward) and GAGGGCGACCACTGTCGCTATGACAACAC (641-644_646_reverse). Following PCR amplification, the original plasmid was digested by *Dpn*I and the PCR-product was phosphorylated and ligated.

4.2.2 Cell culture

All cell culture procedures were carried out under a sterile laminar flow cell culture hood (BDK Luft und Reinraumtechnik, Sonnenbühl, Germany). Cells were cultivated at 37 °C and 5 % CO_2 in a cell incubator (Binder, Tuttlingen, Germany).

4.2.2.1 Passaging and cultivation of HepG2 and SH-SY5Y cells

In this study, HepG2 and SH-SY5Y cells were employed (see section 4.1.5). HepG2 cells were cultivated in MEM Eagle medium (cat# P04-08509, PAN Biotech) supplemented with 10 % (v/v) FBS (cat# P30-3031, PAN Biotech), 2 mM stable glutamine (cat# P04-82100, PAN Biotech) and 1 % (v/v) penicillin/streptomycin (cat# P06-07100, PAN Biotech). SH-SY5Y cells were cultivated in DMEM:F12 medium (cat# P04-41500, PAN Biotech) supplemented with 10 % (v/v) FBS and 1 % (v/v) penicillin/streptomycin.

For both cell lines, the medium was routinely replaced every 3 days and both cell types were passaged by trypsination before reaching maximal confluency of ~90 %. To do so, cells were briefly washed with DPBS (cat# P04-36500, PAN-Biotech), followed by incubation with 1-2 mL trypsin (cat# P10-0231SP, PAN Biotech) for 5 min at 37 °C. To stop protease activity, 10 mL cell specific growth medium was added and cells were vigorously resuspended. Thereafter, cells were counted using a Neubauer chamber for transfection or seeding, or directly transferred to a new cell culture flask for further cultivation. SH-SY5Y cells were routinely split at a dilution of 1:3 or larger, but never exceeding a dilution of 1:10. HepG2 cells were diluted 1:5 - 1:30.

4.2.2.2 Freezing and thawing of cells

For cryo-conservation of cells, cells were trypsinated (see 4.2.2.1) and cell suspensions were adjusted to 2 x 10^6 cells per mL growth medium without antibiotics but supplemented with 10 % (*v/v*) DMSO. 1.8 mL cell suspension was transferred to cryo vials, respectively. Aliquots were placed into a cryo-freezing container (cat# 5100-001, Thermo Fisher Scientific) for gradual reduction in temperature to -80 °C before long-term storage in liquid nitrogen.

For thawing, cryo stocks were transferred to a 37 °C waterbath. Immediately after thawing, the cell suspension was mixed with growth medium and centrifuged for 3 min at 1000 x g. After removal of the supernatant, cells were resuspended in growth medium and transferred to cell culture flasks for cultivation.

4.2.2.3 Cleaning and coating of coverslips

For microscopy, cells were seeded onto high precision glass coverlips (cat# 0117650, Paul Marienfeld) coated with PLL. To this end, coverslips were first cleaned by consecutive washes under agitation in 1 M HCl, in 1 M NaOH and in ethanol for 1 h each. In between each step, coverslips were extensively washed with $_{dd}H_2O$. Afterwards, coverslips were either baked at 180 °C and or stored in 70 % (v/v) ethanol to keep them sterile. Coverlips were placed in 6-well plates and coated for 30 min by plating onto the coverslips 0.5 mL of a 100 µg/mL PLL-solution. After removal of the solution, coverslips were dried and subsequently sterilized by exposure to UV light for 20 min.

4.2.2.4 Transfection of cells

The Neon™ Transfection System (cat# MPK10096, Thermo Fisher Scientific) was used for transfection of HepG2 as well as SH-SY5Y cells according to manufacturer's instructions. Cells were trypsinated, counted (see 4.2.2.1) and centrifuged for 3 min at 1000 x g. After washing with DPBS, for each transfection 2 x 10^6 cells were resuspended in 125 µL buffer R (Thermo Fisher Scientific) for SH-SY5Y or in 125 µL DPBS for HepG2 cells and supplemented with 12.5 µg plasmid DNA. The cell suspension was transferred to a 100 µL Neon electroporation tip and electroporated. A single pulse of 1200 V (for HepG2 cells) or 1100 V (for SH-SY5Y) with 50 ms width was applied. Electroporated cells were transferred to growth medium without antibiotics. For fluorescence microscopy, approximately 3 x 10^5 cells in a total volume of 500 µL were transferred to glass coverslips coated with PLL (see above) and allowed to recover for 1 h at 37 °C before adding 1.5 mL growth medium with

antibiotics. For SDS-PAGE/Western blotting or co-immunoprecipitation, 4 x 10^6 cells were seeded directly on 6-well plates in a total volume of 1.5 ml growth medium without antibiotics and serum. If necessary for the experiment, the supplements Batimastat ([10 µM]; #catSML0041; Sigma-Aldrich) as an α-secretase inhibitor (Parvathy *et al,* 1998), GI254023X ([3 µM]; cat#SML0789; Sigma-Aldrich) as a potent ADAM10 inhibitor (Ludwig *et al,* 2005), DAPT ([10 µM]; cat#D5942; Sigma-Aldrich) as a highly specific γ-secretase inhibitor (Dovey *et al,* 2001), or PMA ([1 µM]; cat#P1585; Sigma-Aldrich) for stimulation of α-cleavage were added to the growth medium 1 h after transfection. Because DMSO was used as solvent for all supplements, DMSO was added as a negative control. Cells were generally incubated for 21 h at 37 °C, before further analysis was performed.

4.2.3 Immunoblotting

4.2.3.1 Co-immunoprecipitation

For co-immunoprecipitation, HepG2 cells were transfected to express APP-GFP and grown in the presence or absence of Batimastat. 21 h after transfection, the medium was removed, cells were scraped-off with a cell scraper and washed two times with ice-cold PBS by centrifugation at 1000 x g for 3 min at 4 °C. Cells were incubated with 200 µL ice-cold lysis buffer for 30 min at 4 °C with extensively pipetting every 10 min. The cell lysate was separated from insoluble cell debris by centrifugation at 20000 x g for 10 min at 4 °C. In the meantime, 25 µL GFP-Trap® Agarose beads (cat#gta-20; Chromotek) were washed three times with 500 µL wash buffer by centrifugation at 2500 x g for 2 min at 4 °C. Thereafter, the lysate was diluted with 300 µL wash buffer and mixed with the agarose beads. For immunoprecipitation of APP-GFP, the beads were incubated for 1 h at 4 °C under agitation. The flow-through was separated from the beads by centrifugation at 2500 x g for 2 min at 4 °C. Beads were washed three times by addition of 500 µL wash buffer and centrifugation at 2500 x g for 2 min at 4 °C. Unbinding of the precipitate was achieved by addition of 2.5x sample buffer and incubation of the beads for 10 min at 95 °C. The supernatant with the precipitate was separated from the beads by centrifugation at 2500 x g for 2 min at 4 °C. All samples were resuspended in 1x sample buffer and incubated for 10 min at 95 °C for SDS-PAGE.

4.2.3.2 Harvesting of cells

For quantification of full-length APP or sAPPα cleavage product by Western blot analysis, the growth medium (without antibiotics and serum; 1.5 ml) of cells grown for 21 h after

transfection in a 6-well plate was centrifuged at 1000 x g for 3 min at 4 °C. The supernatant was mixed 1:4 with 0.5 ml 4x sample buffer. The remaining attached cells in the 6-well plate were scraped-off with a cell scraper, washed two times with PBS by centrifugation at 1000 x g for 3 min at 4 °C and the cell pellet was resuspended in 80 µl 1x sample buffer. Samples were agitated at 95 °C for 10 min for later analysis by SDS-PAGE and Western blot.

4.2.3.3 SDS-PAGe and Western blotting

Protein samples were loaded together with Color Prestained Protein Standard (cat# P7719, NEB, Ipswich, USA) onto a 8 % poly-acrylamide SDS running gel with a 4 % SDS stacking gel. Gels were run in SDS running buffer at 70 V until samples had left the stacking gel. Afterwards, voltage was raised to 150 V.

After SDS-PAGE, gels were equilibrated in ice-cold Towbin buffer for 10 min. Whatman paper (cat# 3001-672, GE Healthcare, Chicago, USA) as well as nitrocellulose membrane (cat# HP40.1, Carl Roth) were also incubated in Towbin buffer for 30 min at 4 °C. The transfer of protein from the gel to the nitrocellulose membrane was performed in a Mini-PROTEAN Tetra Cell with a Mini Trans-Blot Module (Bio-Rad) in cooled Towbin buffer under constant buffer agitation at 100 V for 2 h. After blotting, the membrane was washed in PBS for 5 min and blocked for 1 h using blocking buffer. Afterwards, nitrocellulose membranes were incubated with primary antibodies diluted in dilution buffer at 4 °C over night under constant agitation. After washing four times for 10 min with PBS-T, membranes were incubated with secondary antibodies in dilution buffer for 1 h at room temperature. Thereafter, membranes were washed three times with PBS-T and one time with PBS for 10 min each. Fluorescence was detected using the 700 nm and 800 nm channels of an Odyssey® CLx Imaging System.

4.2.4 Microscopy

4.2.4.1 Preparation and treatment of membrane sheets

Coverslips with overexpressing or non-overexpressing cells were briefly washed with ice-cold DPBS and transferred into a petri dish filled with ice-cold sonication buffer with the cells facing up. A sonicator tip was placed above the center of the coverslip at a distance of ~5 mm. Membrane sheets were generated by applying a 100 ms sonication pulse with 15 % power (for SH-SY5Y cells) or 80 % power (for HepG2 cells). For cleavage assays or cross-linking experiments, coverslips remained unfixed. For all other experiments, samples

were fixed at room temperature for 30 min in 4 % (w/v) PFA (in PBS). Afterwards coverslips were incubated in quenching buffer containing 50 mM NH_4Cl for 20 min. Membrane sheets were either imaged directly (for epifluorescence microscopy) or immunostained before imaging (STED and confocal microscopy).

4.2.4.2 Assay of APP cleavage in unfixed membrane sheets

For evaluation of α-processing in plasma membrane sheets (Figure 29B), membrane sheets were generated from cells expressing APP, APP-A2T or APP-A2V double tagged with mCherry and GFP 21 h after transfection. After sonication, coverslips were either directly fixed in 4 % (w/v) PFA (in PBS) or incubated in medium supplemented with the γ-secretase inhibitor DAPT [10 µM] for 10 min at 37 °C in a cell incubator. After incubation of native membrane sheets, coverslips were fixed and quenched as described above and imaged immediately.

4.2.4.3 Cross-linking of APP in unfixed membrane sheets

From cells overexpressing APP or APP-mutants fused to a C-terminal GFP-tag and grown in the presence of 10 µM Batimastat, membrane sheets were produced as described above. For cross-linking of APP-GFP, samples were incubated with a mouse-anti-GFP antibody in 1 % BSA (in PBS) at 37 °C for 15 min, followed by two washing steps with washing buffer (0.5 % BSA in PBS) at room temperature and incubation with a goat-anti-mouse-IRDye800CW antibody in 1 % BSA (in PBS) for 15 min at 37 °C. All steps were performed either in the presence or absence of Batimastat. The total incubation time under unfixed conditions was 45 min. As a control, unfixed membrane sheets were treated the same as ‘Co-Patching’ samples but incubated in dilution buffer without primary and secondary antibodies. ‘Co-Patching’ and control samples were then fixed in 4 % PFA, as described above. Samples directly fixed after sheeting served as an additional control and were named ‘fixed’. All samples were then permeabilized, blocked and immunostained as described below using primary antibodies rabbit polyclonal anti-ADAM10 or anti-ADAM17 in combination with the secondary antibody STARRED goat anti-rabbit (see Table 6 and Table 7).

4.2.4.4 Immunostaining

Fixed membrane sheets were treated with 0.2 % (v/v) Triton X-100 (in PBS) for permeablization for 2 min, before incubation in blocking buffer (4 % BSA in PBS) for 1 h

under agitation. Samples were incubated with the primary antibody and secondary antibody for 1 h at room temperature in dilution buffer (dilutions indicated in Table 6 and Table 7). Both antibody incubation steps were followed by three washing steps for 5 min in washing buffer (0.5 % BSA in PBS). Better detection of cells or membrane sheets was achieved by incubation with Vybrant™ DiO Cell-Labeling Solution (cat#V22886; ThermoFisher Scientific) in a dilution of 1:200 or Rhodamine Phalloidin Reagent (cat#ab235138; Abcam) in a dilution of 1:1000 for 10 min and a final washing step with PBS for 5 min. The cover slips were mounted on microscopy slides with ProLong® Gold antifade mounting medium (cat# P36930, Invitrogen), sealed with colorless nail polish and stored at 4 °C until microscopy.

4.2.4.5 Epifluorescence microscopy

Fixed membrane sheets were imaged directly in PBS containing 10 % of a saturated solution of 1-(4-tri-methyl-ammonium-phenyl)-6-phenyl-1, 3, 5-hexatriene p-toluene-sulfonate (TMA-DPH; cat#T-204, Thermo Fisher Scientific, Waltham, USA) in PBS for selection of intact membranes. Epifluorescence microscopy was either performed using an Olympus IX81-ZDC fluorescence microscope (Olympus) equipped with a 60x 1.49 NA Apochromat oil immersion objective coupled to a 16-bit EMCCD camera (ImagEM C9100-13; Hamamatsu Photonics) (Figure 6). An additional 4x magnifying lens was employed, yielding a pixel size of 66.67 nm.. For Figure 29B, a Zeiss Axio Observer D1 epifluorescence microscope equipped with a Plan-Apochromat 100x/NA 1.4 oil immersion objective and a 12 bit CCD camera (Sensicam QE, PCO AG) was used, yielding a pixel size of 64.5 nm. For illumination, a 150W xenon lamp integrated into the MT20E-fluorescence illumination system (Olympus) (Figure 6) or a 75 W xenon arc lamp (N XBO 75, Zeiss) (Figure 29) were employed using the filter sets F36-500 DAPI HC for TMA-DPH, F36-525 EGFP HC for GFP and F36-503 TRITC HC (AHF Analysetechnik) for mCherry. Exposure times were 100 ms (Figure 6) or 1000 ms for all channels (Figure 29B).

4.2.4.6 STED and confocal microscopy

Confocal and stimulated emission depletion (STED) microscopy were both performed using an Olympus IX83 confocal microscope (Olympus) equipped with an UPlanSApo 100x (1.4 NA) objective (Olympus, Tokyo, Japan). The Pinhole size was adjusted to 60 µm and the pixel size to 25 nm for all experiments.

GFP and VybrantDio were excited with a pulsed 485 nm laser (Abberior Instruments, Göttingen, Germany) and recorded with a 500-520 nm filter (Abberior Instruments, Göttingen, Germany). For excitation and detection of Alexa594 and Rhodamine Phalloidin fluorescence, a pulsed 561 nm excitation laser and a 580-630 nm filter were used. Atto647N and STAR RED were excited with a 640 nm laser and detected with a 650-720 nm filter. Confocal images were recorded with time-gated detection with 0.78 ns delay and 8 ns gate width.

For STED microscopy, the confocal microscope is equipped with a 4-channel easy3D super-resolution STED optics module (Abberior Instruments, Göttingen Germany). A pulsed 775 nm STED laser (Abberior Instruments) was used for depletion of Alexa594, STAR RED and Atto647N. STED micrographs were recorded with 6 line accumulations and time-gated detection with 0.75 ns delay and 8 ns gate width.

4.2.4.7 Fluorescence recovery after photobleaching (FRAP)

For measurement of protein mobility within the plasma membrane, FRAP microscopy was employed. HepG2 cells were transfected to express APP or APP-mutants fused to a C-terminal GFP-tag and grown for 21 h in the absence or presence of 10 µM Batimastat. Live cells were studied in Ringer solution containing 10 µM Batimastat or the corresponding volume of DMSO as control for a maximum of 40 min per coverslip using a Zeiss LSM 880 with Airyscan confocal microscope (see Table 1) with a LD LCI Plan-Apochromat 40x (1.2) water immersion objective. The microscope was also equipped with a laser diode 405 nm and Argon Multiline laser (458 nm, 488 nm, 514 nm) (Carl Zeiss, Jena, Germany). The microscope was controlled by the ZEN 2.3SP 1 software (Carl Zeiss, Jena, Germany). GFP was excited with the 488 nm Argon multiline laser at a laser power of 0.8 %, while detection of emGFP was performed at 450-550 nm. The focal plane was adjusted to the plane of the basal plasma membrane and the scanning field was set to 161 x 161 pixels with a pixel size of 400 nm and images were taken at 2.5 Hz with an acquisition time of 60 s. After the first three frames, a circular region of interest (ROI) within the cell measuring 40 x 40 pixels (ROI_{bleach}) was photobleached at 100 % laser power of the 405 nm, 458 and 488 nm lasers with a total bleaching time of 800 ms. Recovery of fluorescence was monitored for an additional 147 frames post-bleach.

4.2.5 Image analysis

Micrographs and Western blot images were analysed with the ImageJ software (see Table 8). For analysis, rectangular regions of interest (ROIs) were used, if not stated otherwise. ROIs were placed in one reference channel and propagated to the other respective channel(s), if needed.

Average fluorescence intensity: One ROI was placed onto a membrane sheet and one was placed next to it for determination of the background intensity. The mean signal intensity within the first ROI was quantified and corrected for background.

Relative standard deviation of the mean (rSDM): The rSDM was already used previously (Zilly *et al,* 2011; Schreiber *et al,* 2012) as a measure for the degree of clustering and was used in this study to determine the degree of patching/cross-linking. To this end, the standard deviation of the mean pixel intensity in a ROI was determined by ImageJ and related to the average fluorescence intensity.

Pearson correlation coefficient (PCC): An overlay of images from two channels was created using the 'merge channels' option in ImageJ. ROIs were placed in one reference channel and propagated to the other respective channel and the PCC was calculated using a custom ImageJ macro (written by Dr. Jan-Gero Schloetel).

Maxima analysis: For analysis of spots (maxima density, size, shortest distance and intensity), a custom ImageJ macro (written by Dr. Jan-Gero Schloetel) was used. Before analysis, pixel noise was reduced by smoothing the images with a Gaussian blur ($\sigma = 1$) and thereby improving maxima identification. A threshold of 1 a. u. mean signal intensity was chosen to minimize the chance of including maxima resulting from background signal. Maxima were recognized and counted within each ROI based on the 'Find Maxima' ImageJ function.

For calculation of the maxima density, the number of maxima identified was normalized to the analyzed ROI area. For the maxima average intensity, the macro places circular ROIs with a radius of 2 pixels centered to the spot position and determines the mean signal intensity within this ROI. The mean intensities of all maxima within a ROI were corrected for the average intensity of the background ROI (see above). The maxima size was obtained by line scan analysis. For each maximum, vertical and a horizontal 15 x 3 pixel

line scans were centrally placed at the maxima location. Both line scans were fitted to a Gaussian function obtaining the intensity profile, and the vertical or horizontal fit was chosen, depending on the best fit quality. The full width at half maximum (FWHM) of the Gaussian fit was taken as the maxima size. Maxima where excluded when the fit quality of R^2 was lower than 0.8 and the peak was non-centered (not in the middle third of the linescan). The spot sizes of all maxima within a ROI were averaged for each membrane sheet.

FRAP analysis: For analysis, three circular ROIs with a diameter of 40 pixels were placed inside the scanning field: one corresponding to the photobleached region (ROI_{bleach}), one next to the cell for determining the background fluorescence intensity (ROI_{BG}) and one in an unbleached region of the cell ($ROI_{control}$). The average intensities of ROI_{bleach} and $ROI_{control}$ were corrected for the mean signal intensities of ROI_{BG}. The pre-bleach intensity of $ROI_{control}$ was averaged for all 3 frames and compared to the averaged intensity in the last three frames to identify out-of-focus drift or cell movement during the measurement. If the difference in intensity was higher than 15 %, the cell was excluded from further analysis. The post-bleach intensities in ROI_{bleach} were normalized to the averaged pre-bleach intensity and plotted against the time. For each experimental day and condition, plotted values were averaged and fitted to a hyperbolic function with a fixed offset (y_0) to obtain the half-time of recovery ($t_{1/2}$) and the maximal recovery ($\mathrm{Rec}_{\max}$).

$$y(t) = y_0 + \frac{Rec_{max} * t}{t_{1/2} + t}$$

Western blot analysis: In Western blot images, freehand ROIs were drawn around the bands of interest and the band intensity was determined by measurement of the integrated fluorescence density of the ROI. The same ROI was moved to a region within the same lane with no visible band and the measured background integrated density was substracted from the respective band intensity. For quantification of sAPPα, the sAPPα band integrated density in one condition was divided by the integrated density of full-length APP (sum of mature and immature APP) to normalize for different transfection efficiencies or expression levels of APP-mutants. Normalized sAPPα values were then related to the normalized sAPPα signal of APP wild-type as control. For determination of the cellular level of full-length APP under different conditions, the integrated fluorescence density of full-length

APP was divided by the integrated fluorescence density of Actin to normalize for the amount of cells loaded onto the gel. Values were related to the control condition, which was set to 100 %.

5 Results

5.1 Organisation of APP, ADAM10 and ADAM17 in the plasma membrane

In the cleavage reaction, APP takes the role of the substrate and secretases act as proteases. APP has been demonstrated to organize in clusters in the plasma membrane (Schneider *et al,* 2008; Schreiber *et al,* 2012) and those nanodomains have already been characterized in several cell lines (de Coninck *et al,* 2018; Schneider *et al,* 2008). For the α-secretases an organisation in nanodomains, possibly important for their sheddase function, has only been postulated (Reiss & Bhakdi, 2017). In this study, the substrate and protease organisation in the plasma membrane were examined to better understand the mechanisms regulating APP cleavage.

5.1.1 Impact of familial mutations in the Aβ region on APP clustering

The organisation of APP into clusters is regulated by the first 5 amino acids of the Aβ region (Schreiber *et al,* 2012). Moreover, clustering is a prerequisite for APP endocytosis (Schreiber *et al,* 2012; Schneider *et al,* 2008) and consequently amyloidogenic processing. Several pathological mutations in the APP gene are located within or close to this N-terminal Aβ region and confer increased Aβ production (Chen *et al,* 2012; Di Fede *et al,* 2009; Zhou *et al,* 2011). The only known protective mutation at position 2 of the Aβ region results in reduced β- and improved α-cleavage (Jonsson *et al,* 2012). We followed the hypothesis that the different propensity for Aβ generation is caused by a change in the plasmalemmal clustering degree of these APP mutants which might regulate the accessibility of the substrate for α-secretase cleavage.

The initial aim of this study was to elucidate, if the pathological mutants APP-A2V and APP-E11K as well as the protective mutant APP-A2T display different clustering behaviours which might explain their contrasting propensity for amyloidogenic processing. For this purpose, membrane sheets from HepG2 cells expressing APP, APP-A2V, APP-E11K or APP-A2T were generated. The preparation of membrane sheets (see section 4.2.4.1) is useful to study the organisation of proteins in the plasma membrane as this method allows imaging of the plasma membrane with a high signal-to-noise ratio and without background signals arising from cytosolic structures close to the basal membrane. Membrane sheets were imaged by Epifluorescence microscopy and the APP fluorescence distribution was analyzed by determining its relative standard deviation of the mean (rSDM). This parameter describes the degree of signal clustering and increases upon aggregation (Zilly *et al,* 2011).

As can be seen in Figure 6A, APP and its mutants displayed a similar distribution pattern upon overexpression with the majority of APP fluorescence concentrated into punctate clusters. When looking at the clustering degree, no significant change in the rSDM value between wild-type and the pathological APP-mutants was observed (Figure 6B). Regarding the protective A2T mutant, only a small non-significant decline in the rSDM could be observed. Therefore, a reduced propensity to form oligomers reported for the Aβ peptide carrying the protective A2T mutation (Benilova *et al,* 2014) does not seem to be reflected in the full-length APP molecule. Likewise, the examined pathological mutations do not seem to be more prone to aggregation.

However, the protein expression level represented by the average GFP intensity differed between APP and its mutants. The mutants displayed a higher expression compared to wild-type APP (Figure 6C). To evaluate if differences in the clustering degree are obscured by different expression levels, the rSDM of individual membrane sheets was plotted against the average intensity (Figure 6D). Indeed, the rSDM decreased with increasing fluorescence intensity in APP wild-type as well as in the mutants. The majority of the analyzed sheets from the APP-mutants had an average intensity in the same range as the wild-type with only a minority of membrane sheets from highly expressing cells (Figure 6D). Comparing values from a similar expression level suggests that the slightly higher average expression level of the mutants do not conceal differences in the clustering degree of the mutants.

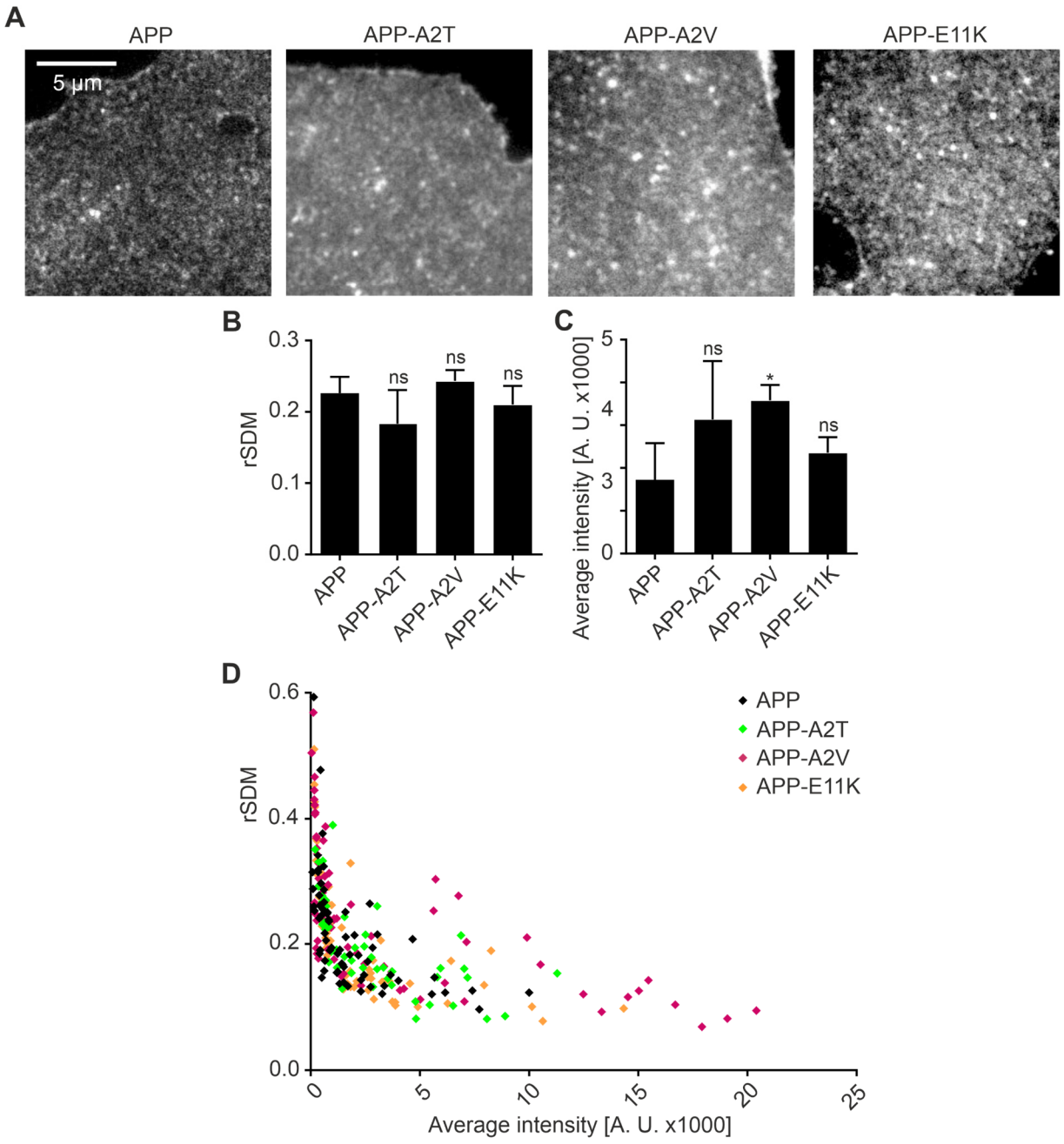

Figure 6. Familial mutants of APP display the same degree of clustering as wild-type (A) Epifluorescence micrographs of membrane sheets from HepG2 cells grown for 21 h, expressing APP, APP-A2T, APP-A2V and APP-E11K fused to a C-terminal GFP-tag. Images are displayed at arbitrary intensity scalings using a linear lookup table for the GFP fluorescence intensity. (B) Relative standard deviation of the mean (rSDM) and (C) average intensity of APP and APP mutants. (D) The rSDM was plotted against the average GFP intensity. Single Values are given (n = 47 - 73 membrane sheets per condition collected from 3 - 5 experiments). (B, C) Values are given as means ± SD (n = 3 - 5 experiments per cell line; 14 - 29 membrane sheets per experiment and condition). Unpaired Student's t-tests compare APP mutants to APP (****p <0.0001; ***p <0.001; **p <0.01; *p <0.05; ns (not significant) p >0.05).

To investigate if the plasmalemmal dynamics are changed by the point mutations, the mobility of APP and its mutants was analyzed. Because mobility is reciprocally related to clustering (Zilly *et al,* 2011; Schreiber *et al,* 2012; He & Marguet, 2011), the analysis also served to confirm the evaluation of the clustering degree. HepG2 cells expressing APP, APP-A2T, -A2V or -E11K fused to a GFP-tag were analyzed by fluorescence recovery after photobleaching (FRAP) microscopy. This technique utilizes a confocal microscope to monitor the diffusion of a fluorophore-tagged protein in living cells over time. In Figure 7A the experimental procedure is depicted. A circular ROI was placed on the basal membrane of the cell, followed by three frames measuring the baseline fluorescence intensity (pre-bleach). GFP fluorescence was bleached within the ROI and the fluorescence was recorded every 400 ms for 1 min. Lateral diffusion of GFP-tagged proteins into the ROI, exchanging the photobleached ones, results in an increase of fluorescence in the bleached region. The recovery of fluorescence was followed over time (see Figure 7B). The recovery traces from each condition and experiment were averaged and fitted with a hyperbolic function to determine the half-time of recovery (see Figure 7C). The recovery half-time is a measure for the mobility of a protein and thus is a suitable parameter for quantitative comparison of the dynamics of wild-type APP and its mutants.

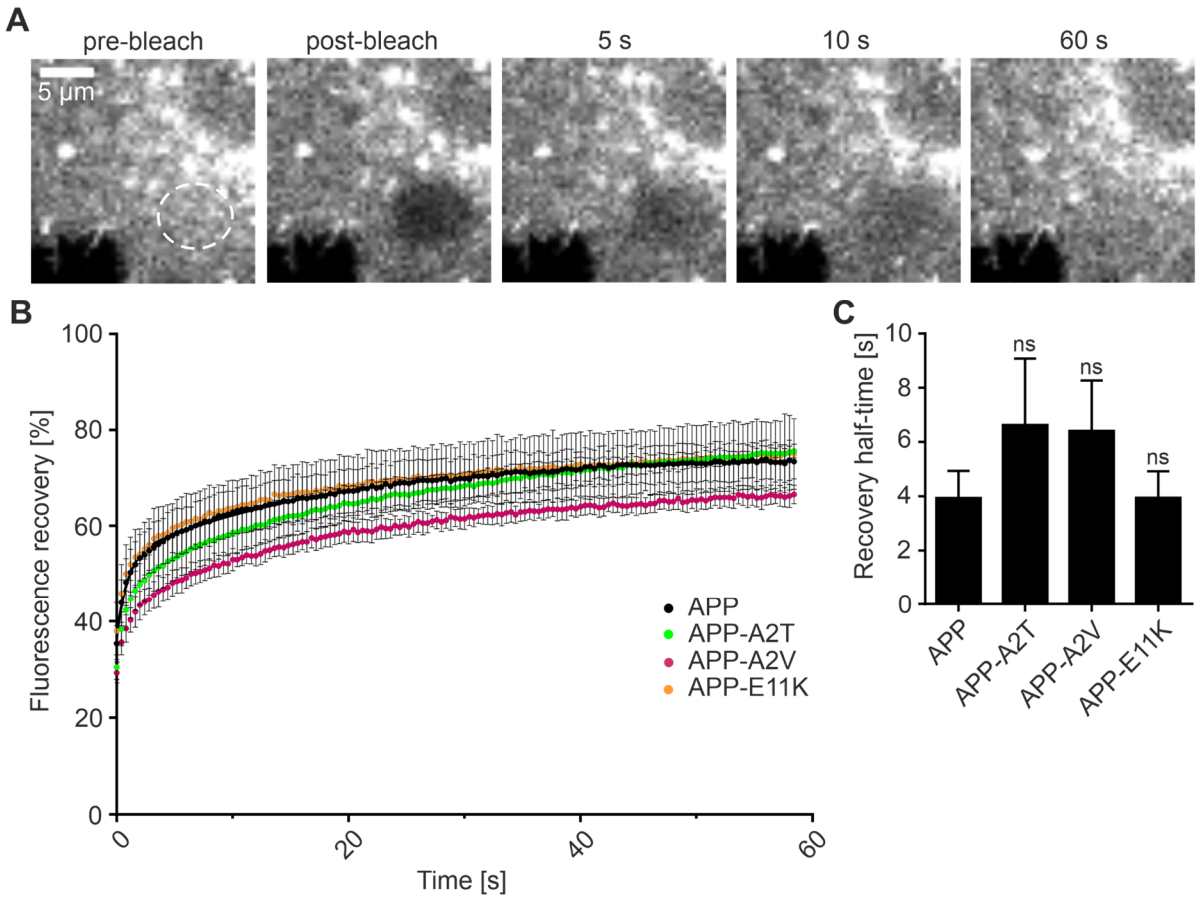

Figure 7. Mobility of APP mutants
HepG2 cells were transfected to express APP, APP-A2T, APP-A2V and APP-E11K fused with a C-terminal GFP-tag and grown for 21 h. (A) Confocal micrographs of representative FRAP experiments from HepG2 cells expressing APP-GFP. Fluorescence bleaching was performed in a circular ROI (dashed circle) at the basal plasma membrane. Shown are the frames preceding bleaching (pre-bleach; first column), directly after bleaching (post-bleach; second column) and 5 s (third column), 10 s (fourth column) and 60 s (fifth column) after bleaching. (B) The recovering GFP fluorescence is related to the pre-bleach value and plotted over time. From the averaged normalized recovery traces of each experimental day (C) the recovery half-time was calculated. (B and C) Values are given as means ± SD (n = 3 - 6 experiments, 10 – 15 membrane sheets per experiment and condition). (C) Unpaired Student's t-tests compare APP mutants to APP (****p <0.0001; ***p <0.001; **p <0.01; *p <0.05; ns (not significant) p >0.05).

In the graph depicting the relative fluorescence recovery over time (Figure 7B), fluoresecence was bleached to ~30-35 % of the pre-bleach value. A fast recovery of roughly ~25 % of GFP fluorescence is observed for wild-type APP as well as for the mutants in the first 5 seconds after bleaching. In the remaining time of the measurement a slow increase indicates a much slower continuing recovery (Figure 7B). These differences in the velocity of the recovery may be due to different APP species. The faster recovery might be caused by APP monomers, small oligomers or cleavage products of APP which should diffuse fast. The slower APP species might be

molecules exchanged in the APP clusters, followed by diffusion. When comparing the overall fluorescence recovery (slow and fast component) of APP and the mutants, it is noticeable that APP-E11K displays a recovery very similar to wild-type APP while the fluorescence recovery of APP-A2T is slightly lower in the first 25 seconds but reaches the same maximal recovery as wild-type APP at the end of the measurement. APP-A2V displayed a slower recovery and also a lower maximal recovery (Figure 7B). These observations are summarized in the half-times of recovery with values of ~4 s for APP wild-type and APP-E11K, while recovery half-times of APP-A2T and -A2V are slightly increased to ~6.6 s and ~6.4 s, respectively (see Figure 7C).

In conclusion, the propensity to form oligomers does not differ from wild-type in the examined protective or pathological mutants of full-length APP and subsequently the plasmalemmal dynamics are also not changed.

5.1.2 Plasma membrane distribution of APP

Next, we wanted to examine the plasmalemmal organisation of APP in more detail. Because the familial APP mutants displayed no difference in the degree of clustering and mobility (Figure 6 and Figure 7), cluster analysis focused only on the organisation of APP wild-type.

For the characterization of nanodomains with a typical size of membrane protein clusters between 50-200 nm, conventional confocal or epifluorescence microscopy are not suitable due to their diffraction-limited resolution. For this reason, STED microscopy was employed, which consists of a confocal microscope and uses a circular STED laser in addition to an excitation laser. After excitation, fluorophores are depleted by the STED laser with only fluorophores in the center of the ring remaining excited. In this way, the spot size is decreased from which fluorescence is collected and resolutions below the diffraction limit are possible.

The difference between classic confocal and STED imaging is illustrated on membrane sheets from HepG2 cells expressing APP-GFP (shown in Figure 8). A comparison of confocal and STED imaging (Figure 8) demonstrates that merged structures appearing to be continuous in confocal images are resolved into smaller entities with STED microscopy and are in fact many closely associated signal maxima.

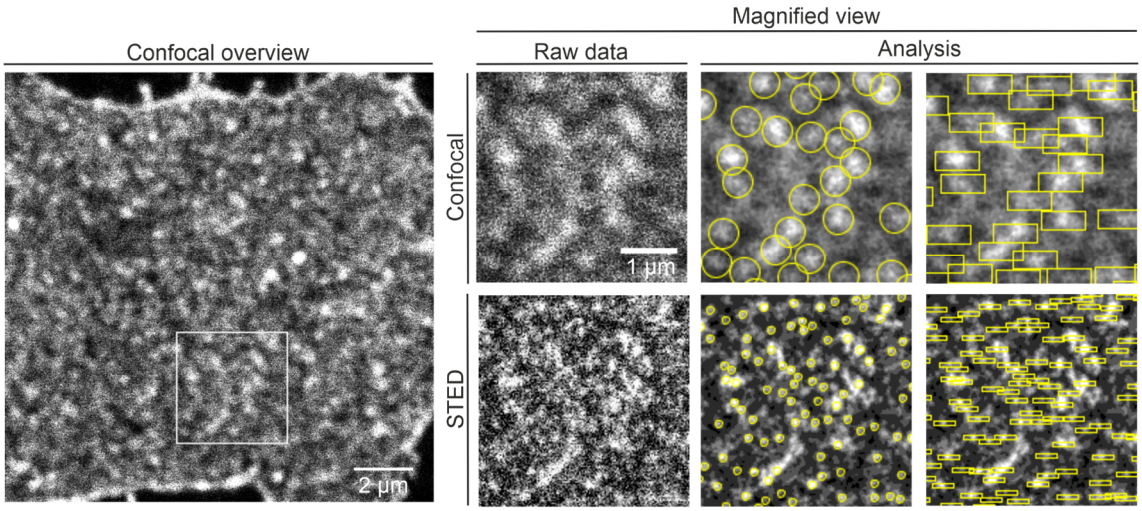

Figure 8. Increase in resolution by STED microscopy and analysis of maxima
Overview of a membrane sheet from HepG2 cells expressing APP-GFP in the confocal channel. GFP fluorescence is visualized by an Atto647N-coupled nanobody. The ROI (white square) is displayed in magnified views in the confocal and STED channel. Magnified views in the left column show raw data, the middle and right column illustrate smoothed images used for maxima detection. Maxima detected by a customized ImageJ macro are delineated using a circle with a pre-set radius (middle column). The total intensity within this circle is measured and defined as maxima intensity. One horizontal and one vertical line scan is drawn around the weighted center of the maxima (horizontal line scan shown in right column) and used for calculation of the FWHM, defined as maxima size.

From the obtained high resolution images, maxima are detected and parameters such as maxima intensity, density and size are extracted using a customized ImageJ macro (described in section 4.2.5). The maxima analysis is illustrated in Figure 8. For determination of the maxima intensity, detected maxima are delineated with a circle of a pre-defined size and the total intensity within this circle is measured. Maxima sizes are determined by centrally placing a line scan on the detected maxima and applying a Gaussian fit to its intensity profile. Maxima were only included in the analysis when the Gaussian fit of an analysed maximum was above a R^2 value of 0.8 and the Gaussian peak was positioned in the central third of the line scan. In this way, poorly separated, merged maxima which could falsify the size determination are excluded. The full width at half maximum (FWHM) of the chosen Gaussian fit was defined as the maxima size.

This method was used to study the organisation of APP in the plasma membrane.The cluster organisation has already been characterized in neuronal SH-SY5Y cells for endogenous APP (de Coninck *et al,* 2018) or neuronal N2a cells for overexpressed APP (Schneider *et al,* 2008). In later experiments of this project examining interaction of APP and α-secretases, overexpression of APP-GFP was necessary (see section 5.3.2). Therefore, cluster formation of overexpressed as well as endogenous APP are examined and the effect of different protein levels on APP cluster organisation is investigated. Additionally, cluster organisation in neuronal as well

as non-neuronal cell lines is compared. For this purpose, neuronal SH-SY5Y cells already expressing endogenous APP were used. Human hepatocyte HepG2 cells were selected as a non-neuronal cell-line due to their low expression of APP to study characteristics of overexpressed APP without high endogenous background expression (in Western blots of HepG2 lysates no endogenous APP was detectable, see Figure 12).

For the visualization of APP clusters, two types of APP staining were utilized. For the visualization of APP-GFP, membrane sheets of HepG2 cells as well as SH-SY5Y cells transfected to express APP-GFP were stained with a Atto647N-congutated nanobody raised against GFP. For the visualization of endogenous APP clusters, membrane sheets of SH-SY5Y cells grown without subsequent transfection were stained with an anti-APP primary antibody and a secondary STARRED-conjugated antibody. Due to these different staining techniques, the intensity counts of visualized endogenous APP are not comparable to fluorescence intensities determined for APP-GFP.

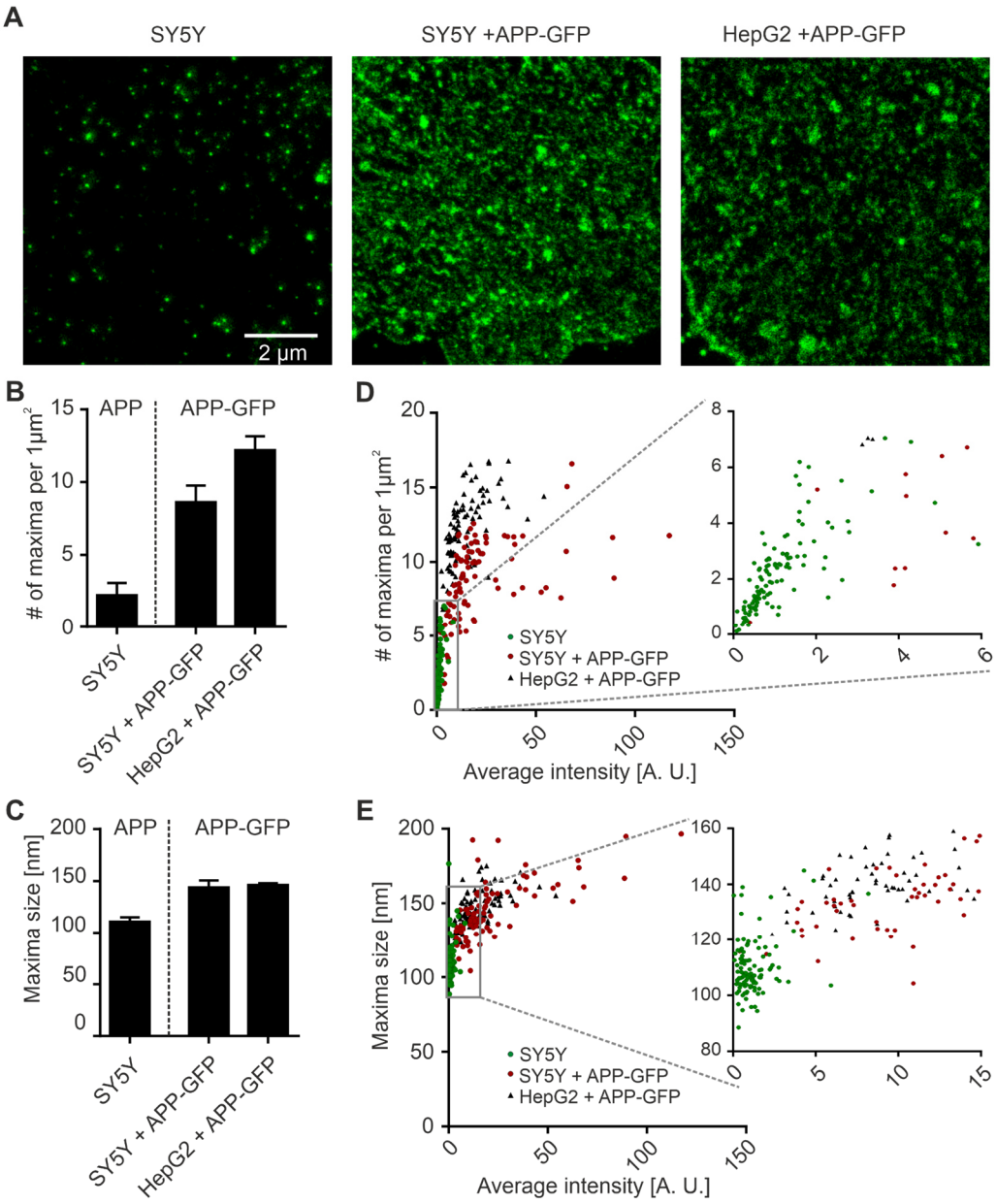

Figure 9. Characteristics of endogenous and overexpressed APP clusters in the plasma membrane

(A) STED micrographs of membrane sheets from SH-SY5Y cells fixed 21 h after growth and immunostained for endogenous APP (SY5Y; left) or from SH-SY5Y (SY5Y + APP-GFP; middle) or HepG2 cells expressing APP-GFP (HepG2 + APP-GFP; right). For STED microscopy, APP-GFP is visualized with an Atto647N-conjugated nanobody raised against GFP and APP is labelled with a STARRED-conjugated antibody. Images are displayed at arbitrary scaling. The maxima (B) density and (C) size were quantified. Maxima (D) density and (E) size of individual membrane sheets were plotted against the average Atto647N or STARRED intensity (magnified views help to distinguish the maxima sizes and densities at lower average intensities). (B-C) Values are given as means ± SD (n = 3 - 4 experiments per cell line; 10 - 40 membrane sheets per experiment and condition; values were first averaged per membrane sheet and then averaged per experimental day). (D, E) Single values are given (n = 89 - 115 membrane sheets collected from 3 - 4 experiments).

When looking at the fluorescence distribution of endogenous APP in SH-SY5Y cells, a concentration of the APP fluorescence signal into individual punctate structures is observed (Figure 9A). In the plasma membrane, a density of 2.2 APP maxima per μm^2 was determined (Figure 9B). Upon overexpression of APP-GFP the number of clusters is higher in HepG2 cells with 12.2 maxima per μm^2 than in SH-SY5Y cells with 8.6 maxima per μm^2 (Figure 9B). Average maxima sizes are 110 nm for endogenous APP clusters. For overexpressed APP-GFP cluster sizes of 143 - 146 nm were determined (Figure 9C). The different sizes of the antibody or nanobody used for visualization of APP and APP-GFP, respectively, may also influence the determined maxima sizes. Additionally, an increase of the maxima size with overexpression could also be emphasized by the addition of the ~ 27 kDa big GFP-tag which increases the bulkiness of the molecule and may therefore also influence the cluster size. The high maxima size upon overexpression might also indicate that the number of APP molecules within these clusters rises upon elevation of the protein level.

To verify if the protein level indeed has an influence on the maxima characteristics, maxima density and maxima size were plotted against the average staining intensity of APP as well as APP-GFP (a measure for the plasmalemmal APP concentration), respectively. Both parameters increased with rising APP levels (Figure 9D and E). This effect was observed for endogenous APP as well as for overexpressed APP-GFP (Figure 9D and E) and confirms that the protein level influences maxima density as well as size.

5.1.3 Plasma membrane distribution of ADAM10 and ADAM17

For ADAM10 and ADAM17 cluster formation has only been postulated, to date (Reiss & Bhakdi, 2017). As the organisation of the secretases in the plasma membrane might also give insights into their interaction with the substrate APP, it is characterized as well in this study.

For this purpose, HepG2 as well as SH-SY5Y cells were grown and 21 h after seeding membrane sheets were generated, followed by fixation, permeabilisation and staining for endogenous ADAM10 and ADAM17 with a primary anti-ADAM10 or anti-ADAM17 antibody and secondary Alexa594-conjugated antibody.

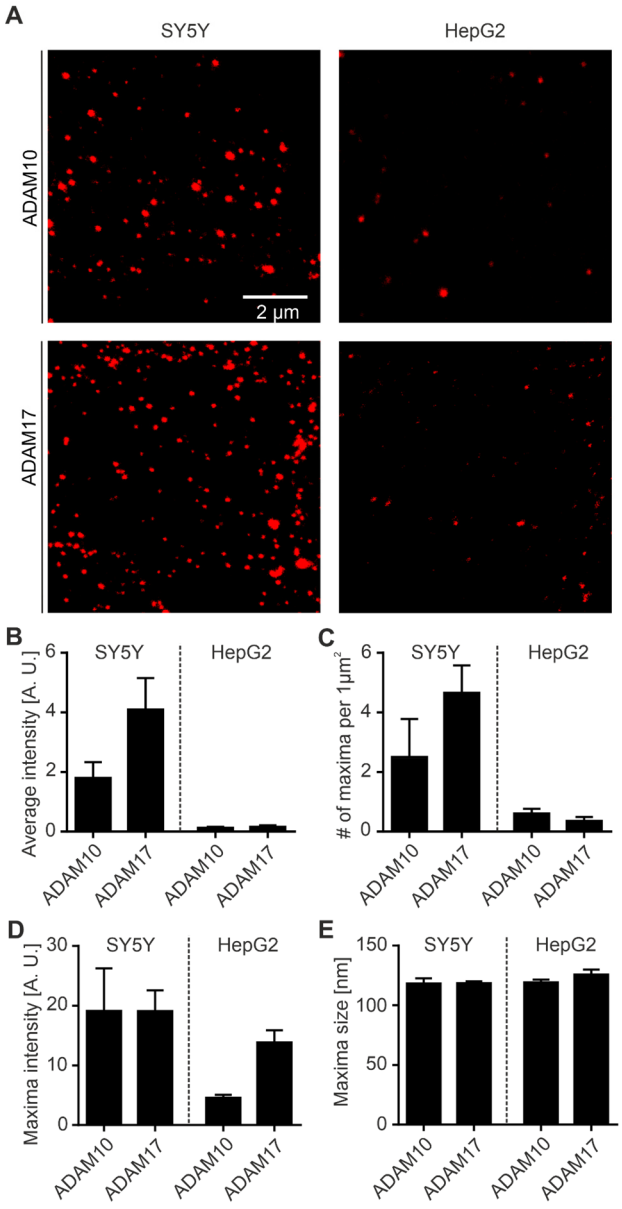

Figure 10. Characteristics of endogenous ADAM10 and ADAM17 clusters in the plasma membrane
(A) STED micrographs of membrane sheets from SH-SY5Y (SY5Y; left) or HepG2 cells (right) fixed 21 h after growth and immunostained for endogenous ADAM10 (upper panels) or ADAM17 (lower panels) Images are displayed at arbitrary scaling. On STED micrographs, the (B) average intensity, maxima (C) density, (D) intensity and (E) size of ADAM10 and ADAM17 were quantified. Values are given as means ± SD (n = 3 - 4 experiments per cell line; 10 - 20 membrane sheets per experiment and condition; values were first averaged per membrane sheet and then averaged per experimental day).

As shown in Figure 10A, the majority of ADAM10 and ADAM17 fluorescence was concentrated in segregated structures. The signal intensity was too high for single molecules (Figure 10B). Therefore, both proteins seem to be indeed organized in plasmalemmal clusters. The

abundances of both secretases were manyfold higher in SH-SY5Y than in HepG2 cells (Figure 10B, C), pointing towards strongly different expression levels in different cellular systems. Additionally, there was a difference in maxima frequency, as ADAM17 maxima density was twice as high as the number of ADAM10 maxima in SH-SY5Y cells, whereas in HepG2 cells it was the other way around (Figure 10C). The different expression levels in the cell lines also had an effect on the cluster intensity, as the average maxima intensity of the secretases was higher in SH-SY5Y than in HepG2 cells (Figure 10D). In contrast to that, a higher expression level in SH-SY5Y cells did not result in an increased cluster size. In fact, the average cluster size of ADAM10 and ADAM17 was ~ 120-125 nm in SH-SY5Y and HepG2 cells (Figure 10E).

This raised the question if the maxima sizes are defined or if they cover a wide size range in the different cell lines. To answer these questions, all individual maxima sizes were pooled and the size distribution for each protein was plotted into histograms. Both, ADAM10 (in black) and ADAM17 (in grey) displayed a similar cluster size distribution in the respective cellular system (Figure 11). The cluster sizes of ADAM10 and ADAM17 were widely distributed with most of the clusters displaying a size of 90 – 130 nm in SH-SY5Y cells (Figure 11A). The distribution was shifted towards higher maxima sizes of 110 – 160 nm in HepG2 cells (Figure 11B).

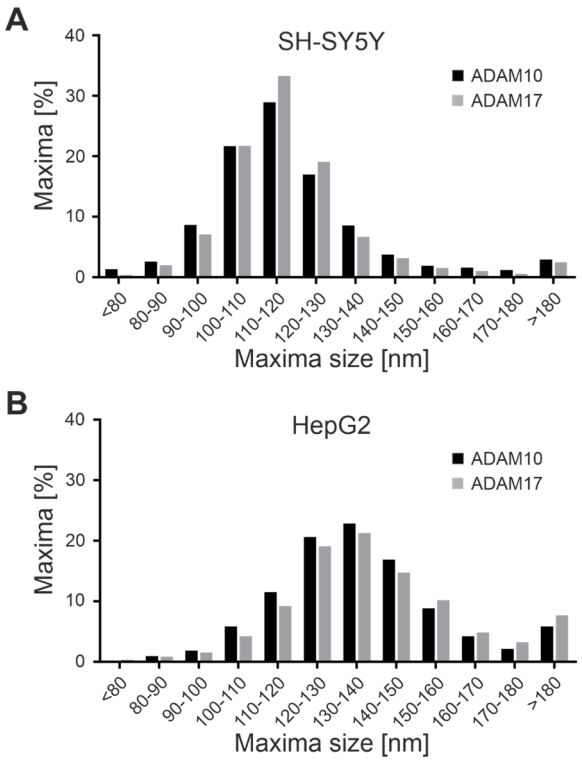

Figure 11. Cluster size distribution of ADAM10 and ADAM17
Based on Figure 10A, the size distribution of all analysed ADAM10 (black) and ADAM17 (grey) maxima was plotted in frequency distribution histograms. Frequency distribution of maxima sizes in membrane sheets generated from (A) SH-SY5Y or (B) HepG2 cells. Bin size 10 nm (for clarity sizes <80 nm and >180 nm were summarized in one bin each). Single values of cluster sizes were pooled from 45 – 61 membrane sheets collected from 3 - 4 experiments.

5.2 Effect of α-processing on APP/α-secretase organisation in the plasma membrane

APP processing by secretases has been found to be influenced by several agents. For example, phorbol esters, interleukin 1, cholinergic agonists and cholesterol depletion increased α-secretase cleavage (Buxbaum *et al,* 1992; Buxbaum *et al,* 1998; Kojro *et al,* 2001). Iron chelators or metalloproteinase inhibitors had the opposite effect (Bodovitz *et al,* 1995; Parvathy *et al,* 1998). However, little is known about how α-secretase activity affects APP concentration in the plasma membrane, and consequently cluster organisation and characteristics. Therefore, the effect of α-secretase inhibition on APP/α-secretase cluster density, size and intensity was investigated.

5.2.1 Impact of α-secretase inhibition on APP organisation

First, the effect of α-secretase inhibition on the total cellular APP level was determined. HepG2 cells were transfected with APP double tagged with mCherry and GFP and incubated with the

broad α-secretase inhibitor Batimastat (Parvathy *et al,* 1998). 21 h after transfection, lysed cells were analysed by Western blot and the bands of overexpressed immature and mature APP were quantified (Figure 12). Upon inhibition of α-secretases by Batimastat (BATI), the cellular concentration of labelled APP triples (Figure 12), which is reflected in a similar increase of signal arising from GFP-labelled APP in membrane sheets (Figure 13B).

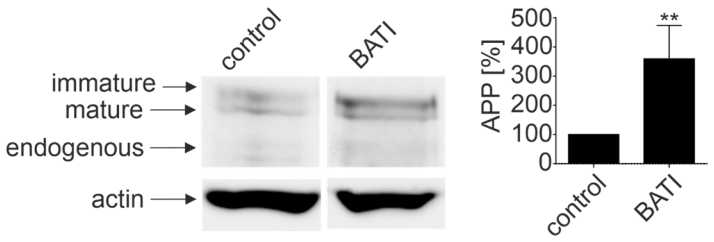

Figure 12. Elevation of the cellular APP level upon α-secretase inhibition.
Double tagged APP (mCherry-APP-GFP, see Figure 29B) is transfected into HepG2 cells, grown for 21 h without (control) or with 10 µM Batimastat (BATI). Immature and mature mCherry-APP-GFP (see arrows) is quantified by Western blot using an antibody raised against β-Amyloid amino acids 1-16. Endogenous APP was not detected (position marked with an arrow). APP band intensities are normalized to actin used as loading control, and the control value is set to 100 %. Value is given as mean ± SD (n = 4 experiments).

The impact of α-secretase inhibition on the APP cluster density, size and intensity in the plasma membrane was examined as well. In confocal micrographs of the control condition, a distribution of the APP signal is observed that can be described as rather undefined spots. Upon α-secretase inhibition, the APP signal appears more uniform (Figure 13A). Possible explanations for this effect could either be that APP clustering depends on the APP level or diffraction-limited microscopy is not capable to resolve an increase in cluster density. For clarification, superresolution STED microscopy was used and APP-GFP was visualized with an Atto647N-labelled nanobody raised aigainst GFP. When looking at STED micrographs in Figure 13A, it becomes clear that rather undefined spots in confocal images turn out to be several sharply defined maxima, which could not be resolved by confocal microscopy. Inhibition of α-cleavage and the resulting elevation of the APP level (Figure 13B) changes the cluster characteristics. Batimastat has the strongest effect on the maxima intensity that increases by ~ 107 % (Figure 13C). The number of APP clusters increases by only ~40 % (Figure 13D) and maxima size hardly increases by only ~12 % (Figure 13E). In conclusion, α-secretase inhibition strongly elevates the plasmalemmal APP. The number of maxima increases less compared to the APP level, but the

intensity of maxima more than doubles. Together, the findings suggest that the number of APP molecules per cluster scales with the expression level.

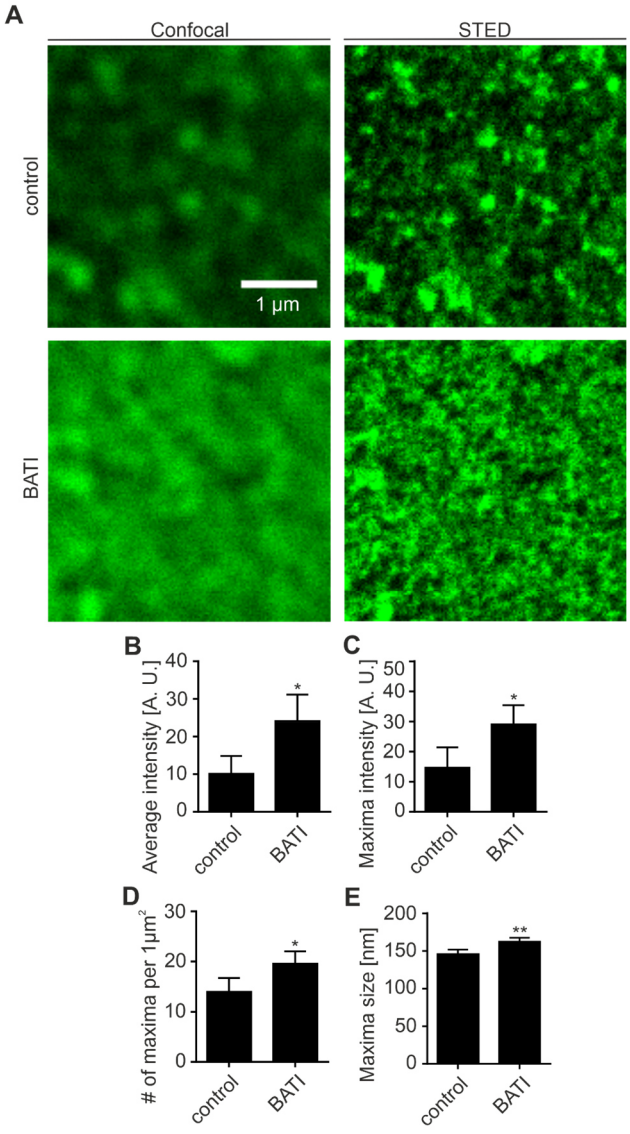

Figure 13. Change of cluster characteristics upon elevation of overexpressed APP by α-secretase inhibition in HepG2 cells
(A) Confocal (left) and STED (right) micrographs of membrane sheets from control (top) and 10 µM Batimastat treated (BATI; bottom) HepG2 cells expressing APP-GFP, grown for 21 h. Images are displayed at arbitrary scaling. For STED microscopy, APP-GFP is visualized with an Atto647N-conjugated nanobody raised against GFP. On STED micrographs, (B) the average Atto647N-intensity, the maxima (C) intensity, (D) density and (E) size were quantified. Values are given as means ± SD (n = 4 experiments; 14 - 37 membrane sheets per experiment and condition; values were first averaged per membrane sheet and then averaged per experimental day). Unpaired Student's t-tests compare control to BATI (****p <0.0001; ***p <0.001; **p <0.01; *p <0.05; ns (not significant) p >0.05). Figure and legend taken and modified from Hitschler & Lang (submitted 2021).

To rule out the possibility that the observed changes in clustering behaviour are caused by the GFP-tag, overexpression of APP or usage of a non-neuronal cell line, the experiment was performed as well with neuronal SH-SY5Y cells. Endogenous APP was visualized directly by immunostaining against the C-terminal domain of APP (Figure 14).

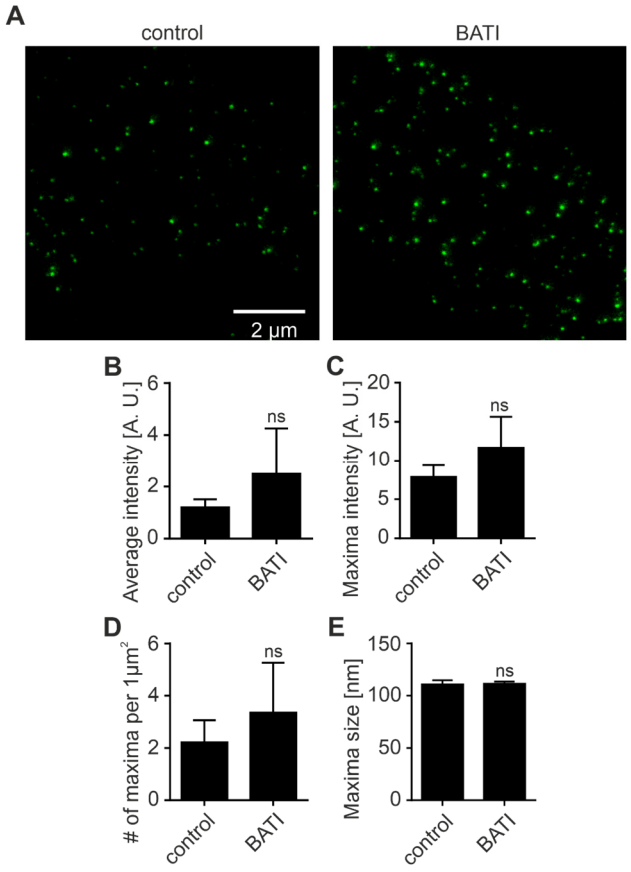

Figure 14. Change of cluster characteristics upon elevation of endogenous APP by α-secretase inhibition in SH-SY5Y cells
(A) STED micrographs of membrane sheets from SH-SY5Y cells, grown for 21 h without (control; left panel) or with 10 µM Batimastat (BATI; right panel), fixed and immunostained for APP. Images are displayed at arbitrary intensity scalings. (B) Average intensity, maxima (C) intensity, (D) density and (E) size of APP. Values are given as means ± SD (n = 4 experiments, 10 - 40 membrane sheets per experiment and condition; values were first averaged per membrane sheet and then averaged per experimental day). Unpaired Student's t-tests compare control to BATI (****p <0.0001; ***p <0.001; **p <0.01; *p <0.05; ns (not significant) p >0.05).

In membrane sheets generated from SH-SY5Y cells, a rise of the average staining intensity to ~208 % was observed upon addition of Batimastat (Figure 14B), which is in the range of the

increase displayed by overexpressed APP (Figure 13). In the presence of Batimastat, the maxima intensity (Figure 14C) as well as the density (Figure 14D) increase by ~50 % while the size of clusters does not change at all (Figure 14E). In general, upon α-secretase inhibition the changes in cluster characteristics observed for overexpressed APP-GFP in HepG2 cells are mirrored in endogenous APP clusters in SH-SY5Y cells.

As a higher clustering degree correlates with a reduced mobility of APP in the plasma membrane (Schreiber *et al,* 2012), the question arose if the higher number of molecules per cluster upon α-secretase inhibition has an effect on the mobility of APP. To this end, HepG2 cells expressing APP-GFP in the presence or absence of Batimastat were analyzed by FRAP microscopy and the maximal recovery of fluorescence as well as the half-time of recovery (Figure 15C) were determined.

In the confocal micrographs (Figure 15A) as well as in the graph depicting the relative fluorescence recovery over time (Figure 15B), a much slower fluorescence recovery is observed in HepG2 cells treated with Batimastat compared to the control condition. The control and BATI condition still reach the same maximal recovery of ~40 % and ~38 % (Figure 15C), respectively. The recovery half-time of APP-GFP more than doubles from ~4 s to ~9 s upon α-secretase inhibition (Figure 15C), indicating that the change in cluster characteristics observed in Figure 13 and Figure 14 indeed has an impact on the mobility of APP. The slower recovery of BATI treated cells might be explained by an increase of molecules per cluster associated with a slower exchange rate between clustered and freely diffusing APP molecules. In fact, α-secretase inhibition increased the intensity of APP clusters (see Figure 13 and Figure 14) and thereby likely the number of molecules within those clusters. Alternatively, upon elevation of APP the relative fraction of freely diffusing APP molecules becomes smaller. Finally, without α-secretase inhibition a large fraction of APP may be cleaved. As α-secretaste cleavage removes the APP clustering region (the first 5 amino acids of the Aβ region, (Schreiber *et al,* 2012)), the cleaved fraction would diffuse faster.

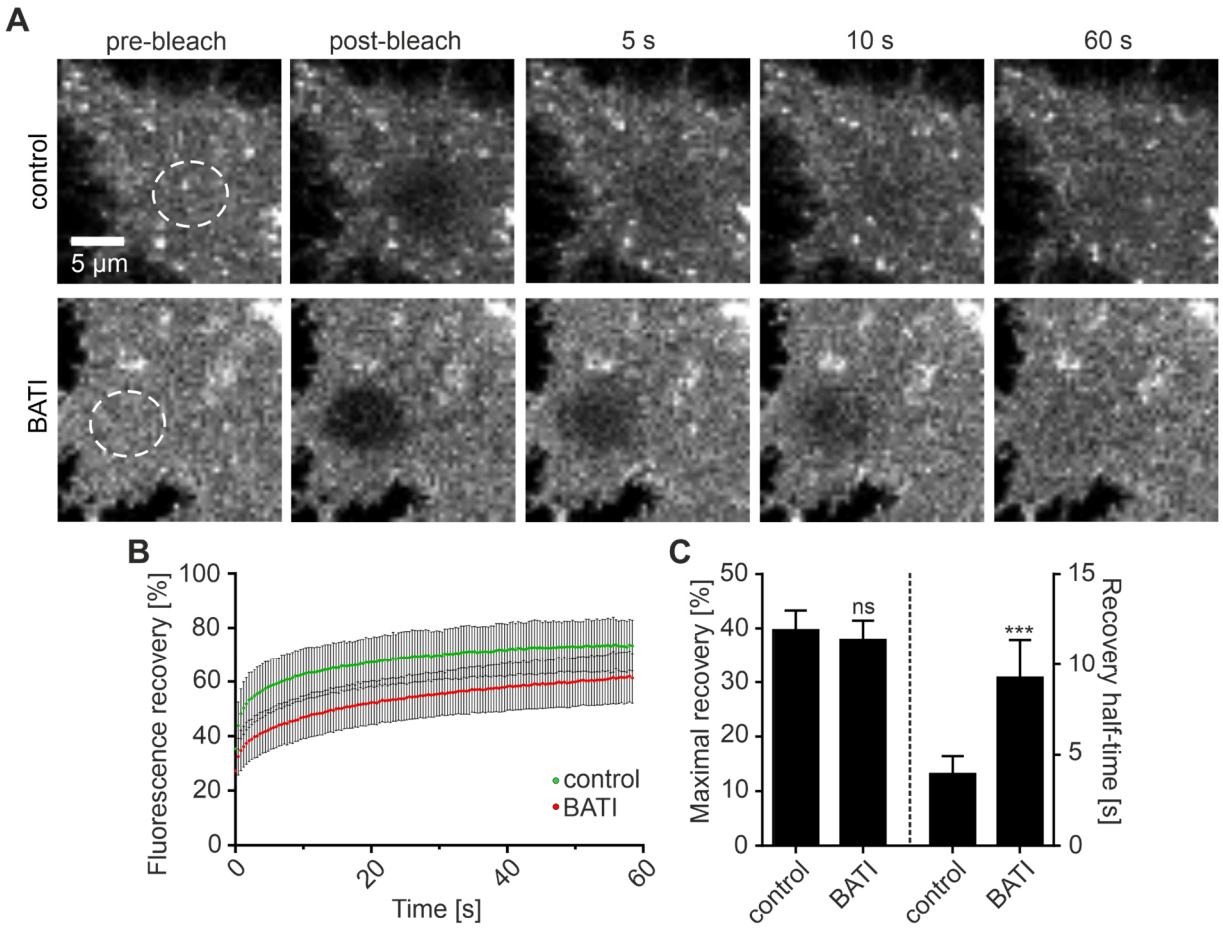

Figure 15. APP mobility is reduced upon inhibition of α-secretase cleavage
(A) Confocal micrographs of representative FRAP experiments from HepG2 cells expressing APP-GFP, grown for 21 h in the absence (control; upper panels) or presence of 10 µM Batimastat (BATI; bottom). Fluorescence bleaching was performed in a circular ROI (dashed circle) at the basal plasma membrane. Shown are the frames preceding bleaching (pre-bleach; first column), directly after bleaching (post-bleach; second column) and 5 s (third column), 10 s (fourth column) and 60 s (fifth column) after bleaching. (B) Recovering GFP fluorescence is related to the pre-bleach value and plotted over time. (C) From the averaged normalized recovery traces of each experimental day the maximal recovery and recovery half-time were calculated. (B and C) Values are given as means ± SD (n = 6 experiments, 10 membrane sheets per experiment and condition). (C) Unpaired Student's t-tests compare control to BATI (****p <0.0001; ***p <0.001; **p <0.01; *p <0.05; ns (not significant) p >0.05).

5.2.2 Impact of α-secretase inhibition on ADAM10 and ADAM17 clustering

It has already been demonstrated in section 5.2.1 that the inhibition of α-secretases elevates the cellular and plasmalemmal level of APP which affects the characteristics of APP clusters in the plasma membrane. It may be possible that the inhibition of α-secretase activity has an effect on the organisation of the secretases itself. For adressing this question, membrane sheets from SH-

SY5Y cells grown in the presence or absence of Batimastat were immunostained for ADAM10 or ADAM17 and analyzed by STED microscopy. The number, size and intensity of clusters did not change upon treatment with Batimastat (Figure 16).

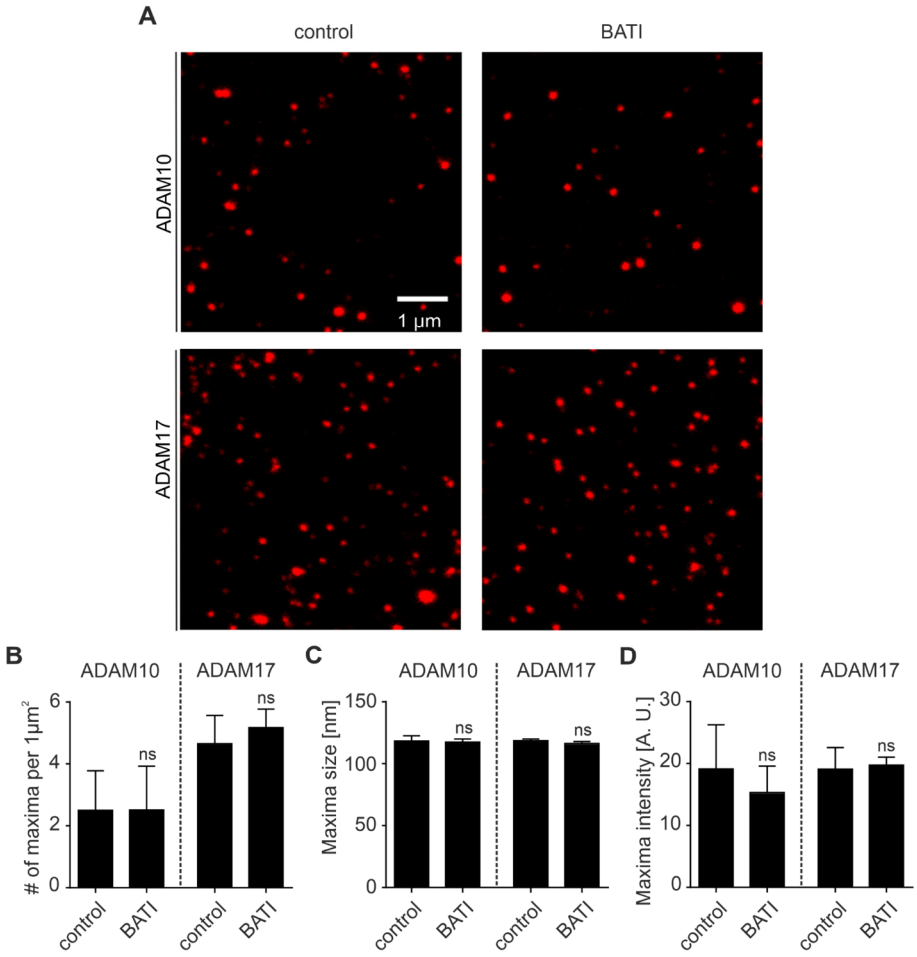

Figure 16. Characteristics of ADAM10 and ADAM17 clusters upon α-secretase inhibition
(A) STED micrographs of membrane sheets from SH-SY5Y cells grown for 21 h without (control; left panel) or with 10 µM Batimastat (BATI; right panel), fixed and immunostained for ADAM10 (upper panels) or ADAM17 (lower panels). Images are displayed at arbitrary intensity scalings. Maxima (B) density, (C) size and (D) intensity of ADAM10 and ADAM17. Values are given as means ± SD (n = 4 experiments, 10 - 20 membrane sheets per experiment and condition; values were first averaged per membrane sheet and then averaged per experimental day). Unpaired Student's t-tests compare control to BATI (****p <0.0001; ***p <0.001; **p <0.01; *p <0.05; ns (not significant) p >0.05).

5.2.3 Impact of ADAM10 inhibition on APP level in the plasma membrane

In section 5.2.1 it was demonstrated that α-secretase inhibition increases the cellular as well as the plasmalemmal APP level and that cluster characteristics change. However, it remains unclear, which α-secretase is mainly responsible for this effect.

For several members of the ADAM family, such as ADAM10, ADAM17, ADAM9 and ADAM19, α-secretase activity has been described (Buxbaum *et al,* 1998; Fahrenholz *et al,* 2000; Koike *et al,* 1999; Lammich *et al,* 1999). Overexpression, knockdown or mutation studies revealed that ADAM10 is the main secretase responsible for constitutive α-cleavage (Lammich *et al,* 1999; Kuhn *et al,* 2010; Jorissen *et al,* 2010; Jouannet *et al,* 2016; Postina *et al,* 2004; Xu *et al,* 2009). However, the extent of ADAM10-mediated processing depends on the experimental system. To elucidate to which extent ADAM10 is responsible for α-processing in the cellular systems used in this study, or in other words, if the observed elevation of APP is mainly caused by inhibition of ADAM10 cleavage activity, the broad inhibitor Batimastat (Parvathy *et al,* 1998) was compared to the ADAM10 specific inhibitor GI254023X (Ludwig *et al,* 2005).

APP-GFP was overexpressed in SH-SY5Y as well as HepG2 cells and the effect of the inhibitors on the plasmalemmal APP level was quantified by STED microscopy (Figure 17A). *In case the whole α-secretase activity would be based on ADAM10, both inhibitors would diminish α-processing and increase the APP level to the same extent (*text passage in *italic* taken and modified from Hitschler & Lang (submitted 2021)*).* In SH-SY5Y as well as HepG2 cells, the average fluorescence intensity of APP increased slightly less with GI254023X when compared to Batimastat. More precisely, the rise in average intensity by specific ADAM10 inhibition was 70 % (Figure 17B; SH-SY5Y cells) and 60 % (Figure 17C; HepG2 cells) of the increase caused by the broad inhibitor. These results confirm that ADAM10 is also the main secretase responsible for α-processing in these cellular systems.

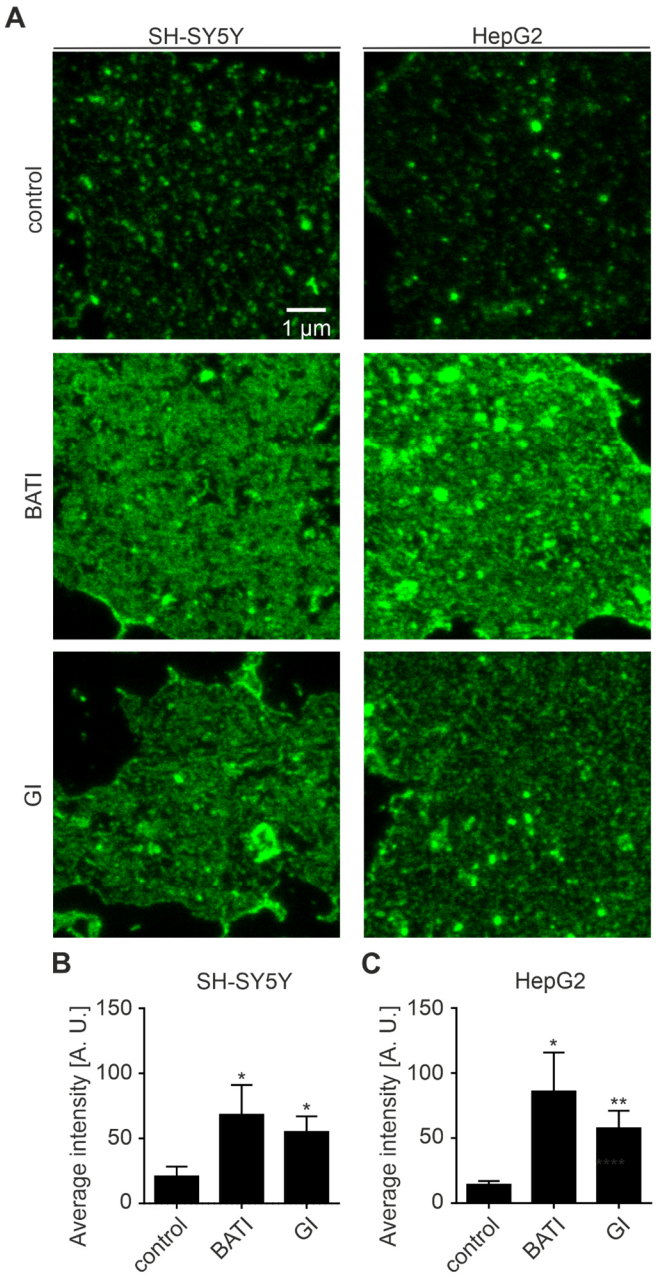

Figure 17. ADAM10 is the main α-secretase involved in APP processing
(A) STED micrographs of membrane sheets from SH-SY5Y (left) and HepG2 cells (right) expressing APP-GFP, incubated for 21 h without inhibitor (control; top), the broad inhibitor Batimastat (BATI; middle), or the ADAM10 specific inhibitor GI254023X (GI; bottom). After incubation, membrane sheets were fixed and APP-GFP was visualized with an anti-GFP nanobody coupled to Atto647N. Images are shown at arbitrary scaling. (B and C) Atto647N nanobody intensity quantified on membrane sheets from (B) SH-SY5Y and (C) HepG2 cells. Values are given as means ± SD (n = 3 experiments per cell line, 13 - 40 membrane sheets per experiment and condition). Unpaired Student's t-tests compare the control to BATI or GI (****p <0.0001; ***p <0.001; **p <0.01; *p <0.05; ns (not significant) p >0.05). Figure and legend taken and modified from Hitschler & Lang (submitted 2021).

5.3 Characterization of the association of APP with ADAM10 and ADAM17

In our cellular systems, ADAM10 is the main α-secretase responsible for α-cleavage of APP (see section 5.2.3). Yet, it remains unkown why. The predominant role of ADAM10 as α-secretase may be explained by a higher abundance, closer proximity to APP, or higher affinity to the substrate APP. To elucidate these questions, the association of APP with ADAM10 is characterized in comparison to another, less dominant α-secretase, ADAM17.

5.3.1 Lateral organisation of ADAM10/ADAM17 and APP

To address the issue, if the physiologically relevant α-secretase ADAM10 is located closer to its substrate APP than ADAM17, the association of APP clusters with ADAM10/ADAM17 was examined. ADAM17 is mainly known for regulated α-processing (Buxbaum *et al,* 1998) but constitutive α-cleavage upon overexpression was observed as well (Slack *et al,* 2001).

The lateral organisation of APP with ADAM10 and ADAM17 was examined in HepG2 cells overexpressing APP-GFP (Figure 18) and at endogenous expression levels in SH-SY5Y cells (Figure 19). Cluster analysis of the obtained STED micrographs revealed that the abundance of the secretases and APP differ in several aspects in the two cell types. *In HepG2 cells, APP maxima are present in an up to ~30–fold excess over the secretase maxima* (Figure 18A, B)*. This is the result of APP overexpression in combination with low secretase expression levels in this cell type. In contrast, secretase and APP maxima are equally abundant in SH-SY5Y cells with densities in the range of 2.2 – 4.7 maxima per µm²* (Figure 19A, B)*. That secretase maxima are up to 10-fold more abundant in SH-SY5Y than in HepG2 cells* (*compare* Figure 19B *and* Figure 18B) *points towards strongly different expression levels in different cellullar systems. Another difference is that ADAM10 maxima are 2-times more frequent than ADAM17 maxima in HepG2 cells* (Figure 18B)*, whereas in SH-SY5Y cells it is the other way around* (Figure 19B; text passage in *italic* taken and modified from Hitschler & Lang (submitted 2021)).

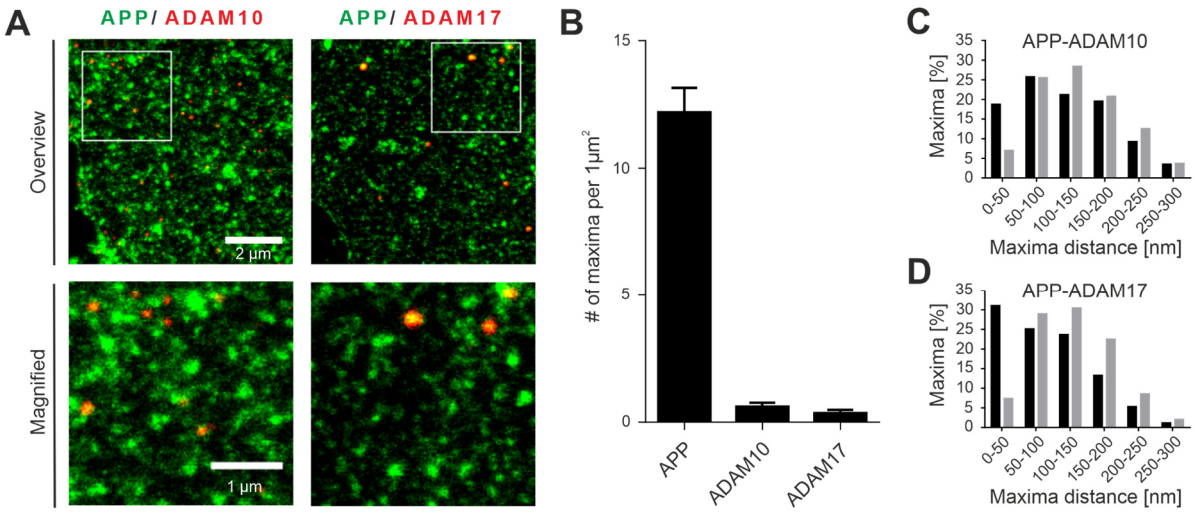

Figure 18. Lateral organisation of secretases and APP in the plasma membrane of HepG2 cells
(A) STED micrographs of membrane sheets from HepG2 cells expressing APP-GFP, grown for 21 h. Membrane sheets are double stained for secretases (red; left ADAM10; right ADAM17) and APP-GFP (green). Shown are channel overlays of overviews (top panels) and magnified views from the boxed regions (bottom panels), at arbitrary intensity scaling. (B) Maxima density of APP-GFP and the secretases. (C, D) Frequency distribution histograms of shortest inter-maxima distances between (C) ADAM10 and APP or (D) ADAM17 and APP maxima. For clarity, only distances ≤ 300 nm are included. Bars show frequencies of original (black) and flipped images (grey), used as reference for randomized distribution. (B) Values are given as means ± SD (n = 3 experiments, 10 - 20 membrane sheets per experiment and condition; values were first averaged per membrane sheet and then averaged per experimental day). (C, D) Single values of maxima distances were pooled from 43 - 61 membrane sheets collected from 3 experiments. Figure and legend taken and modified from Hitschler & Lang (submitted 2021).

To examine the lateral association between APP and ADAM10 or ADAM17, the shortest distance between APP and the secretase maxima was determined. As can be seen in Figure 18C and D, in HepG2 cells roughly half of ADAM10 and ADAM17 maxima are located at a distance of 100 nm or lower to the next APP maximum. As a control, the image of one channel within the analysed region of interest was flipped vertically and horizontally to simulate a random relationship between the channels. In the flip control, this distribution pattern is shifted towards higher distances, indicating that the close distances of ADAM maxima to APP in the original images are not due to a random distribution. *The maxima arise from clusters that have a certain physical size (e.g. APP clusters have a diameter of ~150 nm;* Figure 13E*), and the resolution of the microscope is in the range of 60 – 90 nm (Finke et al, 2020). Therefore, two intensity maxima arising from physically interacting APP and secretase species are not expected to exhibit zero distance to each other. For this study, ADAM maxima were considered closely associated with*

APP if their maxima distance was 50 nm or shorter. This is the case for ~18 % and ~31 % of the ADAM10 and ADAM17 maxima (Figure 18C and D)*, respectively. Relating the percentages of closely associated secretases to the total secretase maxima density* (Figure 18B)*, it can be concluded that 0.12 ADAM10 and 0.10 ADAM17 maxima per µm² are potentially in physical contact with APP* (text passage in *italic* taken and modified from Hitschler & Lang (submitted 2021)). In conclusion, both secretases are equally close to APP in HepG2 cells.

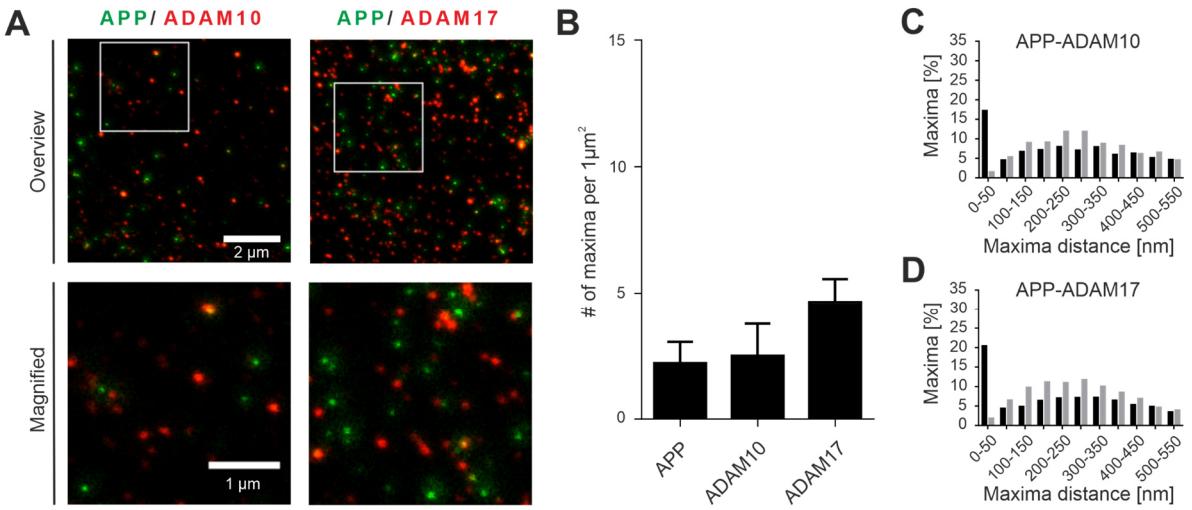

Figure 19. Lateral organisation of secretases and APP in the plasma membrane of SH-SY5Y cells
(A) STED micrographs of membrane sheets from SH-SY5Y cells grown for 21 h. Membrane sheets are double stained for secretases (red; left ADAM10; right ADAM17) and endogenous APP (green). Shown are channel overlays of overviews (top panels) and magnified views from the boxed regions (bottom panels), at arbitrary intensity scaling. (B) Maxima density of APP and the secretases. (C, D) Frequency distribution histograms of shortest inter-maxima distances between (C) ADAM10 and APP or (D) ADAM17 and APP maxima. For clarity, only distances ≤ 550 nm are included. Bars show frequencies of original (black) and flipped images (grey), used as reference for randomized distribution. (B) Values are given as means ± SD (n = 4 experiments, 10 - 20 membrane sheets per experiment and condition; values were first averaged per membrane sheet and then averaged per experimental day). (C, D) Single values of maxima distances were pooled from 43 - 61 membrane sheets collected from 4 experiments. Figure and legend taken and modified from Hitschler & Lang (submitted 2021).

In SH-SY5Y cells, the fraction of closely associated secretase maxima was in the same range as in HepG2 cells with a proportion of ~17 % and ~20 % of the ADAM10 and ADAM17 maxima (Figure 19C and D). *Relating these percentages to the total secretase maxima per µm²* (Figure 19B), *0.44 ADAM10 and 1.1 ADAM17 maxima per µm² in close proximity to APP were determined.*

In conclusion, the dominant role of ADAM10 in α-processing cannot be explained by a closer lateral organisation between ADAM10 and APP. The results obtained in SH-SY5Y cells particularly speak against this idea. *Here, although 70 % of processing is mediated by ADAM10* (Figure 17B)*, the maxima distance analysis revealed that ADAM10 associates with APP actually less frequently than ADAM17. The same is true for the abundance of the secretases. Even when ADAM17 maxima are two-fold more abundant than ADAM10 maxima in SH-SY5Y cells* (Figure 19B)*, 70% of APP is processed by ADAM10* (Figure 17B; text passages in *italic* taken and modified from Hitschler & Lang (submitted 2021)).

5.3.2 Physical interaction of α-secretases with APP

While the lateral organisation or the abundance of the secretases did not explain the predominant role of ADAM10 as α-secretase, a higher affinity of ADAM10 to the substrate APP was not examined, yet. Therefore, APP is probed for a physical interaction with the secretases.

A classical method often used for the analysis of interactions between multiple proteins is co-immunoprecipitation. In this procedure, an antibody against the target protein is linked to Sepharose or Agarose beads. The primary target protein is immunoprecipitated with the antibody-coupled beads by centrifugation, while any proteins not precipitated are washed off. Proteins which are bound to the target protein by native interactions are co-immunoprecipitated and can be identified by Western blot analysis after elution of the target protein. To test for a physical interaction of APP with ADAM10, HepG2 cells expressing APP-GFP in the presence or absence of Batimastat were lysed and APP-GFP was immunoprecipitated using GFP-Trap® Agarose beads. After removal of the flow-through, three washing steps and unbinding of the target protein followed. Samples were tested by SDS-PAGE and Western blot analysis for the presence of APP and ADAM10 using a monoclonal mouse antibody raised against APP and a polyclonal rabbit antibody raised against ADAM10. While APP was found in the eluate indicating a successful immunoprecipitation, ADAM10 was not co-precipitated with APP but remained in the flow-through (Figure 20). Besides, there are no reports in the literature about any ADAM10/APP or ADAM17/APP co-immunoprecipitations, to date.

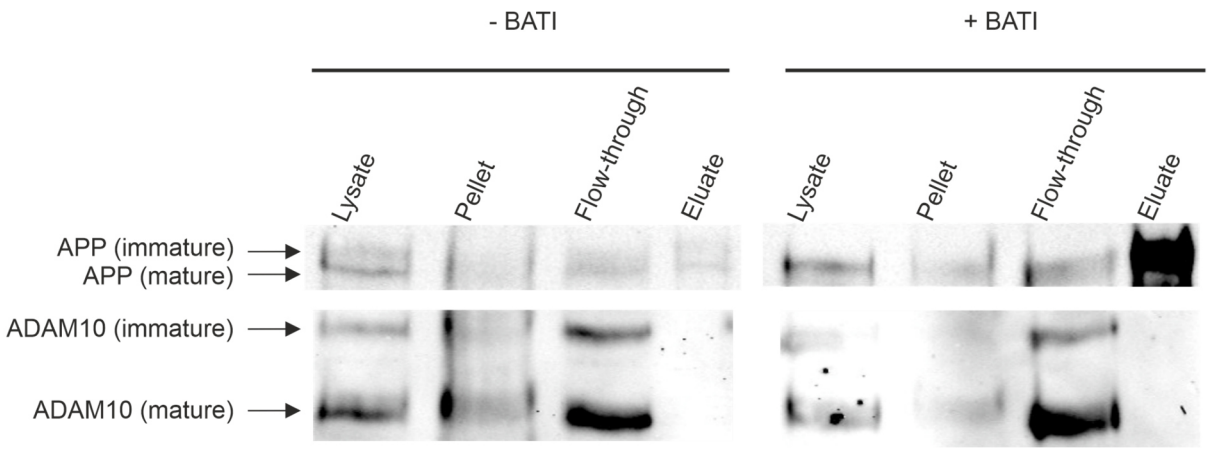

Figure 20. Co-immunoprecipitation of APP and ADAM10 is not successful
HepG2 cells transfected to express APP-GFP were supplemented with 10 µM Batimastat (+ BATI; right panel), or the same volume of DMSO (- BATI; left panel) 1 h after transfection. 21 h after transfection, cells were lysed, resulting in a cell lysate (Lysate) and cell debris (Pellet) fraction. GFP-tagged APP was immunoprecipitated from the lysate using GFP-Trap® Agarose and eluted (Eluate) after removal of the flow-through and three washing steps. APP-GFP (upper panel) and ADAM10 (lower panel) were detected by immunoblotting using antibodies against APP and ADAM10. n = 3 (- BATI) or 2 (+ BATI) independent experiments.

The classical immunoprecipitation method may be unfeasible for several reasons. First, as an enzyme-substrate complex the APP-ADAM10 complex is presumably short lived, because shortly after the secretase binds to the substrate APP it is already cleaved. Second, even if the cleavage rate would be slow or could be inhibited, the complex may dissociate during the usually long lasting immunoprecipitation or due to the mechanical and chemical stresses applied during incubation and washing steps. Therefore, low-affinity or transient protein-protein interactions may not be detected. Third, a prerequisite for the protein-protein interaction may be an intact cell membrane which is dissolved during cell lysis.

Therefore, to avoid cell solubilization and to minimize the duration of the experiment, the APP-ADAM interaction was examined directly in native membranes by antibody-induced co-aggregation. In this assay, one interaction partner is cross-linked by antibodies, yielding a more aggregates-prone distribution pattern when compared to directly fixed proteins, while interaction partners are pulled indirectly into these patches upon physical interaction. For this experiment, HepG2 cells expressing APP-GFP were grown in the presence of Batimastat to increase the plasmalemmal APP level. After generation of membrane sheets, APP-GFP was cross-linked in two subsequent 15 min incubation steps at 37 °C. In the first incubation step a monoclonal antibody raised against GFP maximally binds to two APP-GFP molecules. After washing, a secondary antibody cross-links the APP-GFP-primary antibody complexes. Afterwards, samples were fixed, stained for ADAM10 or ADAM17, and the ADAM10/ADAM17 and GFP fluorescence

signals were recorded by confocal microscopy (Figure 21; text passage in *italic* taken and modified from Hitschler & Lang (submitted 2021)).

Upon cross-linking, a more aggregation-prone distribution pattern can be observed for APP (Figure 21A). For evaluation of the cross-linking effect, the APP fluorescence distribution was analyzed by determining its relative standard deviation of the mean (rSDM). This parameter describes the degree of signal clustering and increases upon aggregation (Zilly *et al,* 2011). Cross-linking tripled the rSDM, whereas incubation in the absence of antibodies only led to a doubling of the rSDM (Figure 21B), which is likely due to spontaneous APP protein aggregation as observed previously for other proteins (Zilly *et al,* 2011). In conclusion, the analysis suggests that the antibody treatment cross-links APP molecules in the native cell membrane into less aggregates, which is also obvious when looking at the images (Figure 21A). *Occasionally, a reduction of GFP intensity was observed in control or cross-linked samples (*see Figure 21C*).* This decline in fluorescence intensity may be caused by enhanced α-secretase cleavage which might be due to a concentration of substrate and enzymes in the aggregates, followed by γ-secretase cleavage and wash-off of the cleavage products. To test this theory, Batimastat was added for α-secretase inhibition during the incubation steps necessary for antibody-induced cross-linking (Figure 22). However, GFP intensity diminished also when Batimastat was present during cross-linking (Figure 22B) indicating that enhanced α-secretase cleavage is not the cause of the reduced fluorescence intensity. *GFP-self-quenching is probably responsible for this effect, which can occur upon oligomerization of GFP-labelled proteins (Schneider et al, 2021; Ochiishi et al, 2016)* (text passage in *italic* taken from Hitschler & Lang (submitted 2021)).

To quantify a potential physical interaction between APP and the secretases, co-aggregation of ADAM10/17 with APP was evaluated by calculating the Pearson correlation coefficient (PCC). It is utilized in image analysis to quantify the degree of colocalization of fluorescence intensity peaks in two different channels and ranges from 1 for perfect colocalization and -1 for perfect negative colocalization. In practice, due to technical limitations PCCs are much lower than 1 even if both proteins would be 100% associated. Although APP becomes spontaneously more aggregated in the absence of cross-linking antibodies (control; Figure 21B), the signal overlap does not change compared to directly fixed samples (Figure 21D). Upon cross-linking of APP (CoP), the PCC value for APP/ADAM10 more than doubles, whereas for APP/ADAM17 it remains the same (control sample, Figure 21D). These results indicate that ADAM10 is probably pulled together with APP into the forming aggregates due to a physical association, resulting in a higher signal overlap. ADAM17 does not co-aggregate, either because there is no or a weaker physical association. The detection of a physical interaction of ADAM10 but not of ADAM17 with APP is

the first difference found in the relationship of the secretases towards APP and might provide an explanation why ADAM10 is more effective in the processing of APP than ADAM17.

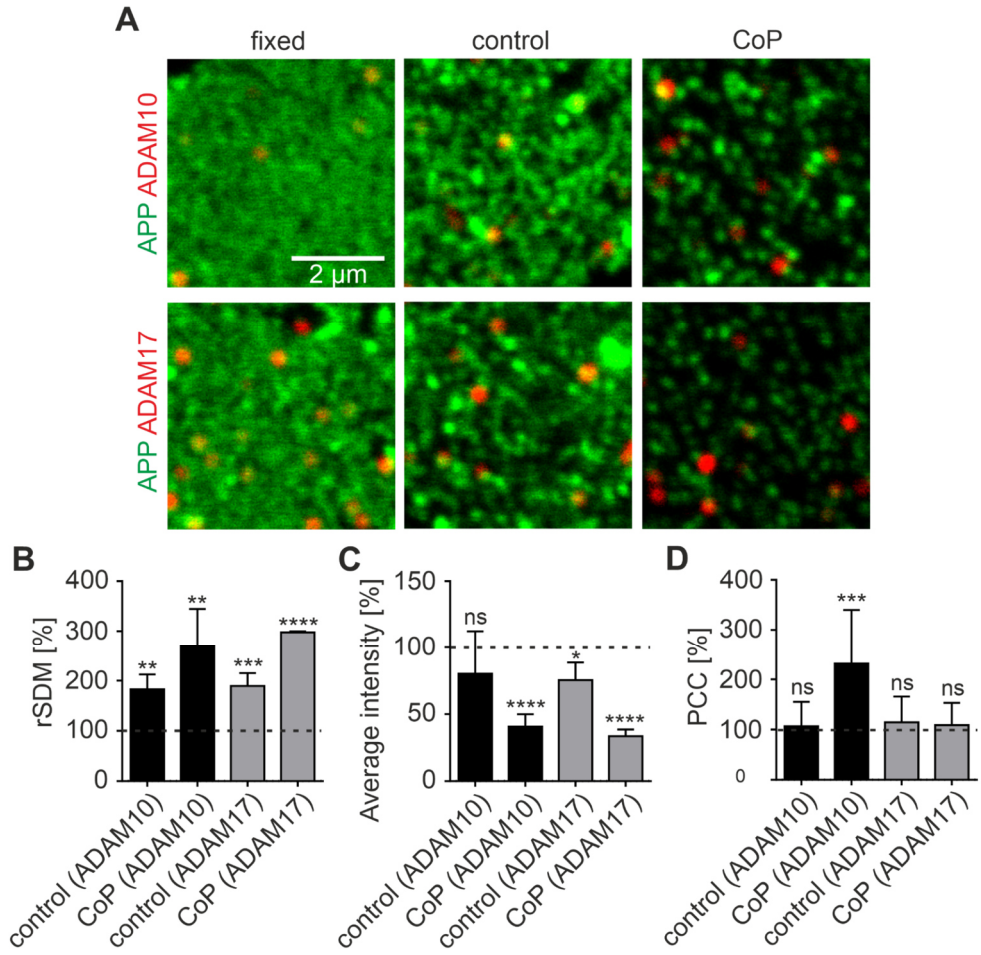

Figure 21. Co-aggregation reveals a physical interaction of APP with ADAM10 but not with ADAM17

(A) Confocal micrographs of membrane sheets from HepG2 cells expressing APP-GFP and grown for 21 h. Membrane sheets were directly fixed (left), incubated without (control; middle) or with cross-linking antibodies (CoP; right), followed by immunostaining for ADAM10 (upper panels) or ADAM17 (lower panels). Images are displayed at arbitrary scalings using linear lookup tables for APP-GFP (green) and ADAM10/ADAM17 (red), respectively. (B) Relative standard deviation of the mean (rSDM) and (C) average intensity of APP-GFP. (D) Overlap through cross-linking is quantified by the Pearson correlation coefficient (PCC) between APP and ADAM10 or APP and ADAM17. (B - D) Values are expressed as percentage of the condition 'fixed' (100% reference line). Values are given as the means ± SD (n = 4 experiments; 10 - 20 membrane sheets per experiment and condition). Unpaired Student's t-tests compare the conditions control and CoP to fixed (****p <0.0001; ***p <0.001; **p <0.01; *p <0.05; ns (not significant) p >0.05). Figure and legend taken and modified from Hitschler & Lang (submitted 2021).

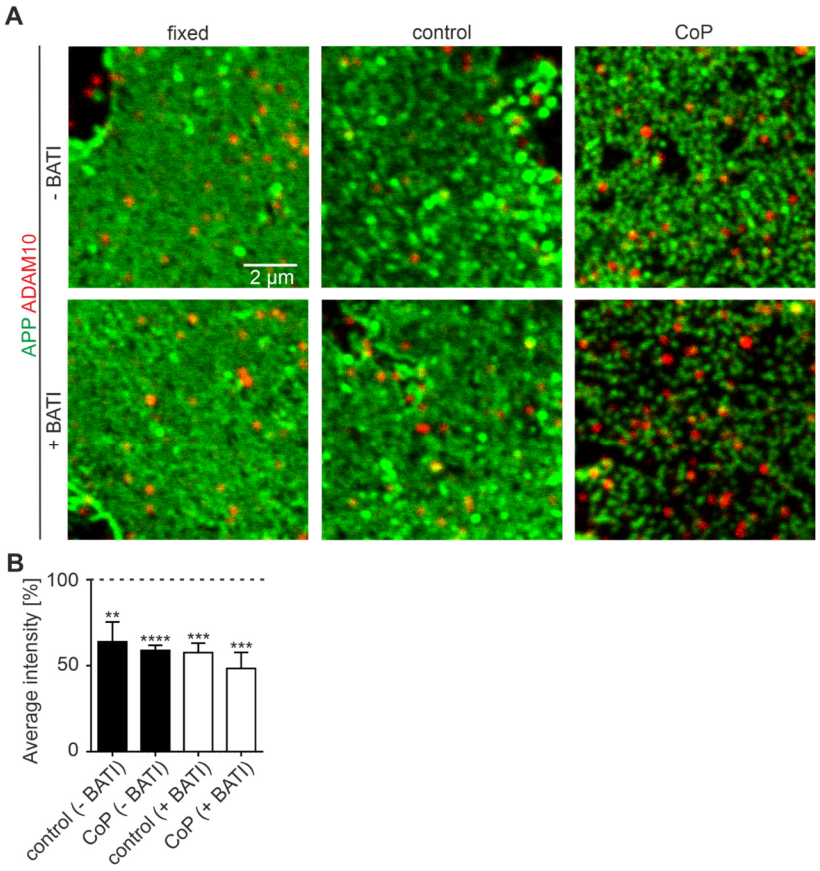

Figure 22. Antibody-induced cross-linking of APP in the presence of Batimastat
(A) Confocal micrographs of membrane sheets from HepG2 cells expressing APP-GFP directly fixed (left panel) 21 h after transfection, or incubated without (control; middle panel) or with cross-linking antibodies (CoP; right panel) in the absence (- BATI) or presence of α-secretase inhibitor (+ BATI), followed by immunostaining for ADAM10. Images are overlays of the green (APP-GFP) and red (ADAM10) channel shown at arbitrary intensity scalings. (B) Average intensity of the APP-GFP intensity. Values are expressed as percentage of the condition 'fixed' (100% reference line). Values are given as means ± SD (n = 3 experiments, 20 membrane sheets per experiment and condition). Unpaired Student's t-tests compare the condition fixed to control and CoP (****p <0.0001; ***p <0.001; **p <0.01; *p <0.05; ns (not significant) p >0.05). Figure and legend taken and modified from Hitschler & Lang (submitted 2021).

5.3.3 Specification of the APP domain responsible for the interaction with ADAM10

After the detection of a physical interaction between APP and ADAM10, the question arises which domain of the APP protein is responsible for this interaction. To address this issue, *two deletion constructs were compared to wild-type APP: APP-ΔN, lacking the extracellular domain (aa 22-626), and APP-ΔC, lacking the cytoplasmic fragment (aa 649-695*; (Schreiber et al, 2012)*). Additionally, APP-TMS was constructed, in which the transmembrane segment (TMS; aa 627-647) is exchanged by the TMS of the epidermal growth factor receptor (EGFR; aa 646-668).*

In the confocal micrographs (Figure 23A), *APP-ΔN already displayed a markedly more punctate distribution pattern in the fixed sample, consequently leading to higher rSDM values. This is probably because a fraction of APP-ΔN remains in the endoplasmic reticulum, and ER-PM contact sites are present on membrane sheets, visible as bright spots (Merklinger et al, 2016)* (text passage in *italic* taken and modified from Hitschler & Lang (submitted 2021)). Nevertheless, the rSDM of all samples increased with antibody-induced cross-linking relative to the fixed sample (Figure 23B) showing that the method efficiently cross-links all constructs. Cross-linking increased the signal overlap of ADAM10 with APP, APP-ΔN and APP-ΔC, but not with APP-TMS (Figure 23C). These results indicate that co-patching and consequently the physical interaction of APP and ADAM10 depend on the transmembrane segment of APP.

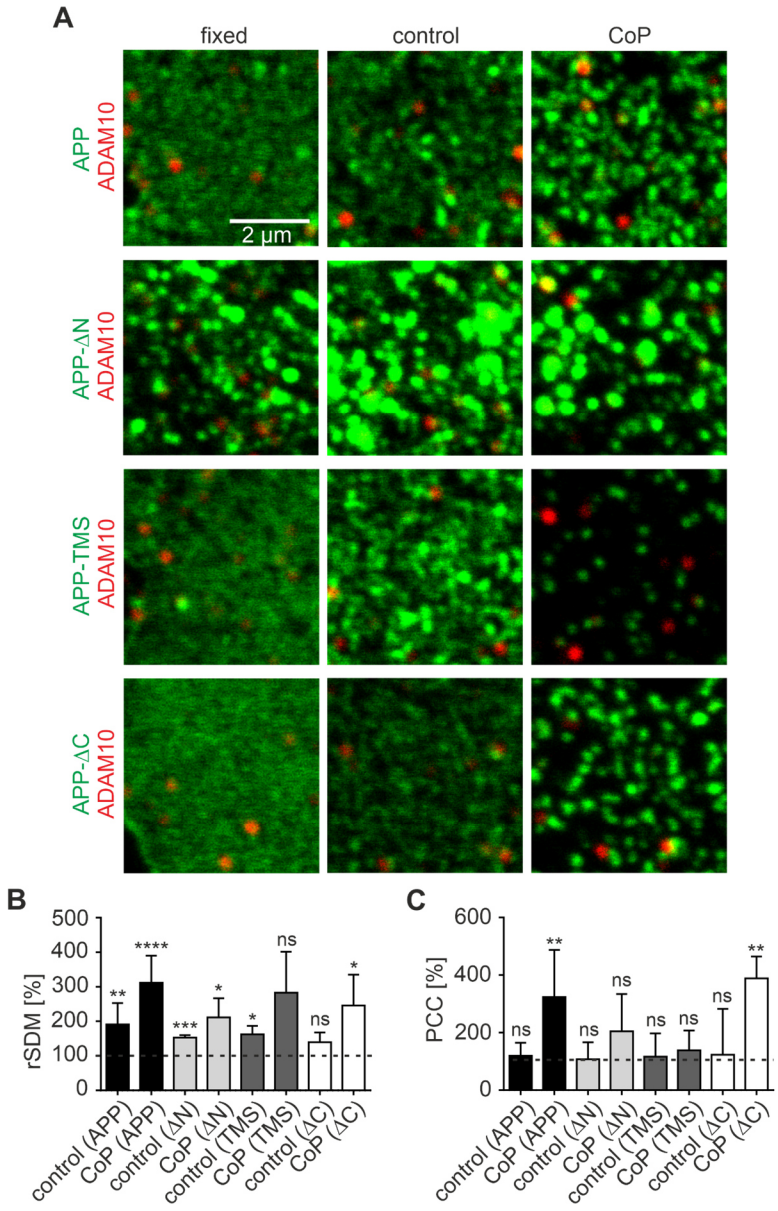

Figure 23. APP co-aggregation with ADAM10 depends on the transmembrane segment of APP

(A) Confocal micrographs of membrane sheets from HepG2 cells expressing APP, APP-ΔN, APP-ΔC and APP-TMS fused to a C-terminal GFP-tag. Membrane sheets were either directly fixed (left column) 21 h after transfection, incubated without (control; middle column) or with crosslinking antibodies (CoP; right column), followed by immunostaining for ADAM10. Images are displayed at arbitrary intensity scalings using linear lookup tables for the GFP-tag (green) and ADAM10 immunostaining (red). (B) Relative standard deviation of the mean (rSDM) of APP and APP mutants. (C) Pearson correlation coefficient (PCC) between ADAM10 and APP, APP-ΔN, APP-ΔC and APP-TMS. (B, C) Values are expressed as percentage of the condition 'fixed' (100% reference line). Values are given as the means ± SD (n = 3 - 6 experiments; 10 - 20 membrane sheets per experiment and condition). Unpaired Student's t-tests compare fixed to control and CoP (****p <0.0001; ***p <0.001; **p <0.01; *p <0.05; ns (not significant) p >0.05). Figure and legend taken and modified from Hitschler & Lang (submitted 2021).

After identification of the APP domain responsible for the interaction with ADAM10, the question arose if the physical APP-ADAM10 association is a prerequisite for APP processing. To this end, α-secretase cleavage efficiency of APP and APP-TMS was compared by Western Blot analysis. Because the exchange of the TMS leads to a loss of the γ-cleavage site, HepG2 cells transfected to express APP or APP-TMS were grown in the presence of the γ-secretase inhibitor DAPT for comparison of α-processing in the absence of γ-cleavage in all conditions. *One day after transfection, lysed cells as well as growth medium were analysed by Western blot using an antibody raised against aa 1-16 of the Aβ region.* Therefore, only full-length APP and sAPPα but not sAPPβ are detected, because the α-secretase cleaves after aa 16 and the β-secretase cleaves before aa 1 of the Aβ region (see Figure 3B). Western blot analysis revealed that exchange of the TMS reduced α-cleavage of the APP-TMS construct to less than 50 % (Figure 24). *These results indicate that the physical link between the transmembrane domain of APP and ADAM10 is functionally important* (text passage in *italic* taken and modified from Hitschler & Lang (submitted 2021)).

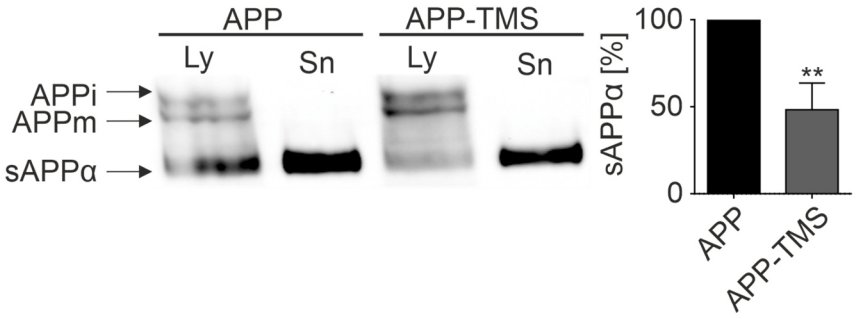

Figure 24. α-Cleavage depends on the transmembrane segment of APP
Western blot quantification of sAPPα in lysate (Ly) and supernatant (Sn) of HepG2 cells grown for 21 h in the presence of 10 µM DAPT, expressing either GFP-labelled APP or APP-TMS. The sum of sAPPα band intensities (Ly + Sn) is related to the sum of the band intensities of immature (APPi) and mature (APPm) APP; APP-TMS is related to APP (set to 100%). Value is given as the mean ± SD (n = 3 experiments). Unpaired Student's t-test compares APP-TMS to APP (****p <0.0001; ***p <0.001; **p <0.01; *p <0.05; ns (not significant) p >0.05). Figure and legend taken and modified from Hitschler & Lang (submitted 2021).

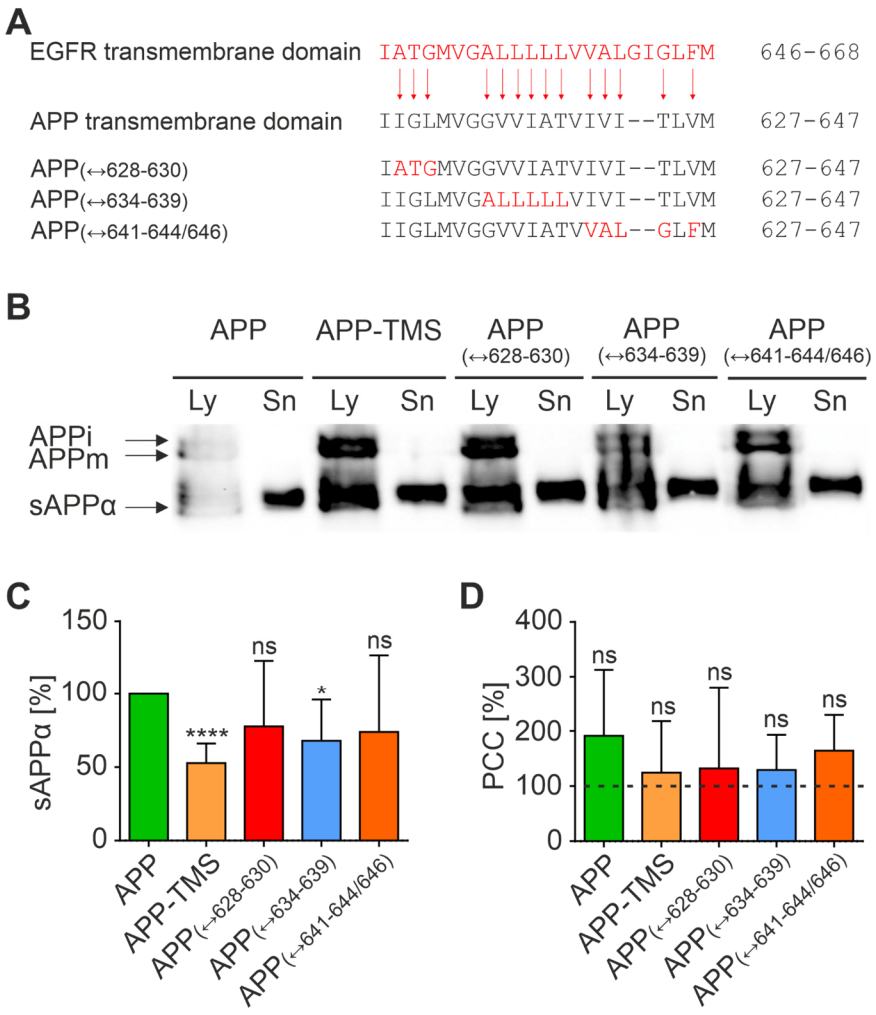

Figure 25. Effect of modifications of the TMS on α-processing and crosslinking with ADAM10

(A) Amino acid sequences of the transmembrane segment (TMS) of the EGFR (aa 646-668) and APP (aa 627-647). Compared to the TMS of EGFR, the TMS of APP lacks two amino acids and differs at position 628-630, 634-639, 641-644 and 646 (see red arrows). APP(↔628-630) carries the mutations I628A, G629T, L630G, APP(↔634-639) the mutations G634A, V635L, V636L, I637L, A638L, T639L, and APP(↔641-644/646) the mutations I641V, V642A, I643L, T644G, V646F. (B) HepG2 cells were transfected with GFP-tagged APP, APP-TMS, APP(↔628-630), APP(↔634-639) or APP(↔641-644/646) and grown in the presence of 10 µM DAPT. 21 h after transfection, lysate (Ly) and supernatant (Sn) were analyzed by Western blot. (C) The sAPPα band intensities are normalized to the sum of immature (APPi) and mature (APPm) APP band intensities, and related to the APP value, which is set to 100 %. Values are given as means ± SD (n = 5 experiments). (D) Pearson Correlation Coefficient (PCC) between ADAM10 and APP constructs as indicated. Analysis as in Figure 21 and Figure 23, showing only the CoP condition. For example images see Figure 26. Values are given as means ± SD (n = 3 - 6 experiments, 15 - 20 membrane sheets per experiment and condition. (C, D) Unpaired Student's t-tests compare (C) APP to APP-mutants or (D) fixed to CoP (****p <0.0001; ***p <0.001; **p <0.01; *p <0.05; ns (not significant) p >0.05). Figure and legend taken and modified from Hitschler & Lang (submitted 2021).

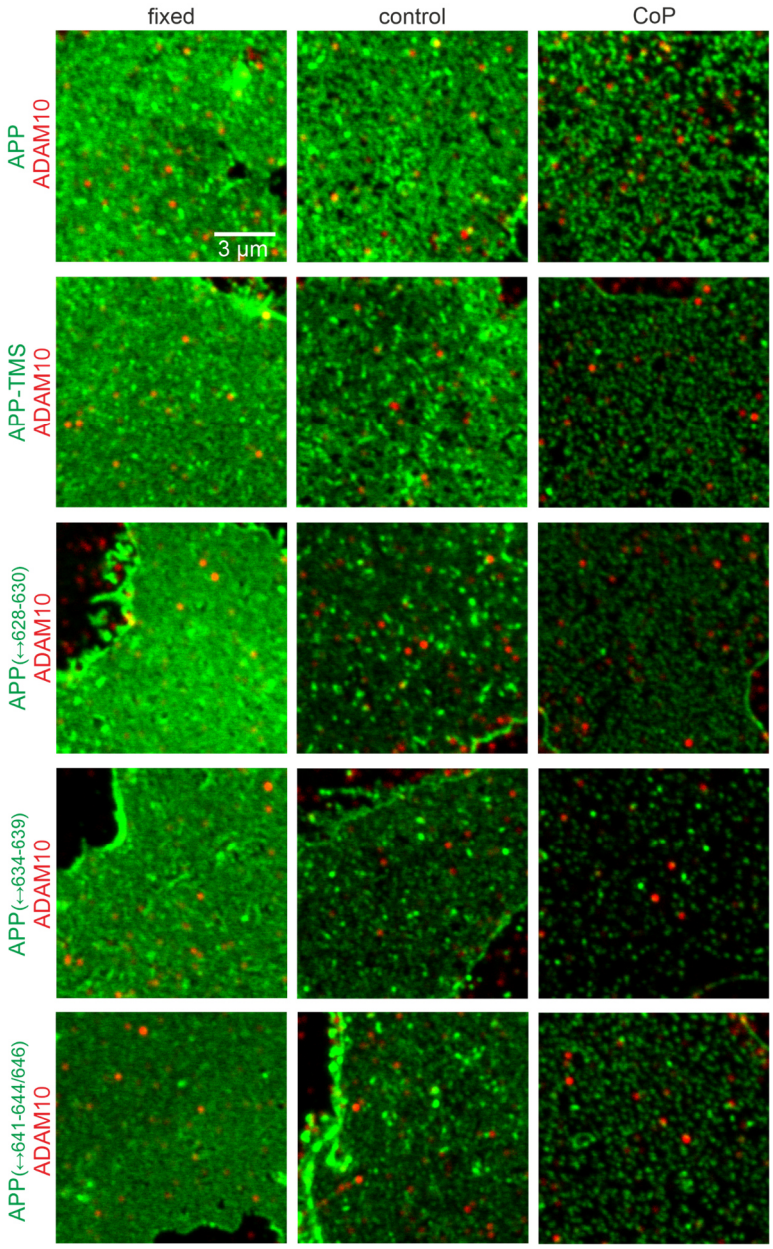

Figure 26. Crosslinking of GFP-tagged APP with modifications of the transmembrane segment
Confocal micrographs of membrane sheets generated from HepG2 cells expressing the indicated constructs, either directly fixed (left column) 21 h after transfection, or incubated without (control; middle column) or with crosslinking antibodies (CoP; right column), followed by immunostaining for ADAM10. Images are displayed at arbitrary intensity scalings using linear lookup tables for the GFP-tag (green) and ADAM10 immunostaining (red). For analysis of the PCC see Figure 25. Figure and legend taken and modified from Hitschler & Lang (submitted 2021).

Next, we aimed to specify the region within the TMS responsible for the physical link with ADAM10. The TMS of APP differs from the two amino acids longer EGFR-TMS at four positions,

628-630, 634-639, 641-644 (in this section the EGFR-TMS has two additional amino acids) and 646 (Figure 25A)*. Based on these deviations, three constructs were generated and in the TMS of APP the amino acids at positions 628-30 (APP(↔628-630)), 634-639 (APP(↔634-639)) and 641-644/646 (APP(↔641-644/646)) were exchanged by the respective amino acids of the EGFR-TMS* (Figure 25A)*.* For these constructs a cross-linking assay (Figure 25D, Figure 26) as well as a cleavage analysis by Western blot (Figure 25B, C) were performed. *In the cross-linking-assay, APP(↔628-630) and APP(↔634-639) displayed no co-patching with ADAM10 similar to APP-TMS (*Figure 25D*). The APP(↔641-644/646) mutant showed a tendency towards co-aggregation but the increase in PCC was not as high as for wild-type APP. Hence, the interaction with ADAM10 is not mediated by a single small region but rather stabilized by several regions distributed along the TMS* (text passages in *italic* taken and modified from Hitschler & Lang (submitted 2021)). Western blot analysis supports this finding, as α-cleavage of all APP-mutants is reduced but not to the same extent as processing of APP-TMS (Figure 25B and C).

5.3.4 Modulation of the interaction between APP and α-secretases

A physical association of APP and ADAM10 has been identified utilizing an antibody-induced cross-linking assay (see Figure 21D). However, for ADAM17 no co-aggregation with APP was observed. These results indicate that there is no physical interaction with APP or one with lower affinity and might be a reason why ADAM17 only contributes to a small extent to constitutive α-secretase activity, as knockdown studies revealed (Kuhn *et al,* 2010). ADAM17 seems to be responsible for the majority of the α-secretase cleavage regulated by protein kinase C, which can be stimulated by phorbol esters (Buxbaum *et al,* 1998). Stimulation of ADAM17 has been proposed to cause a conformational change in the extracellular catalytic domain (Le Gall *et al,* 2010). Therefore, it remains to be tested whether a physical association between ADAM17 and APP is observed under stimulated conditions.

First, the efficiency of α-cleavage stimulation by the phorbol ester PMA was evaluated. HepG2 cells were transfected to express APP-GFP and grown in the presence or absence of PMA for 21 h before lysis of the cells and Western blot analysis of lysate and supernatant for sAPPα cleavage product. Upon PMA addition, sAPPα generation was increased by ~50 % (Figure 27) indicating that stimulation by PMA was efficient.

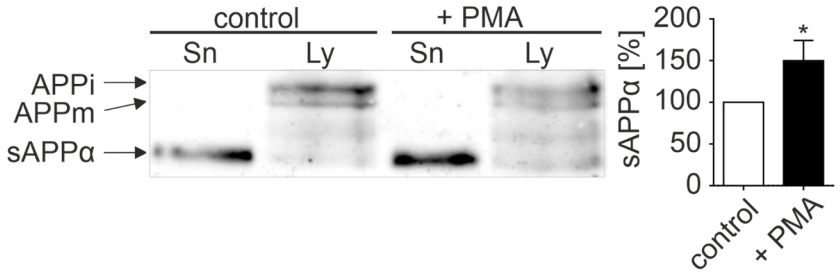

Figure 27. Effect of phorbol ester stimulation on α-processing
Western blot quantification of sAPPα in lysate (Lys) and supernatant (Sn) of HepG2 cells grown for 21 h in the absence (control) or presence of 1 µM PMA (+ PMA), expressing GFP-labelled APP. The sum of sAPPα band intensities (Lys + Sn) is related to the sum of the band intensities of immature (APPi) and mature (APPm) APP; + PMA is related to control (set to 100%). Value is given as the mean ± SD (n = 3 experiments). Unpaired Student's t-test compares + PMA to control (****p <0.0001; ***p <0.001; **p <0.01; *p <0.05; ns (not significant) p >0.05). Figure and legend taken and modified from Hitschler & Lang (submitted 2021).

The effect of PMA stimulation on co-aggregation was examined for ADAM17 as well as ADAM10. Cross-linking of APP was equally efficient in the absence or presence of PMA (Figure 28A, B). However, PMA did not change the propensity of ADAM10 to co-aggregate with APP and the PCC of ADAM17 still did not increase (Figure 28C). Hence, the stimulation of α-cleavage by PMA had no obvious effect on the physical interaction of the ADAMs with APP.

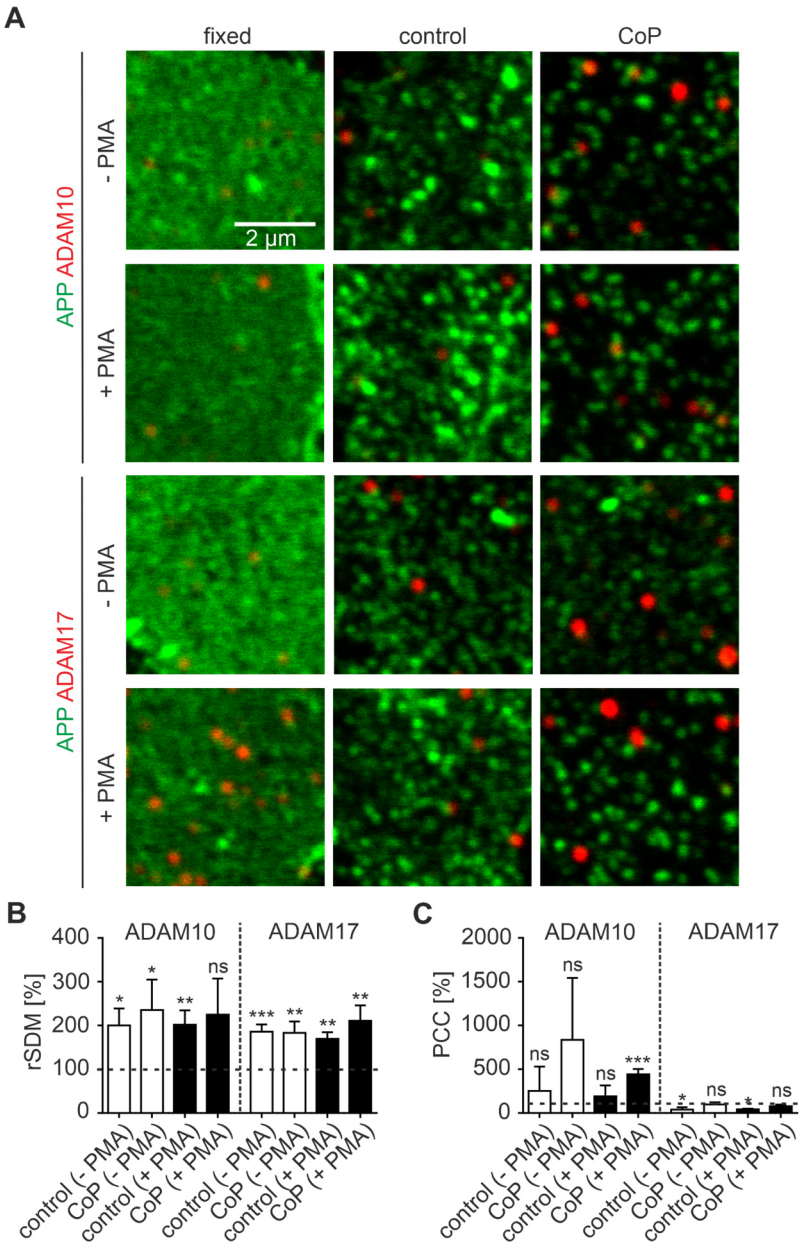

Figure 28. Phorbol ester stimulation of α-processing has no effect on the physical interaction of APP with ADAM10 or ADAM17

(A) Confocal micrographs of membrane sheets from HepG2 cells grown for 21 h in the absence (- PMA) or presence of 1 µM PMA (+ PMA), expressing APP-GFP. Membrane sheets were directly fixed (left), incubated without (control; middle) or with cross-linking antibodies (CoP; right), followed by immunostaining for ADAM10 (upper panels) or ADAM17 (lower panels). Images are displayed at arbitrary scalings using linear lookup tables for APP-GFP (green) and ADAM10/ADAM17 (red), respectively. (B) Relative standard deviation of the mean (rSDM) of APP. (C) Pearson correlation coefficient (PCC) between APP and ADAM10 or ADAM17. (B, C) Values are expressed as percentage of the condition 'fixed' (100% reference line). Values are given as the means ± SD (n = 3 experiments; 15 - 20 membrane sheets per experiment and condition). Unpaired Student's t-tests compare fixed to control and CoP (****p <0.0001; ***p <0.001; **p <0.01; *p <0.05; ns (not significant) p >0.05). Figure and legend taken and modified from Hitschler & Lang (submitted 2021).

5.3.5 Impact of APP mutations on the interaction with ADAM10

Next, we wanted to examine if the physical link of ADAM10 and APP is affected by other factors. For the protective mutation at position 2 of the Aβ region (A673T or APP-A2T) a decreased β-secretase cleavage and reduced Aβ peptide generation was observed, while sAPPα production was slightly increased (Jonsson *et al,* 2012). For the pathological A2V mutation it was the other way around with increased β-cleavage and reduced α-cleavage (Jonsson *et al,* 2012). These results demonstrate that position 2 in the Aβ region is critical for the regulation of non-amyloidogenic as well as amyloidogenic processing of APP. The modulation of α-secretase cleavage might be due to a change in the physical interaction of the APP-mutants with ADAM10. To address this issue, we first tested if α-cleavage of the APP-mutants is changed in the cell line used in this study. Western blot analysis revealed that α-cleavage of APP-A2V was almost completely abolished (Figure 29A). α-Cleavage of APP-A2T was similar to APP wild-type. The originally published increase of APP-A2T α-cleavage was very small (Jonsson *et al,* 2012) and might not be detectable under the test conditions used in this study. Additionally, the Western blot analysis cannot differentiate between a possible difference between intracellular and plasmalemmal processing. Therefore, cleavage of the APP-mutants was additionally examined in native plasma membrane sheets (Figure 29B). To this end, HepG2 cells express APP or the mutants *double tagged with mCherry and GFP (see illustration of the construct in* Figure 29B*). Membrane sheets are generated 21 h after transfection in ice-cold solution, which immediately stops intracellular trafficking. Then, native membranes are either directly fixed, or incubated for 10 min in a cell incubator in medium containing the γ-secretase inhibitor DAPT. Under these conditions, we expect any occurrence of cleavage caused rather by α-secretases, as β-secretases are active at low pH (Haass et al, 1993; Koo & Squazzo, 1994). In any case, cleavage yields a soluble, mCherry-tagged ectodomain that is washed-off, whereas the GFP-tagged C-terminal fragment remains in the cell membrane. Hence, in comparison to directly fixed membranes, GFP-fluorescence does not diminish upon processing, in contrast to mCherry fluorescence* (text passage in *italic* taken from Hitschler & Lang (submitted 2021)). In the cleavage assay, the GFP signal of APP, APP-A2T and APP-A2V indeed is unchanged upon incubation with DAPT (Figure 29B). The mCherry signal is strongly reduced by ~60 % and ~69 % in membrane sheets with APP and APP-A2T, respectively, while it is only diminished by ~33 % in APP-A2V containing membrane sheets. The assay thus confirms that α-cleavage of APP-A2T is slightly increased at the plasma membrane, while α-processing of APP-A2V is strongly reduced.

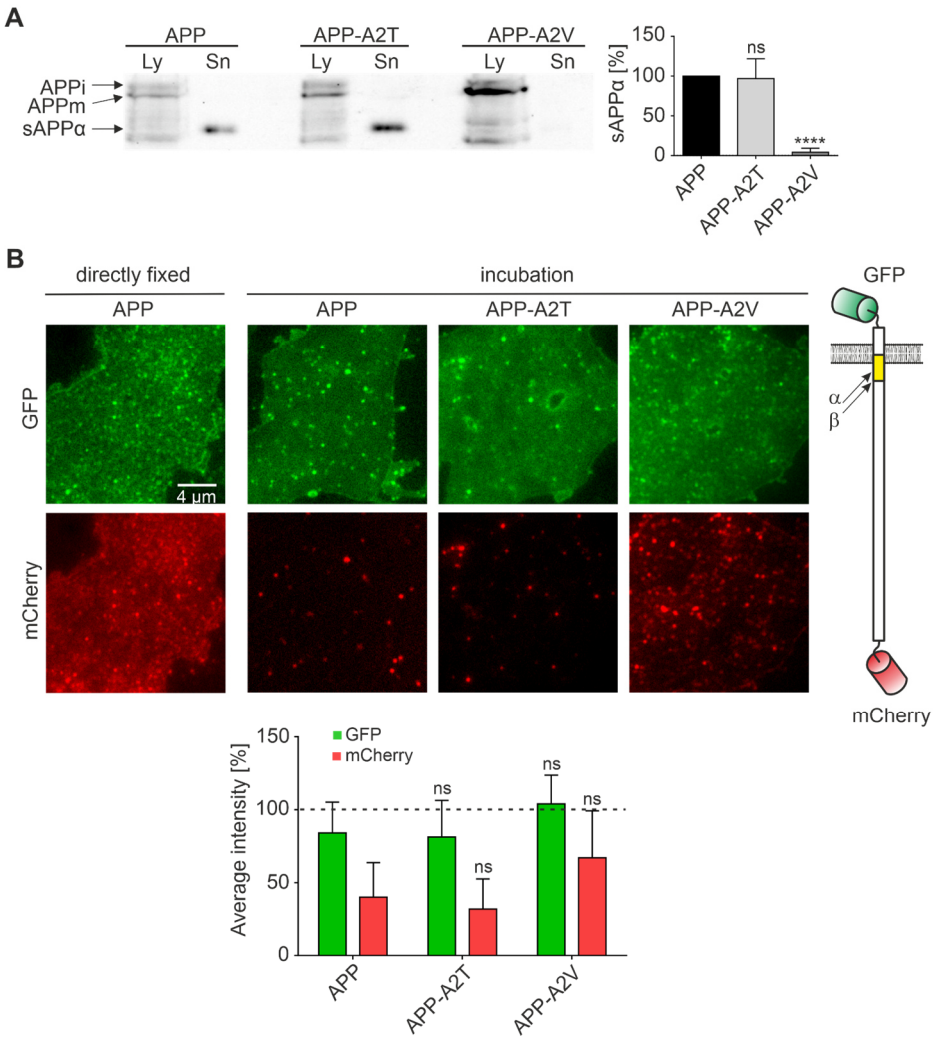

Figure 29. α-Processing of APP mutants
(A) Western blot quantification of sAPPα in lysate (Ly) and supernatant (Sn) of HepG2 cells grown for 21 h, expressing GFP-labelled APP, APP-A2T or APP-A2V. The sum of sAPPα band intensities (Ly + Sn) is related to the sum of the band intensities of immature (APPi) and mature (APPm) APP; APP mutants are related to APP (set to 100%). Values are given as the means ± SD (n = 4 experiments). (B) APP processing in native plasma membrane sheets. Epifluorescence micrographs show images of membrane sheets generated from HepG2 cells expressing APP, APP-A2T or APP-A2V double tagged with mCherry and GFP (see illustration to the right; arrows point towards the α- and β-cleavage site; yellow, Aβ region). Membrane sheets are either directly fixed (left images) 21 h after transfection or fixed after incubation for 10 min at 37 °C in medium containing 10 µM DAPT (right images). Images from the same channels are displayed with the same scaling using linear lookup tables. Bar chart, quantification of GFP and mCherry average intensity of incubated membrane sheets related to the condition 'directly fixed' (100% reference line). Values are given as means ± SD (n = 9 experiments, 10 - 20 membrane sheets per experiment and condition). (A, B) Unpaired Student's t-tests compare APP to APP mutants (****p <0.0001; ***p <0.001; **p <0.01; *p <0.05; ns (not significant) p >0.05). Figure and legend taken and modified from Hitschler & Lang (submitted 2021).

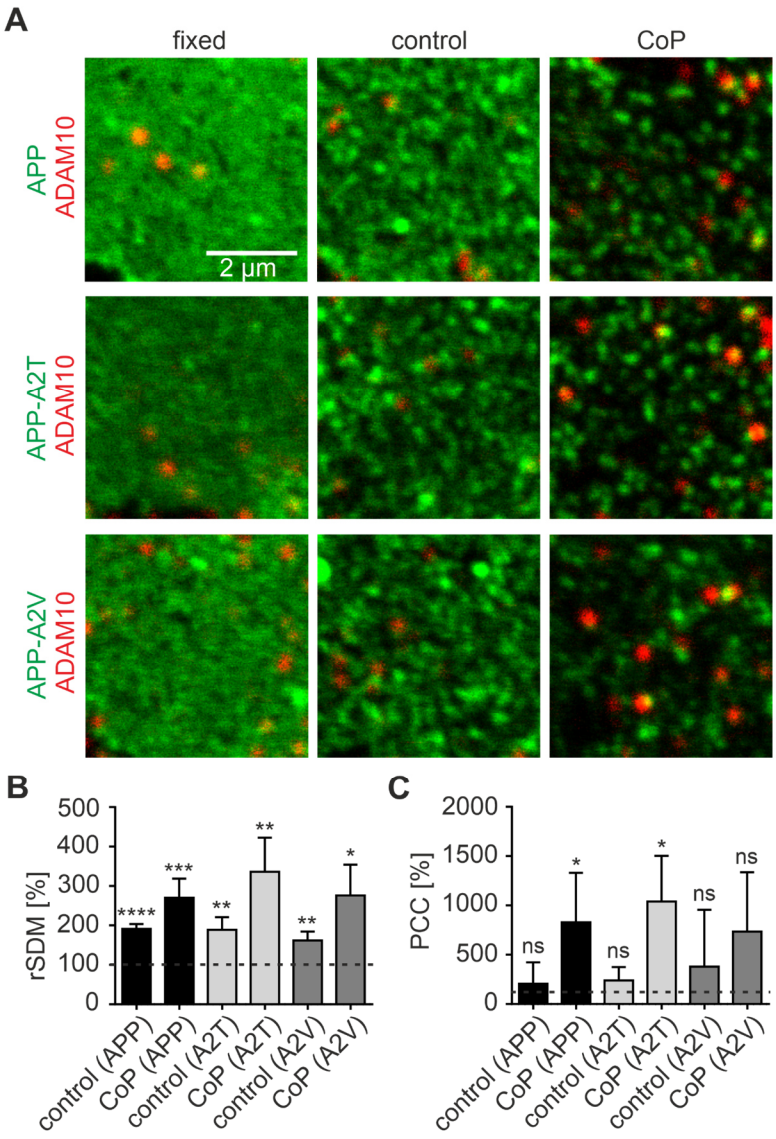

Figure 30. Co-aggregation of APP mutants with ADAM10
(A) Confocal micrographs of membrane sheets from HepG2 cells expressing APP, APP-A2T and APP-A2V fused to a C-terminal GFP-tag. Membrane sheets were either directly fixed (left column) 21 h after transfection, incubated without (control; middle column) or with crosslinking antibodies (CoP; right column), followed by immunostaining for ADAM10. Images are displayed at arbitrary intensity scalings using linear lookup tables for the GFP-tag (green) and ADAM10 immunostaining (red). (B) Relative standard deviation of the mean (rSDM) of APP and APP mutants. (C) Pearson correlation coefficient (PCC) between ADAM10 and APP, APP-A2T or APP-A2V. (B, C) Values are expressed as percentage of the condition 'fixed' (100% reference line). Values are given as the means ± SD (n = 3 - 4 experiments; 20 membrane sheets per experiment and condition). Unpaired Student's t-tests compare fixed to control and CoP (****p <0.0001; ***p <0.001; **p <0.01; *p <0.05; ns (not significant) p >0.05).

Next, the APP mutants were tested for their co-aggregation with ADAM10 to examine if the different propensity for α-cleavage is due to a change in physical interaction with the secretase.

As could be observed in the confocal micrographs and the rSDM determination, the cross-linking of APP was equally efficient for all mutants (Figure 30A and B). For both APP-mutants the same increase in PCC as for APP wild-type is observed, indicating a similar physical link to ADAM10. The reduction in α-cleavage observed for APP-A2V (Figure 29) is not paralleled by a similar decrease of the PCC (Figure 30C), although the A2V PCC increase is the smallest and not significant.

6 Discussion

Amyloidogenic processing of the amyloid precursor protein (APP) to neurotoxic Aβ peptides is one of the main causatives of Alzheimer's disease. Neurotoxic Aβ accumulation can be precluded by increasing non-amyloidogenic processing of APP mediated by α-secretases at the plasma membrane. Enhancement of α-secretase cleavage may be achieved by increasing the accessibility of the substrate, that may be limited through clustering. Alternatively, other avenues may open by gaining a deeper understanding of the organisation and interaction of APP and the α-secretases at the cell surface.

First, this study analyzed whether pathogenic mutants more prone for amyloidogenic processing are more tightly clustered and therefore less accessible for α-secretases. However, epifluorescence microscopy and FRAP revealed no change in the clustering degree and mobility of the examined APP mutants. Next, the substrate-secretase association was studied in more detail by examining the lateral organisation and association of APP and the α-secretases ADAM10 and ADAM17. High-resolution STED microscopy demonstrated that all three proteins are present in nanodomains at the cell surface. While clustering of APP has been described previously, it was only postulated for ADAM10 and ADAM17 to date (Reiss & Bhakdi, 2017). Although ADAM10 is the predominant constitutive α-secretase, no difference in the substrate-secretase spatial proximity could be observed for ADAM10 and ADAM17 as both located at equal frequency closer than 50 nm to their substrate APP. However, for ADAM10 a physical link to APP mediated by the transmembrane segment of APP could be demonstrated by antibody-induced cross-linking of APP in native membranes, while for ADAM17 no physical interaction to APP could be detected. A more detailed understanding of this interaction may allow for developing a therapeutic strategy in the future based on promoting α-cleavage of APP.

6.1 Lateral organisation of APP in plasmalemmal clusters

A non-uniform distribution of plasmalemmal APP into protein clusters was first described in N2a cells (Schneider *et al,* 2008). Later, it could be shown that the majority of the plasmalemmal APP in PC12 as well as HepG2 cells is organized in clustered structures (Schreiber, 2012). The anatomy of APP clusters has been examined in more detail in the plasma membrane of SH-SY5Y cells (de Coninck *et al,* 2018), describing them as nanodomains. Most of the endogenous APP clusters have a diameter between 65 and 85

nm and contain roughly 20 – 30 APP molecules in this cell line (de Coninck *et al,* 2018). It has been shown previously that APP clustering is a prerequisite for endocytosis and subsequent amyloidogenic processing (Schneider *et al,* 2021; Schreiber *et al,* 2012). In this model, clustering stimulates endocytosis of APP, and consequently reduces the possibility of non-amyloidogenic processing by α-secretases at the plasma membrane. This indirectly promotes amyloidogenic processing. Moreover, aggregation of APP into tight clusters may decrease the accessibility to α-secretases, a second mechanism by which clustering may favour Aβ generation.

6.1.1 Impact of familial mutations on APP clustering and processing

APP has been reported to form plasmalemmal clusters via the 5 N-terminal amino acids of the Aβ region (Schreiber *et al,* 2012). Interestingly, several pathological mutations causing familiar AD (Lan *et al,* 2014; Zhou *et al,* 2011; Di Fede *et al,* 2009; Wakutani *et al,* 2004), as well as the only mutation known to protect against AD (Jonsson *et al,* 2012), are located within or close to the region required for APP clustering (Schreiber *et al,* 2012). For a pathological mutation at position 2 of the Aβ region (A2V) it was already demonstrated that it causes dramatically increased β-cleavage and Aβ generation and slightly decreased α-processing (Di Fede *et al,* 2009; Jonsson *et al,* 2012). A mutation at position 11 of the Aβ region (E11K) had a similar effect on β-cleavage and Aβ generation (Zhou *et al,* 2011). Conversely, in the A2T mutation conferring improved cognitive function and protection against AD β-secretase processing and Aβ generation was reduced, whereas α-cleavage was slightly increased (Jonsson *et al,* 2012).

As those familial mutations affect processing and lie within or close to the region required for APP clustering, it is tempting to speculate that these mutations affect clustering and subsequently regulate the accessibility of the substrate to α-secretases. To elucidate if a change in APP clustering may underlie the alterations in APP processing, the clustering degree and dynamics of the APP-A2T, -A2V and -E11K mutant were examined in this study. However, no change in the mobility or degree of clustering could be observed compared to wild-type APP (Figure 6 and Figure 7). A previous study reported a slight decline in the rSDM and half-time recovery of APP-A2T compared to wild-type in HepG2 as well as SH-SY5Y cells (de Coninck, 2020). However, the clustering degree was only decreased slightly by ~ 20–25 % in the previous study (de Coninck, 2020). Different expression levels of the APP-mutants compared to wild-type may affect the clustering degree (see Figure 6D). However, a repetition of the experiment with the APP-mutants

APP-A2T and APP-A2V displaying similar expression levels to wild-type did not result in a change of the clustering degree in this study (data not shown). Furthermore, that post-fixation aggregation artifacts distort the results can never be completely excluded. A previous study utilizing photoactivated localization microscopy (PALM) reported that a fraction of APP molecules were still mobile after fixation with 4 % PFA (de Coninck, 2020) and may therefore self-aggregate post-fixation. Additionally, for the transferrin receptor, which shares with APP a similar size and protein structure, it was demonstrated that ~40 % of the molecules were still mobile even after prolonged fixation with 4 % PFA (Tanaka *et al,* 2010). Such a mobile fraction of APP molecules could still spontaneously aggregate, as previously observed for other proteins under unfixed conditions (Zilly *et al,* 2011), and diminish the differences between the mutants and wild-type. Nonetheless, a difference in the clustering degree of the examined APP-mutants and the wild-type could not be proofed at this point.

That a change in the mobility of the APP mutants could not be detected in this study (Figure 7) in contrast to the aforementioned study (de Coninck, 2020) might be explained by the short recovery half-times in this study. Schreiber (2012) reported that the half-time of recovery strongly diminishes 8 h after transfection from ~9 s to ~4s within the next 12 h. Likely, this is due to APP processing, or in other words, 21 h after transfection (in this study) most APP is present in the cleaved form. This would explain as well why no difference in clustering is observed (see above). The observation that α-secretase inhibition upon treatment with Batimastat increases the recovery half-times 21 h after transfection (Figure 15) supports this hypothesis. Moreover, a fast recovery in the first seconds after bleaching and a much slower continuing increase of fluorescence recovery was observed (Figure 7B), which might hint towards different APP species. The faster recovery might be due to APP monomers, small oligomers or APP cleavage products which should diffuse faster. The slower fluorescence recovery might be caused by slow release of single molecules from clusters. However, if the observed recovery is the mixed effect of slow and fast APP species, the half-times determined from this curve might obscur differences between APP-mutants. Additionally, if the proportion of fast and slow species was different in this study from the previous study (de Coninck, 2020) this might explain why the results from the previous study could not be reproduced. In the previous study a fast recovery of ~40 % was observed in the first 5 seconds of the measurement for APP-A2T (de Coninck, 2020), while the recovery was only ~25 % in the first 5 seconds in this study (Figure 7B). The total recovery was lower in this study with ~45 % compared to ~70 % in the previous study (de

Coninck, 2020). Moreover, the expression level, which can affect the membrane dynamics (as shown in Figure 15), may have differed in the APP mutants. Furthermore, FRAP measurements in the previous study were performed at 37 °C (de Coninck, 2020), whereas samples in this study were removed from the incubator. This procedure may greatly affect the mobility, as the unrestricted diffusion of a particle is dependent on the temperature (Reits & Neefjes, 2001). These considerations hint towards a not yet understood complexity in the FRAP read-out precluding a final conclusion.

Apart from the clustering efficiency and mobility, the α-secretase processing of the mutants A2V and A2T was examined. For the APP-A2T mutant no change in the sAPPα generation could be observed in Western blot analysis and only a slight increase of α-cleavage was observed in native membranes (Figure 29). A previous study reported a slight apparent increase of sAPPα generation by ~ 10-20 % for the A2T mutant (Jonsson *et al,* 2012), which might not have been detected in this study using Western blot analysis. To detect a possible difference in the processing of APP-A2T a different incubation time or higher cell number may be needed. Besides, the additional analysis of β-cleavage products might allow for a more complete understanding of the processing mechanism. In contrast to that, sAPPα generation was dramatically reduced in the APP-A2V mutant (Figure 29) which was an even greater decrease than reported in a previous study (Jonsson *et al,* 2012). As a change in APP clustering could not be observed in this study, there has to be another cause for the different processing of the APP-A2V mutant compared to wild-type. In an antibody-induced cross-linking assay of APP-A2V and APP it was examined if a reduced affinity between the main physiological α-secretase and the mutant may be responsible for the diminished α-cleavage. However, the increasing signal overlap with ADAM10 upon APP-A2V cross-linking indicated a co-aggregation with ADAM10 and demonstrated that the physical interaction between ADAM10 and the mutant was comparable to APP (Figure 30). The reduced α-cleavage of APP-A2V is probably not due to a difference in the interaction with the α-secretase, but most likely caused by a change in β-secretase cleavage. It has been reported that wild-type APP is preferentially cleaved by the β-secretase BACE1 at the β'-cleavage site before position 11 of the Aβ region (Figure 3) to generate C89 and truncated Aβ (Deng *et al,* 2013). The A2V mutation has been demonstrated to shift the preferential cleavage site of the β-secretase from position 11 to position 1 of the Aβ region, resulting in a much higher Aβ level (Zhang *et al,* 2017). As β- and α-secretase may compete for substrate, the change in β-secretase specificity and

increase in β-cleavage might be responsible for the reduced sAPPα generation observed in this study.

In summary, the different propensity for amyloidogenic processing of the examined APP mutants could not be associated with an altered clustering degree or interaction with ADAM10.

6.1.2 Influence of the APP expression level on cluster organisation

As the cross-linking assays and mutant studies required overexpressed APP and there was an even further increase of the protein level by α-secretase inhibition, this study first aimed to characterize possible differences in the plasmalemmal organisation of APP dependant on the protein level.

When endogenously expressed in SH-SY5Y cells, APP was found to be concentrated in clusters with an average density of ~ 2.2 maxima per μm^2 and a cluster size of ~ 110 nm (Figure 9). Maxima sizes may be oversestimated, as maxima are enlarged due to the excitation point spread function (PSF). That the determined cluster size is higher than a previously reported cluster size of ~ 70 nm (de Coninck *et al,* 2018) is not due to this effect, as both cluster sizes were not corrected for the PSF. The difference can be partly explained by technical limitations in obtaining absolute values of cluster size. For high-resolution STED microscopy high staining intensities are required for image acquisition. For this purpose, first and secondary antibodies are commonly used. However, when using this method labelled proteins might be coated by a shell of multivalent antibodies, which can potentially increase the estimated maxima size. It was estimated that the primary-secondary antibody complex increases the diameter of labelled structures by ~ 20 nm, as has been observed when analyzing the size of microtubuli (Aquino *et al,* 2011). Moreover, a high deexcitation laser power during image acquisition is accompanied by a general reduction in signal intensity and a higher resolution. In this study, a lower STED laser power was used than in the previous study (de Coninck *et al,* 2018) which could result in more fluorophores remaining excited around the center of the deexcitation donut accounting for a lower resolution. Another challenge in the determination of cluster sizes is the analysis of microscopy data, which involves recognition and delineation of maxima, line scan analysis and fitting of the line scan with a Gaussian function to obtain the full-width at half maximum (FWHM; Figure 8). During this analysis, different thresholds compared to de Coninck *et al* (2018) were chosen for excluding maxima from the analysis, which may also have an impact on the determined average cluster size. Furthermore, the expression level

also has an influence on the cluster size and density as already demonstrated in Figure 9. In the cell passage or growth phase of the cells used in this project the APP expression might have been higher leading to a higher size and number of clusters than determined in a previous study (de Coninck *et al,* 2018).

In any case, overexpression of APP-GFP in SH-SY5Y and HepG2 cells yields high concentrations of APP in membrane sheets. Inhibition of α-secretase cleavage by the broad metalloprotease inhibitor Batimastat proved to further increase the cellular as well as the plasmalemmal protein level of overexpressed APP (Figure 12 and Figure 13). The higher protein level resulted in a change of the cluster characteristics. Upon α-secretase inhibition a strong effect on the maxima intensity was observed (Figure 13C), which hints towards a higher number of APP molecules within each cluster. Additionally, a slightly higher density of clusters could be determined (Figure 13D), that however correlates less with the increase in expression level. Therefore, the elevation of the protein level seems to increase the number of molecules within each cluster which probably results in a higher packing density and clustering degree rather than an enlargement of clusters.

It was tested next, how the increased protein level and consequently more cluster formation affected the dynamics of APP in the plasma membrane. The inhibition of α-secretase cleavage led to doubling of the half time of recovery in FRAP experiments from 5 s to 10 s (Figure 15). The higher cluster number and higher number of molecules within clusters caused by the protein elevation likely reduced the mobility of APP in the membrane. These results are in line with previous studies, as clustered membrane proteins have been shown to be restricted in diffusion (He & Marguet, 2011; Zilly *et al,* 2011) and it was already demonstrated that an increasing clustering degree reduced the mobility of APP (Schreiber *et al,* 2012).

All in all, overexpression as well as α-secretase inhibition resulted in an increase in protein level, a higher degree of clustering and decreased mobility of APP.

6.2 Lateral organisation of ADAM10 and ADAM17 in plasmalemmal clusters and possible physiological function

Even though the most relevant physiological α-secretase ADAM10 and the main regulated α-secretase ADAM17 are the best characterized members of the ADAM family, the nanoscale organisation at the plasma membrane and possible implications for their function have not yet been studied. Therefore, in this study, the distribution of ADAM10

and ADAM17 in the plasma membrane of SH-SY5Y as well as HepG2 cells was examined by STED microscopy.

It is noteworthy that ADAM clusters are 4-10-times more abundant in SH-SY5Y cells compared to HepG2 cells (Figure 18A, B; Figure 19A, B), pointing towards different expression levels in different cellular systems. Additionally, ADAM10 maxima are two-times more frequent than ADAM17 maxima in HepG2 cells, whereas in SH-SY5Y cells it is the other way around. The different abundance of ADAM10 and ADAM17 on the cell surface of different cell lines could be related to their different substrate specifities. While some substrates, such as APP, can be processed by both ADAM10 and ADAM17, other substrates are specifically cleaved by either ADAM10 or ADAM17 (Pruessmeyer & Ludwig, 2009). Hence, the expression of certain substrates might have an influence on the expression of the proteases and might explain the different ADAM10 and ADAM17 abundance in separate cell types. Additionally, cell activation may also play a role for cell surface expression. While ADAM10 is constitutively present in the plasma membrane in most cell types, ADAM17 was only found in low levels on the cell surface, but ADAM17 expression increased when stimulated with phorbol esters (Ebsen *et al,* 2013).

ADAM10 and ADAM17 were found to be concenctrated in punctate nanodomains across the plasma membrane (Figure 11). *This raised the question, what the detected maxima actually represent on the level of molecular architecture; are they monomers, dimers or large clusters? The ADAM maxima intensities are brighter as expected for single molecule labelling, pointing to the presence of more than one molecule at the maxima location*. For these nanodomains an average cluster size of ~ 120 nm in SH-SY5Y cells and ~ 125 nm in HepG2 cells (Figure 10) was determined. This hints towards a supramolecular organisation of ADAMs. *However, the distribution of the secretase maxima sizes are close to the resolution limit of the microscope (*90 – 130 nm in SH-SY5Y cells and 110 – 160 nm in HepG2 cells, Figure 11*). Therefore, it is not possible to come up with a reliable estimate about the real physical size of the secretase architectures, which could clarifiy whether maxima are large membrane domains consisting of many secretase molecules. In any case, molecular species reflected by the secretase maxima likely are too large to enter the APP clusters, for which reason APP may be only accessible for processing at the periphery of the APP cluster* (text passages in *italic* taken and modified from Hitschler & Lang (submitted 2021)).

Protein clustering may therefore be a mechanism to maintain a reservoir of biochemical inactive membrane proteins and to block protein activity and interaction by steric hindrance,

as already described for some membrane proteins (Bethani *et al,* 2007; Bethani *et al,* 2009; Bar-On *et al,* 2009).

6.3 A physical interaction of ADAM10 with APP underlying its predominant role in α-processing

Examining the effect of ADAM10 overexpression, knockdown or mutation on the amount of APP cleavage products and plaque formation *in vitro* and in *vivo* (Jorissen *et al,* 2010; Jouannet *et al,* 2016; Kuhn *et al,* 2010; Lammich *et al,* 1999; Postina *et al,* 2004; Xu *et al,* 2009) revealed that ADAM10 is the physiologically relevant α-secretase. The comparison of a broad to an ADAM10 specific inhibitor in this study confirmed that ADAM10 is responsible for 60 % and 70 % of α-cleavage in HepG2 and SH-SY5Y cells, respectively (Figure 17).

The predominant role of ADAM10 rather cannot be explained by a higher substrate specificity of ADAM10, as ADAM10 and ADAM17 exhibit a broad substrate specificity and share some overlapping substrates such as APP (Caescu et al, 2009). One possibility may be that protease turnover is dependent on the abundance of secretases in the plasma membrane. This hypothesis is supported by a study demonstrating that tetraspanin 15 regulates the cell surface expression and α-secretase activity of ADAM10 (Prox et al, 2012) (text passage in *italic* taken and modified from Hitschler & Lang (submitted 2021)). Another factor could be that the substrate specificity of ADAM10 and ADAM17 might at times be determined by a primary co-localization of enzyme and substrate in a common plasmalemmal nanodomain, as proposed previously (Reiss & Bhakdi, 2017). Finally, the binding affinity of the secretases to APP might resolve the predominant role of ADAM10. To determine if one of the above mentioned factors explains the role of ADAM10 as main physiological α-secretase, secretase abundance and nanoscale organisation of ADAM10 and ADAM17 in relation to APP were studied and the possibility of an interaction between APP and the secretases was investigated in the native membrane.

When looking at the secretase abundance at the cell surface, 2-fold more ADAM10 than ADAM17 maxima are present in HepG2 cells (Figure 18), in like with the predominant role of ADAM10. However, in SH-SY5Y cells the opposite is the case (Figure 19), although 70 % of α-secretase activity can be related to ADAM10 in this cell line (Figure 17). Therefore, protease abundance can be ruled out as the major factor determining the predominant secretase. Another possibility is the proximity of the proteases to their substrate. For example, ADAM10 might locate closer to its substrate APP. However, in HepG2 cells only

~18 % of the ADAM10 and ~31 % of the ADAM17 maxima were located in close proximity to APP (≤ 50 nm), which in principle would allow for a physical interaction. Relating the proportion of maxima close to APP to the total number of ADAM maxima, 0.12 ADAM10 and 0.10 ADAM17 APP-close maxima per μm^2 are obtained. These results indicate no clear preference for ADAM10 association in HepG2 cells. In SH-SY5Y cells, the percentage of ADAM10 and ADAM17 maxima in close proximity to APP was similar with ~ 17 % and ~ 20 %. When the proportion of APP-close secretase maxima is related to the abundance of maxima, 0.44 ADAM10 and 1.10 ADAM17 APP-close maxima per μm^2 are determined. Therefore, more ADAM17 maxima are closely associated with APP in SH-SY5Y cells than ADAM10 maxima. Consequently, the lateral organisation of the secretases and APP provides no explanation for the predominant α-cleavage of APP by ADAM10.

To examine if the binding affinity explains the predominant role of ADAM10, antibody-induced cross-linking of APP in the native membrane of HepG2 cells was utilized. The cross-linking of APP into aggregates increased the signal overlap of APP with ADAM10, but not with ADAM17 (Figure 21D). In conclusion, ADAM10 is dragged into the APP aggregates during cross-linking due to a physical interaction with its substrate. For this physical link, the transmembrane segment of APP seems to be necessary, as the substitution of the TMS diminished co-aggregation of APP and ADAM10 (Figure 23C). Additionally, α-cleavage of the APP-TMS mutant was reduced by half (Figure 24), indicating that the transmembrane segment of APP is necessary for processing. No such physical association was detected for ADAM17. This difference can explain why ADAM10 is the relevant physiological α-secretase.

Despite no detectable physical interaction, ADAM17 clusters associated in similar amounts with APP clusters as ADAM10 in directly fixed membrane sheets. Why the ADAM17 clusters are located in close proximity to APP can only be speculated. Maybe ADAM17 locates close to the substrate in a resting position, even when the substrate is constitutively processed by ADAM10. Recently, binary complexes containing both, α- and ɣ-secretases or β- and ɣ-secretases, have been identified and a model was proposed that proteases may form functional complexes to execute sequential cleavage efficiently (Chen *et al,* 2015). One study even found ternary complexes between α-, β- and ɣ-secretases (Wang & Pei, 2018). It is possible that complexes form between different α-secretases such as ADAM10 and ADAM17, explaining why both locate close to APP even if ADAM10 has a higher affinity to the substrate. In such a functional complex ADAM17 could cleave the substrate immediately when stimulated or make the α-cleavage of APP more efficient with

two α-secretases. ADAM17 might only bind to APP when activitated, which might be the reason why a physical interaction was not detected in the antibody-induced cross-linking assay.

6.4 Putative mechanism of the substrate-enzyme interaction mediated by the transmembrane segment of APP

About the exact mechanism of the physical interaction between APP and ADAM10 and how it affects processing can only be speculated. Little is known about which features of ADAM10, ADAM17 or its substrates determine their substrate affinity or specificity. ADAM substrate specificity does not rely on a specific amino acid signature (Caescu *et al,* 2009) recognized by the protease domain. On the other hand, it is known that non-catalytic domains of ADAM10 and ADAM17 can affect their substrate binding affinity and substrate cleavage site specificity (Stawikowska *et al,* 2013), possibly due to steric hindrance. By this mechanism, access to the secretase transmembrane domain may be regulated. Additionally, the secondary structure of substrates has been shown to regulate the activity and substrate affinity of ADAM10 and ADAM17 (Stawikowska *et al,* 2013). Therefore, certain conformations of the substrate APP may favor a higher substrate affinity of ADAM10 compared to ADAM17.

Cross-linking and processing assays revealed that the transmembrane domain is essential for physical association of ADAM10 to APP and for processing of the substrate (Figure 23 and Figure 24). Further specification of the relevant section within the TMS failed because all three investigated regions within the TMS seem to be required for co-aggregation and processing (Figure 25). One explanation for the importance of the APP transmembrane domain could lie in the four GxxxG or GxxxG-like motifs present in the extracellular juxtamembrane and transmembrane regions of APP (Khalifa *et al,* 2010) (Figure 3B). These motifs have been shown to mediate sequence-specific dimerization of α-helices in other transmembrane proteins (Lemmon *et al,* 1992; Russ & Engelman, 2000). It has been reported previously that pairwise replacement of the Glycines in the GxxxG motifs of APP by unpolar amino acids reduced Aβ production (Kienlen-Campard *et al,* 2008). Accumulation of β-cleavage products suggested that the γ-secretase was inhibited and enhanced dimerization of the CTF via a different α-helical transmembrane interface was proposed as a possible cause (Kienlen-Campard *et al,* 2008). These results indicated that a change in the dimer state of the APP transmembrane region might influence the interaction with and processing by secretases. Additionally, it has been shown that the

disruption of the GxxxG motifs by known FAD mutations destabilized the APP-transmembrane dimer and increased the proportion of monomers (Gorman *et al,* 2008). Additonally, mutations of cysteine residues responsible for dimer stabilization in a substrate of ADAM10, CD44, prevented dimerization of the substrate and consequently led to reduced cleavage by ADAM10 (Hartmann *et al,* 2015), suggesting that substrate dimerization is a prerequisite for induced cleavage by ADAM10. Therefore, the exchange of the TMS or substitution of specific amino acids in the TMS, as performed for the APP-TMS, APP(↔628-630), APP(↔634-639) and APP(↔641-644/646) mutants, might perturb the dimer state of the transmembrane region and explain the reduced interaction with and processing by ADAM10. However, more work is needed to investigate if the APP-TMS mutants used in this study indeed display a changed oligomerization state which could be a cause for the lost interaction with ADAM10. The dimer state could be examined by biochemical purification, followed by native PAGE and Western blot analysis. Another approach could be Fluorescence Resonance Energy Transfer (FRET) microscopy with donor- and acceptor labelled APP proteins.

ADAM10 as well as ADAM17 have been reported to dimerize in co-immunoprecipitation and cross-linking experiments (Xu *et al,* 2012) and the transmembrane domain of ADAM10 was identified to mediate ADAM10 dimerization (Deng *et al,* 2014). Therefore, the dimeric state of substrate and secretase mediated by the transmembrane domains of the proteins could regulate the physical substrate-enzyme interaction.

6.5 Therapeutic potential of the physical interaction identified between APP and ADAM10

α- and β-secretases are generally thought to be inversely active and compete for APP as substrate. Multiple studies already demonstrated that an upregulation of α-cleavage led to a reduction of β-secretase activity (Hung *et al,* 1993; Buxbaum *et al,* 1998; Koike *et al,* 1999; Skovronsky *et al,* 2000; Postina *et al,* 2004; Fu *et al,* 2009). Since the α-secretase cleaves APP within the Aβ region and thereby can preclude neurotoxic Aβ generation, the stimulation of α-secretase cleavage and consequent reduction of β-cleavage is considered a promising therapeutic approach for treating AD. Strategies for enhancing α-secretase cleavage thus far comprise overexpression of the α-secretase ADAM10 (Postina *et al,* 2004), or of the proprotein convertases PC7 and furin to promote ADAM10 maturation (Anders *et al,* 2001), or the use of retinoic acid for induction of the ADAM10 promoter

(Fahrenholz, 2007). However, chronic upregulation of the α-secretase might have negative effects on the cleavage of the multiple other substrates of ADAM10 (Kumar *et al,* 2018).

The physical link between the physiologically relevant α-secretase ADAM10 and APP identified in this study might improve the understanding of the substrate-enzyme interaction and provide new opportunities for enhancing α-secretase cleavage. If the physical interaction between APP and ADAM10 could be strengthened, α-processing of APP might be boosted, preventing Aβ generation. As activation of protein kinase C by the phorbol ester PMA has been shown to stimulate α-cleavage and reduce Aβ generation (Buxbaum *et al,* 1993), it was examined in this study if PMA could improve the interaction of α-secretases with APP. However, PMA did not strengthen the physical interaction of ADAM10 with APP and did not result in an increased affinity of ADAM17 to the substrate APP (Figure 28). Since PMA mainly regulates α-secretase activity of ADAM17 (Buxbaum *et al,* 1998), maybe other stimulators are necessary for the constitutive α-secretase ADAM10. For example, the neurotransmitter PACAP appeared to mainly stimulate ADAM10 mediated processing of APP by activation of different signaling pathways (Kojro *et al,* 2006). The detailed molecular mechanism of PACAP-enhanced α-secretase activity has not been elucidated thus far, but it was proposed that tetraspanins form complexes with ADAMs, G protein-coupled receptors and integrins upon activation of the receptors by PACAP and promote association of ADAM10 and its substrate APP (Kojro *et al,* 2006). Therefore, it might be interesting to examine if the neurotransmitter PACAP may affect the physical interaction of ADAM10 with the substrate APP. Additionally, a possible involvement of tetraspanins in the ADAM10-APP interaction might be interesting to study. Tetraspaning 15 and Tetraspanin 12 have been already demonstrated to interact with ADAM10, stimulate ADAM10 maturation and thereby increase α-cleavage (Prox *et al,* 2012; Xu *et al,* 2009). In contrast to that, tetraspanin 3 does not affect the maturation or cell surface expression of ADAM10 but has been found to bind to ADAM10, APP and the γ-secretase complex which suggested that tetraspanin 3 may stabilize the interaction between the enzymes and its substrate APP (Seipold *et al,* 2017).

In conclusion, the mechanism regulating the physical interaction between the physiologically relevant α-secretase ADAM10 and the substrate APP needs to be better understood and other possibilities need to be exploited to strengthen the substrate-enzyme interaction and enhance α-cleavage for treatment of AD.

6.6 Conclusion

In this study, we investigated why ADAM10 is the predominat, constitutive α-secretase in APP processing. We examined the lateral association and abundance of α-secretases as well as the interaction with APP. Utilizing antibody-induced cross-linking in the native plasma membrane, we identify a physical interaction of APP with ADAM10 but not with ADAM17, explaining the predominant role of ADAM10. More work is needed to understand the precise underlying mechanisms of this physical interaction. This assay may prove to be a useful tool for further analysis of the substrate-secretase interaction, which in turn might help in the development of therapeutic strategies against the progression of Alzheimer's disease by enhancing α-secretase processing.

7 References

Aizenstein HJ, Nebes RD, Saxton JA, Price JC, Mathis CA, Tsopelas ND, Ziolko SK, James JA, Snitz BE, Houck PR et al (2008) Frequent amyloid deposition without significant cognitive impairment among the elderly. *Arch Neuro* 65: 1509–1517

Ali MH, Imperiali B (2005) Protein oligomerization: how and why. *Bioorg Med Chem* 13: 5013–5020

Alonso AC, Zaidi T, Grundke-Iqbal I, Iqbal K (1994) Role of abnormally phosphorylated tau in the breakdown of microtubules in Alzheimer disease. *Proc Natl Acad Sci USA* 91: 5562–5566

Alzheimer A (1907) Über eine eigenartige Erkrankung der Hirnrinde. *Allg Z Psych* 64: 146–148

Alzheimer's Association (2021) Alzheimer's disease facts and figures. *Alzheimers Dement* 17: 327–406

Amtul Z, Wang L, Westaway D, Rozmahel RF (2010) Neuroprotective mechanism conferred by 17beta-estradiol on the biochemical basis of Alzheimer's disease. *Neuroscience* 169: 781–786

Anders A, Gilbert S, Garten W, Postina R, Fahrenholz F (2001) Regulation of the alpha-secretase ADAM10 by its prodomain and proprotein convertases. *FASEB J* 15: 1837–1839

Aquino D, Schönle A, Geisler C, Middendorff CV, Wurm CA, Okamura Y, Lang T, Hell SW, Egner A (2011) Two-color nanoscopy of three-dimensional volumes by 4Pi detection of stochastically switched fluorophores. *Nat Methods* 8: 353–359

Araki W, Kitaguchi N, Tokushima Y, Ishii K, Aratake H, Shimohama S, Nakamura S, Kimura J (1991) Trophic effect of β-amyloid precursor protein on cerebral cortical neurons in culture. *Biochem Biophys Res Commun* 181: 265–271

Arribas J, Coodly L, Vollmer P, Kishimoto TK, Rose-John S, Massagué J (1996) Diverse cell surface protein ectodomains are shed by a system sensitive to metalloprotease inhibitors. *J Biol Chem* 271: 11376–11382

Aydin D, Weyer SW, Müller UC (2012) Functions of the APP gene family in the nervous system: insights from mouse models. *Exp Brain Res* 217: 423–434

Barker WW, Luis CA, Kashuba A, Luis M, Harwood DG, Loewenstein D, Waters C, Jimison P, Shepherd E, Sevush S et al (2002) Relative frequencies of Alzheimer disease, Lewy body, vascular and frontotemporal dementia, and hippocampal sclerosis in the State of Florida Brain Bank. *Alzheimer Dis Assoc Disord* 16: 203

Bar-On D, Gutman M, Mezer A, Ashery U, Lang T, Nachliel E (2009) Evaluation of the heterogeneous reactivity of the syntaxin molecules on the inner leaflet of the plasma membrane. *J Neurosci* 29: 12292–12301

Barrett PJ, Song Y, van Horn WD, Hustedt EJ, Schafer JM, Hadziselimovic A, Beel AJ, Sanders CR (2012) The amyloid precursor protein has a flexible transmembrane domain and binds cholesterol. *Science* 336: 1168–1171

Baruch-Suchodolsky R, Fischer B (2009) Abeta40, either soluble or aggregated, is a remarkably potent antioxidant in cell-free oxidative systems. *Biochemistry* 48: 4354–4370

Beel AJ, Sakakura M, Barrett PJ, Sanders CR (2010) Direct binding of cholesterol to the amyloid precursor protein: An important interaction in lipid-Alzheimer's disease relationships? *Biochim Biophys Acta* 1801: 975–982

Beel AJ, Sanders CR (2008) Substrate specificity of gamma-secretase and other intramembrane proteases. *Cell Mol Life Sci* 65: 1311–1334

Benilova I, Gallardo R, Ungureanu A-A, Castillo Cano V, an Snellinx, Ramakers M, Bartic C, Rousseau F, Schymkowitz J, Strooper B de (2014) The Alzheimer disease protective mutation A2T modulates kinetic and thermodynamic properties of amyloid-β (Aβ) aggregation. *J Biol Chem* 289: 30977–30989

Bertram L, Lill CM, Tanzi RE (2010) The genetics of Alzheimer disease: back to the future. *Neuron* 68: 270–281

Bethani I, Lang T, Geumann U, Sieber JJ, Jahn R, Rizzoli SO (2007) The specificity of SNARE pairing in biological membranes is mediated by both proof-reading and spatial segregation. *EMBO J* 26: 3981–3992

Bethani I, Werner A, Kadian C, Geumann U, Jahn R, Rizzoli SO (2009) Endosomal fusion upon SNARE knockdown is maintained by residual SNARE activity and enhanced docking. *Traffic* 10: 1543–1559

Betts V, Leissring MA, Dolios G, Wang R, Selkoe DJ, Walsh DM (2008) Aggregation and catabolism of disease-associated intra-Abeta mutations: reduced proteolysis of AbetaA21G by neprilysin. *Neurobiol. Dis.* 31: 442–450

Blacker M, Noe MC, Carty TJ, Goodyer CG, LeBlanc AC (2002) Effect of tumor necrosis factor-alpha converting enzyme (TACE) and metalloprotease inhibitor on amyloid precursor protein metabolism in human neurons. *J Neurochem* 83: 1349–1357

Blennow K, Leon MJ de, Zetterberg H (2006) Alzheimer‘s disease. *Lancet* 368: 387–403

Bodovitz S, Falduto MT, Frail DE, Klein WL (1995) Iron levels modulate alpha-secretase cleavage of amyloid precursor protein. *J Neurochem* 64: 307–315

Borg JP, Ooi J, Levy E, Margolis B (1996) The phosphotyrosine interaction domains of X11 and FE65 bind to distinct sites on the YENPTY motif of amyloid precursor protein. *Mol Cell Biol* 16: 6229–6241

Bracco L, Gallato R, Grigoletto F, Lippi A, Lepore V, Bino G, Lazzaro MP, Carella F, Piccolo T, Pozzilli C (1994) Factors affecting course and survival in Alzheimer’s disease. A 9-year longitudinal study. *Arch Neuro* 51: 1213–1219

Brandt R, Lee G (1993) Functional organization of microtubule-associated protein tau. Identification of regions which affect microtubule growth, nucleation, and bundle formation in vitro. *J Biol Chem* 268: 3414–3419

Bulic B, Ness J, Hahn S, Rennhack A, Jumpertz T, Weggen S (2011) Chemical biology, molecular mechanism and clinical perspective of γ-secretase modulators in Alzheimer’s disease. *Curr Neuropharmacol* 9: 598–622

Buxbaum JD, Koo EH, Greengard P (1993) Protein phosphorylation inhibits production of Alzheimer amyloid beta/A4 peptide. *Proc Natl Acad Sci USA* 90: 9195–9198

Buxbaum JD, Liu KN, Luo Y, Slack JL, Stocking KL, Peschon JJ, Johnson RS, Castner BJ, Cerretti DP, Black RA (1998) Evidence that tumor necrosis factor alpha converting enzyme is involved in regulated alpha-secretase cleavage of the Alzheimer amyloid protein precursor. *J Biol Chem* 273: 27765–27767

Buxbaum JD, Oishi M, Chen HI, Pinkas-Kramarski R, Jaffe EA, Gandy SE, Greengard P (1992) Cholinergic agonists and interleukin 1 regulate processing and secretion of the Alzheimer beta/A4 amyloid protein precursor. *Proc Natl Acad Sci USA* 89: 10075–10078

Caccamo A, Oddo S, Billings LM, Green KN, Martinez-Coria H, Fisher A, LaFerla FM (2006) M1 receptors play a central role in modulating AD-like pathology in transgenic mice. *Neuron* 49: 671–682

Caescu CI, Jeschke GR, Turk BE (2009) Active-site determinants of substrate recognition by the metalloproteinases TACE and ADAM10. *Biochem J* 424: 79–88

Caporaso GL, Gandy SE, Buxbaum JD, Ramabhadran TV, Greengard P (1992) Protein phosphorylation regulates secretion of Alzheimer beta/A4 amyloid precursor protein. *Proc Natl Acad Sci USA* 89: 3055–3059

Castellani RJ, Plascencia-Villa G, Perry G (2019) The amyloid cascade and Alzheimer’s disease therapeutics: theory versus observation. *Lab Invest* 99: 958–970

Cebecauer M, Spitaler M, Sergé A, Magee AI (2010) Signalling complexes and clusters: functional advantages and methodological hurdles. *J Cell Sci* 123: 309–320

Chan D, Janssen JC, Whitwell JL, Watt HC, Jenkins R, Frost C, Rossor MN, Fox NC (2003) Change in rates of cerebral atrophy over time in early-onset Alzheimer's disease: longitudinal MRI study. *Lancet* 362: 1121–1122

Chen AC, Kim S, Shepardson N, Patel S, Hong S, Selkoe DJ (2015) Physical and functional interaction between the α- and γ-secretases: A new model of regulated intramembrane proteolysis. *J Cell Biol* 211: 1157–1176

Chen W-T, Hong C-J, Lin Y-T, Chang W-H, Huang H-T, Liao J-Y, Chang Y-J, Hsieh Y-F, Cheng C-Y, Liu H-C et al (2012) Amyloid-beta (Aβ) D7H mutation increases oligomeric Aβ42 and alters properties of Aβ-zinc/copper assemblies. *PLoS One* 7: e35807

Chyung JH, Raper DM, Selkoe DJ (2005) Gamma-secretase exists on the plasma membrane as an intact complex that accepts substrates and effects intramembrane cleavage. *J Biol Chem* 280: 4383–4392

Cissé MA, Sunyach C, Lefranc-Jullien S, Postina R, Vincent B, Checler F (2005) The disintegrin ADAM9 indirectly contributes to the physiological processing of cellular prion by modulating ADAM10 activity. *J Biol Chem* 280: 40624–40631

Citron M, Oltersdorf T, Haass C, McConlogue L, Hung AY, Seubert P, Vigo-Pelfrey C, Lieberburg I, Selkoe DJ (1992) Mutation of the beta-amyloid precursor protein in familial Alzheimer's disease increases beta-protein production. *Nature* 360: 672–674

Citron M, Teplow DB, Selkoe DJ (1995) Generation of amyloid β protein from its precursor is sequence specific. *Neuron* 14: 661–670

Cossec J-C, Simon A, Marquer C, Moldrich RX, Leterrier C, Rossier J, Duyckaerts C, Lenkei Z, Potier M-C (2010) Clathrin-dependent APP endocytosis and Abeta secretion are highly sensitive to the level of plasma membrane cholesterol. *Biochim Biophys Acta* 1801: 846–852

Cureton DK, Harbison CE, Cocucci E, Parrish CR, Kirchhausen T (2012) Limited transferrin receptor clustering allows rapid diffusion of canine parvovirus into clathrin endocytic structures. *J Virol* 86: 5330–5340

Daigle I, Li C (1993) apl-1, a Caenorhabditis elegans gene encoding a protein related to the human beta-amyloid protein precursor. *Proc Natl Acad Sci USA* 90: 12045–12049

de Coninck D (2020) *Structural aspects of the plasmalemmal amyloid precursor protein cluster.* PhD thesis. University of Bonn, Bonn, Germany

de Coninck D, Schmidt TH, Schloetel J-G, Lang T (2018) Packing density of the amyloid precursor protein in the cell membrane. *Biophys J* 114: 1128–1141

de Jonghe C, Esselens C, Kumar-Singh S, Craessaerts K, Serneels S, Checler F, Annaert W, van Broeckhoven C, Strooper B de (2001) Pathogenic APP mutations near the gamma-secretase cleavage site differentially affect Abeta secretion and APP C-terminal fragment stability. *Hum Mol Genet* 10: 1665–1671

DeKosky ST, Scheff SW, Styren SD (1996) Structural correlates of cognition in dementia: quantification and assessment of synapse change. *Neurodegeneration* 5: 417–421

Deng W, Cho S, Su P-C, Berger BW, Li R (2014) Membrane-enabled dimerization of the intrinsically disordered cytoplasmic domain of ADAM10. *Proc Natl Acad Sci USA* 111: 15987–15992

Deng Y, Wang Z, Wang R, Zhang X, Zhang S, Wu Y, Staufenbiel M, Cai F, Song W (2013) Amyloid-β protein (Aβ) Glu11 is the major β-secretase site of β-site amyloid-β precursor protein-cleaving enzyme 1 (BACE1), and shifting the cleavage site to Aβ Asp1 contributes to Alzheimer pathogenesis. *Eur J Neurosci* 37: 1962–1969

Deyts C, Thinakaran G, Parent AT (2016) APP receptor? To be or not to be. *Trends Pharmacol Sci* 37: 390–411

Di Fede G, Catania M, Morbin M, Rossi G, Suardi S, Mazzoleni G, Merlin M, Giovagnoli AR, Prioni S, Erbetta A et al (2009) A recessive mutation in the APP gene with dominant-negative effect on amyloidogenesis. *Science* 323: 1473–1477

Dominguez D, Tournoy J, Hartmann D, Huth T, Cryns K, Deforce S, Serneels L, Camacho IE, Marjaux E, Craessaerts K et al (2005) Phenotypic and biochemical analyses of BACE1- and BACE2-deficient mice. *J Biol Chem* 280: 30797–30806

Dovey HF, John V, Anderson JP, Chen LZ, Saint Andrieu P de, Fang LY, Freedman SB, Folmer B, Goldbach E, Holsztynska EJ et al (2001) Functional gamma-secretase inhibitors reduce beta-amyloid peptide levels in brain. *J Neurochem* 76: 173–181

Drechsel DN, Hyman AA, Cobb MH, Kirschner MW (1992) Modulation of the dynamic instability of tubulin assembly by the microtubule-associated protein tau. *Mol Biol Cell* 3: 1141–1154

Dries DR, Shah S, Han Y-H, Yu C, Yu S, Shearman MS, Yu G (2009) Glu-333 of nicastrin directly participates in gamma-secretase activity. *J Biol Chem* 284: 29714–29724

Drubin DG, Kirschner MW (1986) Tau protein function in living cells. *J Cell Biol* 103: 2739–2746

Dyrks T, Weidemann A, Multhaup G, Salbaum JM, Lemaire HG, Kang J, Müller-Hill B, Masters CL, Beyreuther K (1988) Identification, transmembrane orientation and biogenesis of the amyloid A4 precursor of Alzheimer's disease. *EMBO J* 7: 949–957

Ebsen H, Schröder A, Kabelitz D, Janssen O (2013) Differential surface expression of ADAM10 and ADAM17 on human T lymphocytes and tumor cells. *PLoS One* 8: e76853

Edbauer D, Winkler E, Regula JT, Pesold B, Steiner H, Haass C (2003) Reconstitution of gamma-secretase activity. *Nat Cell Biol* 5: 486–488

Ehehalt R, Keller P, Haass C, Thiele C, Simons K (2003) Amyloidogenic processing of the Alzheimer beta-amyloid precursor protein depends on lipid rafts. *J Cell Biol* 160: 113–123

Esch FS, Keim PS, Beattie EC, Blacher RW, Culwell AR, Oltersdorf T, McClure D, Ward PJ (1990) Cleavage of amyloid beta peptide during constitutive processing of its precursor. *Science* 248: 1122–1124

Fahrenholz F (2007) Alpha-secretase as a therapeutic target. *Curr Alzheimer Res* 4: 412–417

Fahrenholz F, Gilbert S, Kojro E, Lammich S, Postina R (2000) Alpha-secretase activity of the disintegrin metalloprotease ADAM 10. Influences of domain structure. *Ann NY Acad Sci* 920: 215–222

Finke J, Mikuličić S, Loster A-L, Gawlitza A, Florin L, Lang T (2020) Anatomy of a viral entry platform differentially functionalized by integrins α3 and α6. *Sci Rep* 10: 5356

Förstl H, Kurz A (1999) Clinical features of Alzheimer's disease. *Eur Arch Psychiatry Clin Neurosci* 249: 288–290

Fortna RR, Crystal AS, Morais VA, Pijak DS, Lee VM-Y, Doms RW (2004) Membrane topology and nicastrin-enhanced endoproteolysis of APH-1, a component of the gamma-secretase complex. *J Biol Chem* 279: 3685–3693

Francis R, McGrath G, Zhang J, Ruddy DA, Sym M, Apfeld J, Nicoll M, Maxwell M, Hai B, Ellis MC et al (2002) aph-1 and pen-2 are required for Notch pathway signaling, γ-secretase cleavage of βAPP, and presenilin protein accumulation. *Dev Cell* 3: 85–97

Frykman S, Hur J-Y, Frånberg J, Aoki M, Winblad B, Nahalkova J, Behbahani H, Tjernberg LO (2010) Synaptic and endosomal localization of active gamma-secretase in rat brain. *PLoS One* 5: e8948

Fu H, Dou J, Li W, Cui W, Mak S, Hu Q, Luo J, Lam CSC, Pang Y, Youdim MBH et al (2009) Promising multifunctional anti-Alzheimer's dimer bis(7)-Cognitin acting as an activator of protein kinase C regulates activities of alpha-secretase and BACE-1 concurrently. *Eur J Pharmacol* 623: 14–21

Funamoto S, Sasaki T, Ishihara S, Nobuhara M, Nakano M, Watanabe-Takahashi M, Saito T, Kakuda N, Miyasaka T, Nishikawa K et al (2013) Substrate ectodomain is critical for substrate preference and inhibition of γ-secretase. *Nat Commun* 4: 2529

Galmes R, Delaunay J-L, Maurice M, Aït-Slimane T (2013) Oligomerization is required for normal endocytosis/transcytosis of a GPI-anchored protein in polarized hepatic cells. *J Cell Sci* 126: 3409–3416

Gatz M, Reynolds CA, Fratiglioni L, Johansson B, Mortimer JA, Berg S, Fiske A, Pedersen NL (2006) Role of genes and environments for explaining Alzheimer disease. *Arch Gen Psychiatry* 63: 168–174

Glenner GG, Wong CW (1984) Alzheimer's disease and Down's syndrome: Sharing of a unique cerebrovascular amyloid fibril protein. *Biochem Biophys Res Commun* 122: 1131–1135

Goate A, Chartier-Harlin MC, Mullan M, Brown J, Crawford F, Fidani L, Giuffra L, Haynes A, Irving N, James L (1991) Segregation of a missense mutation in the amyloid precursor protein gene with familial Alzheimer's disease. *Nature* 349: 704–706

Goedert M (1987) Neuronal localization of amyloid beta protein precursor mRNA in normal human brain and in Alzheimer's disease. *EMBO J* 6: 3627–3632

Goedert M, Spillantini MG, Cairns NJ, Crowther RA (1992) Tau proteins of alzheimer paired helical filaments: Abnormal phosphorylation of all six brain isoforms. *Neuron* 8: 159–168

Goodman Y, Mattson MP (1994) Secreted forms of beta-amyloid precursor protein protect hippocampal neurons against amyloid beta-peptide-induced oxidative injury. *Exp Neurol* 128: 1–12

Goodsell DS, Olson AJ (2000) Structural symmetry and protein function. *Annu Rev Biophys Biomol Struct* 29: 105–153

Gorman PM, Kim S, Guo M, Melnyk RA, McLaurin J, Fraser PE, Bowie JU, Chakrabartty A (2008) Dimerization of the transmembrane domain of amyloid precursor proteins and familial Alzheimer's disease mutants. *BMC Neurosci* 9: 17

Gouras GK, Xu H, Jovanovic JN, Buxbaum JD, Wang R, Greengard P, Relkin NR, Gandy S (1998) Generation and regulation of beta-amyloid peptide variants by neurons. *J Neurochem* 71: 1920–1925

Green RC, Schneider LS, Amato DA, Beelen AP, Wilcock G, Swabb EA, Zavitz KH (2009) Effect of tarenflurbil on cognitive decline and activities of daily living in patients with mild Alzheimer disease: a randomized controlled trial. *JAMA* 302: 2557–2564

Grundke-Iqbal I, Iqbal K, Tung YC, Quinlan M, Wisniewski HM, Binder LI (1986) Abnormal phosphorylation of the microtubule-associated protein tau (tau) in Alzheimer cytoskeletal pathology. *Proc Natl Acad Sci USA* 83: 4913–4917

Gu Y, Misonou H, Sato T, Dohmae N, Takio K, Ihara Y (2001) Distinct intramembrane cleavage of the beta-amyloid precursor protein family resembling gamma-secretase-like cleavage of Notch. *J Biol Chem* 276: 35235–35238

Guo Q, Wang Z, Li H, Wiese M, Zheng H (2012) APP physiological and pathophysiological functions: insights from animal models. *Cell Res* 22: 78–89

Gustke N, Trinczek B, Biernat J, Mandelkow EM, Mandelkow E (1994) Domains of tau protein and interactions with microtubules. *Biochemistry* 33: 9511–9522

Haapasalo A, Kovacs DM (2011) The many substrates of presenilin/γ-secretase. *J Alzheimers Dis* 25: 3–28

Haass C, Capell A, Citron M, Teplow DB, Selkoe DJ (1995a) The vacuolar H(+)-ATPase inhibitor bafilomycin A1 differentially affects proteolytic processing of mutant and wild-type beta-amyloid precursor protein. *J Biol Chem* 270: 6186–6192

Haass C, Hung AY, Schlossmacher MG, Teplow DB, Selkoe DJ (1993) beta-Amyloid peptide and a 3-kDa fragment are derived by distinct cellular mechanisms. *J Biol Chem* 268: 3021–3024

Haass C, Kaether C, Thinakaran G, Sisodia S (2012) Trafficking and proteolytic processing of APP. *Cold Spring Harb Perspect Med* 2: a006270

Haass C, Koo EH, Mellon A, Hung AY, Selkoe DJ (1992) Targeting of cell-surface beta-amyloid precursor protein to lysosomes: alternative processing into amyloid-bearing fragments. *Nature* 357: 500–503

Haass C, Lemere CA, Capell A, Citron M, Seubert P, Schenk D, Lannfelt L, Selkoe DJ (1995b) The Swedish mutation causes early-onset Alzheimer's disease by beta-secretase cleavage within the secretory pathway. *Nat Med* 1: 1291–1296

Hardy JA, Higgins GA (1992) Alzheimer's disease: the amyloid cascade hypothesis. *Science* 256: 184–185

Hartmann M, Parra LM, Ruschel A, Lindner C, Morrison H, Herrlich A, Herrlich P (2015) Inside-out regulation of ectodomain cleavage of cluster-of-differentiation-44 (CD44) and of neuregulin-1 requires substrate dimerization. *J Biol Chem* 290: 17041–17054

He H-T, Marguet D (2011) Detecting nanodomains in living cell membrane by fluorescence correlation spectroscopy. *Annu Rev Phys Chem* 62: 417–436

He X, Cooley K, Chung CHY, Dashti N, Tang J (2007) Apolipoprotein receptor 2 and X11 alpha/beta mediate apolipoprotein E-induced endocytosis of amyloid-beta precursor protein and beta-secretase, leading to amyloid-beta production. *J Neurosci* 27: 4052–4060

Heber S, Herms J, Gajic V, Hainfellner J, Aguzzi A, Rülicke T, Kretzschmar H, Koch C von, Sisodia S, Tremml P et al (2000) Mice with combined gene knock-outs reveal essential and partially redundant functions of amyloid precursor protein family members. *J Neurosci* 20: 7951–7963

Herms J, Anliker B, Heber S, Ring S, Fuhrmann M, Kretzschmar H, Sisodia S, Müller U (2004) Cortical dysplasia resembling human type 2 lissencephaly in mice lacking all three APP family members. *EMBO J* 23: 4106–4115

Herreman A, Serneels L, Annaert W, Collen D, Schoonjans L, Strooper B de (2000) Total inactivation of gamma-secretase activity in presenilin-deficient embryonic stem cells. *Nat Cell Biol* 2: 461–462

Hesse L, Beher D, Masters CL, Multhaup G (1994) The βA4 amyloid precursor protein binding to copper. *FEBS Lett* 349: 109–116

Hitschler L, Lang T (submitted 2021) The APP transmembrane domain is required for anti-amyloidogenic processing by ADAM10. *(Manuscript submitted)*

Ho A, Südhof TC (2004) Binding of F-spondin to amyloid-beta precursor protein: a candidate amyloid-beta precursor protein ligand that modulates amyloid-beta precursor protein cleavage. *Proc Natl Acad Sci USA* 101: 2548–2553

Hofman EG, Bader AN, Voortman J, van den Heuvel DJ, Sigismund S, Verkleij AJ, Gerritsen HC, van Bergen en Henegouwen PMP (2010) Ligand-induced EGF receptor oligomerization is kinase-dependent and enhances internalization. *J Biol Chem* 285: 39481–39489

Howard L, Lu X, Mitchell S, Griffiths S, Glynn P (1996) Molecular cloning of MADM: a catalytically active mammalian disintegrin-metalloprotease expressed in various cell types. *Biochem J* 317: 45–50

Hu X, He W, Diaconu C, Tang X, Kidd GJ, Macklin WB, Trapp BD, Yan R (2008) Genetic deletion of BACE1 in mice affects remyelination of sciatic nerves. *FASEB J* 22: 2970–2980

Hu X, Hicks CW, He W, Wong P, Macklin WB, Trapp BD, Yan R (2006) Bace1 modulates myelination in the central and peripheral nervous system. *Nat Neurosci* 9: 1520–1525

Hung AY, Haass C, Nitsch RM, Qiu WQ, Citron M, Wurtman RJ, Growdon JH, Selkoe DJ (1993) Activation of protein kinase C inhibits cellular production of the amyloid beta-protein. *J Biol Chem* 268: 22959–22962

Hurd MD, Martorell P, Delavande A, Mullen KJ, Langa KM (2013) Monetary costs of dementia in the United States. *N Engl J Med* 368: 1326–1334

Hussain I, Powell D, Howlett DR, Tew DG, Meek TD, Chapman C, Gloger IS, Murphy KE, Southan CD, Ryan DM et al (1999) Identification of a novel aspartic protease (Asp 2) as beta-secretase. *Mol Cell Neurosci* 14: 419–427

Imbimbo BP (2009) Why did tarenflurbil fail in Alzheimer's disease? *J Alzheimers Dis* 17: 757–760

Imbimbo BP, Panza F, Frisardi V, Solfrizzi V, D'Onofrio G, Logroscino G, Seripa D, Pilotto A (2011) Therapeutic intervention for Alzheimer's disease with γ-secretase inhibitors: still a viable option? *Expert Opin Investig Drugs* 20: 325–341

Iqbal K, Liu F, Gong C-X, Del Alonso AC, Grundke-Iqbal I (2009) Mechanisms of tau-induced neurodegeneration. *Acta Neuropathol* 118: 53–69

Itagaki S, McGeer PL, Akiyama H, Zhu S, Selkoe D (1989) Relationship of microglia and astrocytes to amyloid deposits of Alzheimer disease. *J Neuroimmunol* 24: 173–182

Iwatsubo T (2004) The gamma-secretase complex: machinery for intramembrane proteolysis. *Curr Opin Neurobiol* 14: 379–383

Iwatsubo T, Odaka A, Suzuki N, Mizusawa H, Nukina N, Ihara Y (1994) Visualization of Aβ42(43) and Aβ40 in senile plaques with end-specific Aβ monoclonals: Evidence that an initially deposited species is Aβ42(43). *Neuron* 13: 45–53

Jacobson K, Mouritsen OG, Anderson RGW (2007) Lipid rafts: at a crossroad between cell biology and physics. *Nat Cell Biol* 9: 7–14

Jacobson K, Sheets ED, Simson R (1995) Revisiting the fluid mosaic model of membranes. *Science* 268: 1441–1442

Janes PW, Saha N, Barton WA, Kolev MV, Wimmer-Kleikamp SH, Nievergall E, Blobel CP, Himanen J-P, Lackmann M, Nikolov DB (2005) Adam meets Eph: an ADAM substrate recognition module acts as a molecular switch for ephrin cleavage in trans. *Cell* 123: 291–304

Janus C, Pearson J, McLaurin J, Mathews PM, Jiang Y, Schmidt SD, Chishti MA, Horne P, Heslin D, French J et al (2000) A beta peptide immunization reduces behavioural impairment and plaques in a model of Alzheimer's disease. *Nature* 408: 979–982

Jarrett JT, Berger EP, Lansbury PT (1993) The carboxy terminus of the beta amyloid protein is critical for the seeding of amyloid formation: implications for the pathogenesis of Alzheimer's disease. *Biochemistry* 32: 4693–4697

Jonsson T, Atwal JK, Steinberg S, Snaedal J, Jonsson PV, Bjornsson S, Stefansson H, Sulem P, Gudbjartsson D, Maloney J et al (2012) A mutation in APP protects against Alzheimer's disease and age-related cognitive decline. *Nature* 488: 96–99

Jorissen E, Prox J, Bernreuther C, Weber S, Schwanbeck R, Serneels L, an Snellinx, Craessaerts K, Thathiah A, Tesseur I et al (2010) The disintegrin/metalloproteinase ADAM10 is essential for the establishment of the brain cortex. *J Neurosci* 30: 4833–4844

Jouannet S, Saint-Pol J, Fernandez L, Nguyen V, Charrin S, Boucheix C, Brou C, Milhiet P-E, Rubinstein E (2016) TspanC8 tetraspanins differentially regulate the cleavage of ADAM10 substrates, Notch activation and ADAM10 membrane compartmentalization. *Cell Mol Life Sci* 73: 1895–1915

Kaden D, Munter L-M, Joshi M, Treiber C, Weise C, Bethge T, Voigt P, Schaefer M, Beyermann M, Reif B et al (2008) Homophilic interactions of the amyloid precursor protein (APP) ectodomain are regulated by the loop region and affect beta-secretase cleavage of APP. *J Biol Chem* 283: 7271–7279

Kaden D, Voigt P, Munter L-M, Bobowski KD, Schaefer M, Multhaup G (2009) Subcellular localization and dimerization of APLP1 are strikingly different from APP and APLP2. *J Cell Sci* 122: 368–377

Kalaria RN, Maestre GE, Arizaga R, Friedland RP, Galasko D, Hall K, Luchsinger JA, Ogunniyi A, Perry EK, Potocnik F et al (2008) Alzheimer's disease and vascular dementia in developing countries: prevalence, management, and risk factors. *Lancet Neurol* 7: 812–826

Kandalepas PC, Vassar R (2012) Identification and biology of β-secretase. *J Neurochem* 120: 55–61

Kang J, Lemaire HG, Unterbeck A, Salbaum JM, Masters CL, Grzeschik KH, Multhaup G, Beyreuther K, Müller-Hill B (1987) The precursor of Alzheimer's disease amyloid A4 protein resembles a cell-surface receptor. *Nature* 325: 733–736

Karch CM, Goate AM (2015) Alzheimer's disease risk genes and mechanisms of disease pathogenesis. *Biol Psychiatry* 77: 43–51

Kato T, Hagiyama M, Ito A (2018) Renal ADAM10 and 17: their physiological and medical meanings. *Front Cell Dev Biol* 6: 153

Katzman R, Terry R, DeTeresa R, Brown T, Davies P, Fuld P, Renbing X, Peck A (1988) Clinical, pathological, and neurochemical changes in dementia: a subgroup with preserved mental status and numerous neocortical plaques. *Ann Neurol* 23: 138–144

Khalifa NB, van Hees J, Tasiaux B, Huysseune S, Smith SO, Constantinescu SN, Octave J-N, Kienlen-Campard P (2010) What is the role of amyloid precursor protein dimerization? *Cell Adh Migr* 4: 268–272

Kienlen-Campard P, Tasiaux B, van Hees J, Li M, Huysseune S, Sato T, Fei JZ, Aimoto S, Courtoy PJ, Smith SO et al (2008) Amyloidogenic processing but not amyloid precursor protein (APP) intracellular C-terminal domain production requires a precisely oriented APP dimer assembled by transmembrane GXXXG motifs. *J Biol Chem* 283: 7733–7744

Kim J, Basak JM, Holtzman DM (2009a) The role of apolipoprotein E in Alzheimer's disease. *Neuron* 63: 287–303

Kim M, Suh J, Romano D, Truong MH, Mullin K, Hooli B, Norton D, Tesco G, Elliott K, Wagner SL et al (2009b) Potential late-onset Alzheimer's disease-associated mutations in the ADAM10 gene attenuate alpha-secretase activity. *Hum Mol Genet* 18: 3987–3996

Kimberly WT, LaVoie MJ, Ostaszewski BL, Ye W, Wolfe MS, Selkoe DJ (2003) Gamma-secretase is a membrane protein complex comprised of presenilin, nicastrin, Aph-1, and Pen-2. *Proc Natl Acad Sci USA* 100: 6382–6387

Kimura A, Hata S, Suzuki T (2016) Alternative selection of β-site APP-cleaving enzyme 1 (BACE1) cleavage sites in amyloid β-protein precursor (APP) harboring protective and pathogenic mutations within the Aβ sequence. *J Biol Chem* 291: 24041–24053

King GD, Scott Turner R (2004) Adaptor protein interactions: modulators of amyloid precursor protein metabolism and Alzheimer's disease risk? *Exp Neurol* 185: 208–219

Kinoshita A, Fukumoto H, Shah T, Whelan CM, Irizarry MC, Hyman BT (2003) Demonstration by FRET of BACE interaction with the amyloid precursor protein at the cell surface and in early endosomes. *J Cell Sci* 116: 3339–3346

Knopman DS (2019) Lowering of amyloid-beta by β-secretase inhibitors - some informative failures. *N Engl J Med* 380: 1476–1478

Knops J, Suomensaari S, Lee M, McConlogue L, Seubert P, Sinha S (1995) Cell-type and amyloid precursor protein-type specific inhibition of A beta release by bafilomycin A1, a selective inhibitor of vacuolar ATPases. *J Biol Chem* 270: 2419–2422

Koch CS von, Zheng H, Chen H, Trumbauer M, Thinakaran G, van der Ploeg L, Price DL, Sisodia SS (1997) Generation of APLP2 KO mice and early postnatal lethality in APLP2/APP double KO mice. *Neurobiol Aging* 18: 661–669

Koike H, Tomioka S, Sorimachi H, Saido TC, Maruyama K, Okuyama A, Fujisawa-Sehara A, Ohno S, Suzuki K, Ishiura S (1999) Membrane-anchored metalloprotease MDC9 has an alpha-secretase activity responsible for processing the amyloid precursor protein. *Biochem J* 343 Pt 2: 371–375

Kojro E, Gimpl G, Lammich S, Marz W, Fahrenholz F (2001) Low cholesterol stimulates the nonamyloidogenic pathway by its effect on the alpha -secretase ADAM 10. *Proc Natl Acad Sci USA* 98: 5815–5820

Kojro E, Postina R, Buro C, Meiringer C, Gehrig-Burger K, Fahrenholz F (2006) The neuropeptide PACAP promotes the alpha-secretase pathway for processing the Alzheimer amyloid precursor protein. *FASEB J* 20: 512–514

Koo EH, Squazzo SL (1994) Evidence that production and release of amyloid beta-protein involves the endocytic pathway. *J Biol Chem* 269: 17386–17389

Kornberg LJ, Earp HS, Turner CE, Prockop C, Juliano RL (1991) Signal transduction by integrins: increased protein tyrosine phosphorylation caused by clustering of beta 1 integrins. *Proc Natl Acad Sci USA* 88: 8392–8396

Kuhn P-H, Marjaux E, Imhof A, Strooper B de, Haass C, Lichtenthaler SF (2007) Regulated intramembrane proteolysis of the interleukin-1 receptor II by alpha-, beta-, and gamma-secretase. *J Biol Chem* 282: 11982–11995

Kuhn P-H, Wang H, Dislich B, Colombo A, Zeitschel U, Ellwart JW, Kremmer E, Rossner S, Lichtenthaler SF (2010) ADAM10 is the physiologically relevant, constitutive alpha-secretase of the amyloid precursor protein in primary neurons. *EMBO J* 29: 3020–3032

Kumar D, Ganeshpurkar A, Kumar D, Modi G, Gupta SK, Singh SK (2018) Secretase inhibitors for the treatment of Alzheimer's disease: Long road ahead. *Eur J Med Chem* 148: 436–452

Kumar-Singh S, Theuns J, van Broeck B, Pirici D, Vennekens K, Corsmit E, Cruts M, Dermaut B, Wang R, van Broeckhoven C (2006) Mean age-of-onset of familial alzheimer disease caused by presenilin mutations correlates with both increased Abeta42 and decreased Abeta40. *Hum Mutat* 27: 686–695

Kwok JBJ, Li Q-X, Hallupp M, Whyte S, Ames D, Beyreuther K, Masters CL, Schofield PR (2000) Novel Leu723Pro amyloid precursor protein mutation increases amyloid beta42 (43) peptide levels and induces apoptosis. *Ann Neurol* 47: 249–253

LaFerla FM, Oddo S (2005) Alzheimer's disease: Abeta, tau and synaptic dysfunction. *Trends Mol Med* 11: 170–176

Lambert MP, Barlow AK, Chromy BA, Edwards C, Freed R, Liosatos M, Morgan TE, Rozovsky I, Trommer B, Viola KL et al (1998) Diffusible, nonfibrillar ligands derived from Abeta1-42 are potent central nervous system neurotoxins. *Proc Natl Acad Sci USA* 95: 6448–6453

Lammich S, Kojro E, Postina R, Gilbert S, Pfeiffer R, Jasionowski M, Haass C, Fahrenholz F (1999) Constitutive and regulated alpha-secretase cleavage of Alzheimer's amyloid precursor protein by a disintegrin metalloprotease. *Proc Natl Acad Sci USA* 96: 3922–3927

Lan M-Y, Liu J-S, Wu Y-S, Peng C-H, Chang Y-Y (2014) A novel APP mutation (D678H) in a Taiwanese patient exhibiting dementia and cerebral microvasculopathy. *J Clin Neurosci* 21: 513–515

Lang T, Rizzoli SO (2010) Membrane protein clusters at nanoscale resolution: more than pretty pictures. *Physiology* 25: 116–124

LeBlanc AC, Chen HY, Autilio-Gambetti L, Gambetti P (1991) Differential APP gene expression in rat cerebral cortex, meninges, and primary astroglial, microglial and neuronal cultures. *FEBS Lett* 292: 171–178

Lee VM, Goedert M, Trojanowski JQ (2001) Neurodegenerative tauopathies. *Annu Rev Neurosci* 24: 1121–1159

Le Gall SM, Maretzky T, Issuree PDA, Niu X-D, Reiss K, Saftig P, Khokha R, Lundell D, Blobel CP (2010) ADAM17 is regulated by a rapid and reversible mechanism that controls access to its catalytic site. *J Cell Sci* 123: 3913–3922

Lemere CA, Blusztajn JK, Yamaguchi H, Wisniewski T, Saido TC, Selkoe DJ (1996) Sequence of deposition of heterogeneous amyloid beta-peptides and APO E in Down syndrome: implications for initial events in amyloid plaque formation. *Neurobiol. Dis.* 3: 16–32

Lemmon MA, Flanagan JM, Treutlein HR, Zhang J, Engelman DM (1992) Sequence specificity in the dimerization of transmembrane alpha-helices. *Biochemistry* 31: 12719–12725

Li B, Chohan MO, Grundke-Iqbal I, Iqbal K (2007) Disruption of microtubule network by Alzheimer abnormally hyperphosphorylated tau. *Acta Neuropathol* 113: 501–511

Li C, Ebrahimi A, Schluesener H (2013) Drug pipeline in neurodegeneration based on transgenic mice models of Alzheimer's disease. *Ageing Res Rev* 12: 116–140

Li N, Liu K, Qiu Y, Ren Z, Dai R, Deng Y, Qing H (2016) Effect of presenilin mutations on APP cleavage; insights into the pathogenesis of FAD. *Front Aging Neurosci* 8: 51

Lichtenthaler SF, Dominguez D-I, Westmeyer GG, Reiss K, Haass C, Saftig P, Strooper B de, Seed B (2003) The cell adhesion protein P-selectin glycoprotein ligand-1 is a substrate for the aspartyl protease BACE1. *J Biol Chem* 278: 48713–48719

Lin X, Koelsch G, Wu S, Downs D, Dashti A, Tang J (2000) Human aspartic protease memapsin 2 cleaves the beta-secretase site of beta-amyloid precursor protein. *Proc Natl Acad Sci USA* 97: 1456–1460

Lopez-Perez E, Zhang Y, Frank SJ, Creemers J, Seidah N, Checler F (2001) Constitutive alpha-secretase cleavage of the beta-amyloid precursor protein in the furin-deficient LoVo cell line: involvement of the pro-hormone convertase 7 and the disintegrin metalloprotease ADAM10. *J Neurochem* 76: 1532–1539

Lorenzo A, Yuan M, Zhang Z, Paganetti PA, Sturchler-Pierrat C, Staufenbiel M, Mautino J, Vigo FS, Sommer B, Yankner BA (2000) Amyloid beta interacts with the amyloid precursor protein: a potential toxic mechanism in Alzheimer's disease. *Nat Neurosci* 3: 460–464

Lourenço FC, Galvan V, Fombonne J, Corset V, Llambi F, Müller U, Bredesen DE, Mehlen P (2009) Netrin-1 interacts with amyloid precursor protein and regulates amyloid-beta production. *Cell Death Differ* 16: 655–663

Ludwig A, Hundhausen C, Lambert MH, Broadway N, Andrews RC, Bickett DM, Leesnitzer MA, Becherer JD (2005) Metalloproteinase inhibitors for the disintegrin-like metalloproteinases ADAM10 and ADAM17 that differentially block constitutive and phorbol ester-inducible shedding of cell surface molecules. *Comb Chem High Throughput Screen* 8: 161–171

Luo Y, Bolon B, A Damore M, Fitzpatrick D, Liu H, Zhang J, Yan Q, Vassar R, Citron M (2003) BACE1 (β-secretase) knockout mice do not acquire compensatory gene expression changes or develop neural lesions over time. *Neurobiol. Dis.* 14: 81–88

Luo Y, Bolon B, Kahn S, Bennett BD, Babu-Khan S, Denis P, Fan W, Kha H, Zhang J, Gong Y et al (2001) Mice deficient in BACE1, the Alzheimer's beta-secretase, have normal phenotype and abolished beta-amyloid generation. *Nat Neurosci* 4: 231–232

Marenchino M, Williamson PTF, Murri S, Zandomeneghi G, Wunderli-Allenspach H, Meier BH, Krämer SD (2008) Dynamics and cleavability at the alpha-cleavage site of APP(684-726) in different lipid environments. *Biophys J* 95: 1460–1473

Mattson MP, Cheng B, Culwell AR, Esch FS, Lieberburg I, Rydel RE (1993) Evidence for excitoprotective and intraneuronal calcium-regulating roles for secreted forms of the β-amyloid precursor protein. *Neuron* 10: 243–254

Maurer K, Volk S, Gerbaldo H (1997) Auguste D and Alzheimer's disease. *Lancet* 349: 1546–1549

Maynard CJ, Bush AI, Masters CL, Cappai R, Li Q-X (2005) Metals and amyloid-beta in Alzheimer's disease. *Int J Exp Pathol* 86: 147–159

McDonald JM, Cairns NJ, Taylor-Reinwald L, Holtzman D, Walsh DM (2012) The levels of water-soluble and triton-soluble Aβ are increased in Alzheimer's disease brain. *Brain Res* 1450: 138–147

Merklinger E, Schloetel J-G, Spitta L, Thiele C, Lang T (2016) No evidence for spontaneous lipid transfer at ER-PM membrane contact sites. *J Membr Biol* 249: 41–56

Merlos-Suárez A, Ruiz-Paz S, Baselga J, Arribas J (2001) Metalloprotease-dependent protransforming growth factor-alpha ectodomain shedding in the absence of tumor necrosis factor-alpha-converting enzyme. *J Biol Chem* 276: 48510–48517

Meziane H, Dodart JC, Mathis C, Little S, Clemens J, Paul SM, Ungerer A (1998) Memory-enhancing effects of secreted forms of the beta-amyloid precursor protein in normal and amnestic mice. *Proc Natl Acad Sci USA* 95: 12683–12688

Mills J, Reiner PB (1999) Regulation of amyloid precursor protein cleavage. *J Neurochem* 72: 443–460

Morgan D, Diamond DM, Gottschall PE, Ugen KE, Dickey C, Hardy J, Duff K, Jantzen P, DiCarlo G, Wilcock D et al (2000) A beta peptide vaccination prevents memory loss in an animal model of Alzheimer's disease. *Nature* 408: 982–985

Moss ML, Powell G, Miller MA, Edwards L, Qi B, Sang Q-XA, Strooper B de, Tesseur I, Lichtenthaler SF, Taverna M et al (2011) ADAM9 inhibition increases membrane activity of ADAM10 and controls α-secretase processing of amyloid precursor protein. *J Biol Chem* 286: 40443–40451

Müller U (1994) Behavioral and anatomical deficits in mice homozygous for a modified beta-amyloid precursor protein gene. *Cell* 79: 755–765

Müller UC, Zheng H (2012) Physiological functions of APP family proteins. *Cold Spring Harb Perspect Med* 2: a006288

Munter L-M, Voigt P, Harmeier A, Kaden D, Gottschalk KE, Weise C, Pipkorn R, Schaefer M, Langosch D, Multhaup G (2007) GxxxG motifs within the amyloid precursor protein transmembrane sequence are critical for the etiology of Abeta42. *EMBO J* 26: 1702–1712

Musa A, Lehrach H, Russo VA (2001) Distinct expression patterns of two zebrafish homologues of the human APP gene during embryonic development. *Dev Genes Evol* 211: 563–567

Nhan HS, Chiang K, Koo EH (2015) The multifaceted nature of amyloid precursor protein and its proteolytic fragments: friends and foes. *Acta Neuropathol* 129: 1–19

Nichols E, Szoeke CEI, Vollset SE, Abbasi N, Abd-Allah F, Abdela J, Aichour MTE, Akinyemi RO, Alahdab F, Asgedom SW et al (2019) Global, regional, and national burden of Alzheimer's disease and other dementias, 1990–2016: a systematic analysis for the Global Burden of Disease Study 2016. *Lancet Neurol* 18: 88–106

Nilsberth C, Westlind-Danielsson A, Eckman CB, Condron MM, Axelman K, Forsell C, Stenh C, Luthman J, Teplow DB, Younkin SG et al (2001) The 'Arctic' APP mutation (E693G) causes Alzheimer's disease by enhanced Abeta protofibril formation. *Nat Neurosci* 4: 887–893

Nitsch RM, Slack BE, Wurtman RJ, Growdon JH (1992) Release of Alzheimer amyloid precursor derivatives stimulated by activation of muscarinic acetylcholine receptors. *Science* 258: 304–307

Nordstedt C, Caporaso GL, Thyberg J, Gandy SE, Greengard P (1993) Identification of the Alzheimer beta/A4 amyloid precursor protein in clathrin-coated vesicles purified from PC12 cells. *J Biol Chem* 268: 608–612

Oakley H, Cole SL, Logan S, Maus E, Shao P, Craft J, Guillozet-Bongaarts A, Ohno M, Disterhoft J, van Eldik L et al (2006) Intraneuronal beta-amyloid aggregates, neurodegeneration, and neuron loss in transgenic mice with five familial Alzheimer's disease mutations: potential factors in amyloid plaque formation. *J Neurosci* 26: 10129–10140

O'Brien RJ, Wong PC (2011) Amyloid precursor protein processing and Alzheimer's disease. *Annu Rev Neurosci* 34: 185–204

Ochiishi T, Doi M, Yamasaki K, Hirose K, Kitamura A, Urabe T, Hattori N, Kinjo M, Ebihara T, Shimura H (2016) Development of new fusion proteins for visualizing amyloid-β oligomers in vivo. *Sci Rep* 6: 22712

Okado H, Okamoto H (1992) A Xenopus homologue of the human β-amyloid precursor protein: Development regulation of its gene expression. *Biochem Biophys Res Commun* 189: 1561–1568

Oltersdorf T, Ward PJ, Henriksson T, Beattie EC, Neve R, Lieberburg I, Fritz LC (1990) The Alzheimer amyloid precursor protein. Identification of a stable intermediate in the biosynthetic/degradative pathway. *J Biol Chem* 265: 4492–4497

Ono K, Condron MM, Teplow DB (2010) Effects of the English (H6R) and Tottori (D7N) familial Alzheimer disease mutations on amyloid beta-protein assembly and toxicity. *J Biol Chem* 285: 23186–23197

Parvathy S, Hussain I, Karran EH, Turner AJ, Hooper NM (1998) Alzheimer's amyloid precursor protein alpha-secretase is inhibited by hydroxamic acid-based zinc metalloprotease inhibitors: similarities to the angiotensin converting enzyme secretase. *Biochemistry* 37: 1680–1685

Parvathy S, Hussain I, Karran EH, Turner AJ, Hooper NM (1999) Cleavage of Alzheimer's amyloid precursor protein by alpha-secretase occurs at the surface of neuronal cells. *Biochemistry* 38: 9728–9734

Postina R, Schroeder A, Dewachter I, Bohl J, Schmitt U, Kojro E, Prinzen C, Endres K, Hiemke C, Blessing M et al (2004) A disintegrin-metalloproteinase prevents amyloid plaque formation and hippocampal defects in an Alzheimer disease mouse model. *J Clin Invest* 113: 1456–1464

Prince MJ, Wimo A, Guerchet M, Ali G-C, Wu Y-T, Prina M (2015) *World Alzheimer Report 2015: The global impact of dementia: An analysis of prevalence, incidence, cost and trends.* Alzheimer's Disease International, London, England

Prox J, Willenbrock M, Weber S, Lehmann T, Schmidt-Arras D, Schwanbeck R, Saftig P, Schwake M (2012) Tetraspanin15 regulates cellular trafficking and activity of the ectodomain sheddase ADAM10. *Cell Mol Life Sci* 69: 2919–2932

Pruessmeyer J, Ludwig A (2009) The good, the bad and the ugly substrates for ADAM10 and ADAM17 in brain pathology, inflammation and cancer. *Semin Cell Dev Biol* 20: 164–174

Qi-Takahara Y, Morishima-Kawashima M, Tanimura Y, Dolios G, Hirotani N, Horikoshi Y, Kametani F, Maeda M, Saido TC, Wang R et al (2005) Longer forms of amyloid beta protein: implications for the mechanism of intramembrane cleavage by gamma-secretase. *J Neurosci* 25: 436–445

Rajendran L, Honsho M, Zahn TR, Keller P, Geiger KD, Verkade P, Simons K (2006) Alzheimer's disease beta-amyloid peptides are released in association with exosomes. *Proc Natl Acad Sci USA* 103: 11172–11177

Rajendran L, Schneider A, Schlechtingen G, Weidlich S, Ries J, Braxmeier T, Schwille P, Schulz JB, Schroeder C, Simons M et al (2008) Efficient inhibition of the Alzheimer's disease beta-secretase by membrane targeting. *Science* 320: 520–523

Reddy P, Slack JL, Davis R, Cerretti DP, Kozlosky CJ, Blanton RA, Shows D, Peschon JJ, Black RA (2000) Functional analysis of the domain structure of tumor necrosis factor-alpha converting enzyme. *J Biol Chem* 275: 14608–14614

Refolo LM, Salton SR, Anderson JP, Mehta P, Robakis NK (1989) Nerve and epidermal growth factors induce the release of the Alzheimer Amyloid precursor from PC 12 cell cultures. *Biochem Biophys Res Commun* 164: 664–670

Reinhard C, Hébert SS, Strooper B de (2005) The amyloid-beta precursor protein: integrating structure with biological function. *EMBO J* 24: 3996–4006

Reiss K, Bhakdi S (2017) The plasma membrane: Penultimate regulator of ADAM sheddase function. *Biochim Biophys Acta Mol Cell Res* 1864: 2082–2087

Reits EA, Neefjes JJ (2001) From fixed to FRAP: measuring protein mobility and activity in living cells. *Nat Cell Biol* 3: E145-7

Robakis NK, Ramakrishna N, Wolfe G, Wisniewski HM (1987) Molecular cloning and characterization of a cDNA encoding the cerebrovascular and the neuritic plaque amyloid peptides. *Proc Natl Acad Sci USA* 84: 4190–4194

Roberds SL, Anderson J, Basi G, Bienkowski MJ, Branstetter DG, Chen KS, Freedman SB, Frigon NL, Games D, Hu K et al (2001) BACE knockout mice are healthy despite lacking the primary beta-secretase activity in brain: implications for Alzheimer's disease therapeutics. *Hum Mol Genet* 10: 1317–1324

Roch JM, Masliah E, Roch-Levecq AC, Sundsmo MP, Otero DA, Veinbergs I, Saitoh T (1994) Increase of synaptic density and memory retention by a peptide representing the trophic domain of the amyloid beta/A4 protein precursor. *Proc Natl Acad Sci USA* 91: 7450–7454

Roher AE, Lowenson JD, Clarke S, Wolkow C, Wang R, Cotter RJ, Reardon IM, Zürcher-Neely HA, Heinrikson RL, Ball MJ (1993) Structural alterations in the peptide backbone of beta-amyloid core protein may account for its deposition and stability in Alzheimer's disease. *J Biol Chem* 268: 3072–3083

Rosen DR, Martin-Morris L, Luo LQ, White K (1989) A Drosophila gene encoding a protein resembling the human beta-amyloid protein precursor. *Proc Natl Acad Sci USA* 86: 2478–2482

Rushworth JV, Hooper NM (2010) Lipid rafts: linking Alzheimer's amyloid-β production, aggregation, and toxicity at neuronal membranes. *Int J Alzheimers Dis* 2011: 603052

Russ WP, Engelman DM (2000) The GxxxG motif: a framework for transmembrane helix-helix association. *J Mol Biol* 296: 911–919

Saitoh T, Sundsmo M, Roch J-M, Kimura N, Cole G, Schubert D, Oltersdorf T, Schenk DB (1989) Secreted form of amyloid β protein precursor is involved in the growth regulation of fibroblasts. *Cell* 58: 615–622

Sakono M, Zako T (2010) Amyloid oligomers: formation and toxicity of Abeta oligomers. *FEBS J* 277: 1348–1358

Sambrook J, Russell DW (2006) *The condensed protocols from molecular cloning: a laboratory manual.* Cold Spring Harbor Laboratory Press, New York, USA

Sankaranarayanan S, Holahan MA, Colussi D, Crouthamel M-C, Devanarayan V, Ellis J, Espeseth A, Gates AT, Graham SL, Gregro AR et al (2009) First demonstration of cerebrospinal fluid and plasma A beta lowering with oral administration of a beta-site amyloid precursor protein-cleaving enzyme 1 inhibitor in nonhuman primates. *J Pharmacol Exp Ther* 328: 131–140

Sastre M, Steiner H, Fuchs K, Capell A, Multhaup G, Condron MM, Teplow DB, Haass C (2001) Presenilin-dependent gamma-secretase processing of beta-amyloid precursor protein at a site corresponding to the S3 cleavage of Notch. *EMBO Rep* 2: 835–841

Scheuermann S, Hambsch B, Hesse L, Stumm J, Schmidt C, Beher D, Bayer TA, Beyreuther K, Multhaup G (2001) Homodimerization of amyloid precursor protein and its implication in the amyloidogenic pathway of Alzheimer's disease. *J Biol Chem* 276: 33923–33929

Scheuner D, Eckman C, Jensen M, Song X, Citron M, Suzuki N, Bird TD, Hardy J, Hutton M, Kukull W et al (1996) Secreted amyloid beta-protein similar to that in the senile plaques of Alzheimer's disease is increased in vivo by the presenilin 1 and 2 and APP mutations linked to familial Alzheimer's disease. *Nat Med* 2: 864–870

Schneider A, Rajendran L, Honsho M, Gralle M, Donnert G, Wouters F, Hell SW, Simons M (2008) Flotillin-dependent clustering of the amyloid precursor protein regulates its endocytosis and amyloidogenic processing in neurons. *J Neurosci* 28: 2874–2882

Schneider F, Sych T, Eggeling C, Sezgin E (2021) Influence of nanobody binding on fluorescence emission, mobility, and organization of GFP-tagged proteins. *iScience* 24: 101891

Schreiber A (2012) *Bildungsmechanismus und physiologische Relevanz supramolekularer Proteincluster des Amyloid Precursor Protein APP in der Zellmembran.* PhD thesis. University of Bonn, Bonn, Germany

Schreiber A, Fischer S, Lang T (2012) The amyloid precursor protein forms plasmalemmal clusters via its pathogenic amyloid-β domain. *Biophys J* 102: 1411–1417

Seals DF, Courtneidge SA (2003) The ADAMs family of metalloproteases: multidomain proteins with multiple functions. *Genes Dev* 17: 7–30

Seipold L, Damme M, Prox J, Rabe B, Kasparek P, Sedlacek R, Altmeppen H, Willem M, Boland B, Glatzel M et al (2017) Tetraspanin 3: A central endocytic membrane component regulating the expression of ADAM10, presenilin and the amyloid precursor protein. *Biochim Biophys Acta Mol Cell Res* 1864: 217–230

Selkoe D, Kopan R (2003) Notch and Presenilin: regulated intramembrane proteolysis links development and degeneration. *Annu Rev Neurosci* 26: 565–597

Selkoe DJ (2001) Alzheimer's disease: genes, proteins, and therapy. *Physiol Rev* 81: 741–766

Selkoe DJ (2011) Resolving controversies on the path to Alzheimer's therapeutics. *Nat Med* 17: 1060–1065

Seubert P, Oltersdorf T, Lee MG, Barbour R, Blomquist C, Davis DL, Bryant K, Fritz LC, Galasko D, Thal LJ (1993) Secretion of beta-amyloid precursor protein cleaved at the amino terminus of the beta-amyloid peptide. *Nature* 361: 260–263

Shah S, Lee S-F, Tabuchi K, Hao Y-H, Yu C, LaPlant Q, Ball H, Dann CE, Südhof T, Yu G (2005) Nicastrin functions as a gamma-secretase-substrate receptor. *Cell* 122: 435–447

Shaji KS (2009) Dementia care in developing countries: The road ahead. *Indian J Psychiatry* 51: S5-7

Shaked GM, Kummer MP, Lu DC, Galvan V, Bredesen DE, Koo EH (2006) Abeta induces cell death by direct interaction with its cognate extracellular domain on APP (APP 597-624). *FASEB J* 20: 1254–1256

Shankar GM, Li S, Mehta TH, Garcia-Munoz A, Shepardson NE, Smith I, Brett FM, Farrell MA, Rowan MJ, Lemere CA et al (2008) Amyloid-beta protein dimers isolated directly from Alzheimer's brains impair synaptic plasticity and memory. *Nat Med* 14: 837–842

Shariati SAM, Strooper B de (2013) Redundancy and divergence in the amyloid precursor protein family. *FEBS Lett* 587: 2036–2045

Silvestri R (2009) Boom in the development of non-peptidic beta-secretase (BACE1) inhibitors for the treatment of Alzheimer's disease. *Med Res Rev* 29: 295–338

Sinha S, Anderson JP, Barbour R, Basi GS, Caccavello R, Davis D, Doan M, Dovey HF, Frigon N, Hong J et al (1999) Purification and cloning of amyloid precursor protein beta-secretase from human brain. *Nature* 402: 537–540

Sisodia SS (1992) Beta-amyloid precursor protein cleavage by a membrane-bound protease. *Proc Natl Acad Sci USA* 89: 6075–6079

Sisodia SS, Koo EH, Beyreuther K, Unterbeck A, Price DL (1990) Evidence that beta-amyloid protein in Alzheimer's disease is not derived by normal processing. *Science* 248: 492–495

Skovronsky DM, Moore DB, Milla ME, Doms RW, Lee VM (2000) Protein kinase C-dependent alpha-secretase competes with beta-secretase for cleavage of amyloid-beta precursor protein in the trans-golgi network. *J Biol Chem* 275: 2568–2575

Slack BE, Ma LK, Seah CC (2001) Constitutive shedding of the amyloid precursor protein ectodomain is up-regulated by tumour necrosis factor-α converting enzyme. *Biochem J* 357: 787–794

Smith KM, Gaultier A, Cousin H, Alfandari D, White JM, DeSimone DW (2002) The cysteine-rich domain regulates ADAM protease function in vivo. *J Cell Biol* 159: 893–902

Soba P, Eggert S, Wagner K, Zentgraf H, Siehl K, Kreger S, Löwer A, Langer A, Merdes G, Paro R et al (2005) Homo- and heterodimerization of APP family members promotes intercellular adhesion. *EMBO J* 24: 3624–3634

Stawikowska R, Cudic M, Giulianotti M, Houghten RA, Fields GB, Minond D (2013) Activity of ADAM17 (a disintegrin and metalloprotease 17) is regulated by its noncatalytic domains and secondary structure of its substrates. *J Biol Chem* 288: 22871–22879

Strooper B de (2003) Aph-1, Pen-2, and nicastrin with presenilin generate an active γ-secretase complex. *Neuron* 38: 9–12

Strooper B de (2010) Proteases and proteolysis in Alzheimer disease: a multifactorial view on the disease process. *Physiol Rev* 90: 465–494

Strooper B de, Saftig P, Craessaerts K, Vanderstichele H, Guhde G, Annaert W, Figura K von, van Leuven F (1998) Deficiency of presenilin-1 inhibits the normal cleavage of amyloid precursor protein. *Nature* 391: 387–390

Suh J, Choi SH, Romano DM, Gannon MA, Lesinski AN, Kim DY, Tanzi RE (2013) ADAM10 missense mutations potentiate β-amyloid accumulation by impairing prodomain chaperone function. *Neuron* 80: 385–401

Suzuki N, Cheung TT, Cai XD, Odaka A, Otvos L, Eckman C, Golde TE, Younkin SG (1994) An increased percentage of long amyloid beta protein secreted by familial amyloid beta protein precursor (beta APP717) mutants. *Science* 264: 1336–1340

Takami M, Nagashima Y, Sano Y, Ishihara S, Morishima-Kawashima M, Funamoto S, Ihara Y (2009) Gamma-secretase: successive tripeptide and tetrapeptide release from the transmembrane domain of beta-carboxyl terminal fragment. *J Neurosci* 29: 13042–13052

Takashima A, Wolozin B, Buee L (eds) (2019) *Tau biology.* Springer, Singapore

Takasugi N, Tomita T, Hayashi I, Tsuruoka M, Niimura M, Takahashi Y, Thinakaran G, Iwatsubo T (2003) The role of presenilin cofactors in the gamma-secretase complex. *Nature* 422: 438–441

Tanaka KAK, Suzuki KGN, Shirai YM, Shibutani ST, Miyahara MSH, Tsuboi H, Yahara M, Yoshimura A, Mayor S, Fujiwara TK et al (2010) Membrane molecules mobile even after chemical fixation. *Nat Methods* 7: 865–866

Tanzi RE (2012) The genetics of Alzheimer disease. *Cold Spring Harb Perspect Med* 2: a006296

Tanzi RE, Gusella JF, Watkins PC, Bruns GA, St George-Hyslop P, van Keuren ML, Patterson D, Pagan S, Kurnit DM, Neve RL (1987) Amyloid beta protein gene: cDNA, mRNA distribution, and genetic linkage near the Alzheimer locus. *Science* 235: 880–884

Tate B, McKee TD, Loureiro RMB, Dumin JA, Xia W, Pojasek K, Austin WF, Fuller NO, Hubbs JL, Shen R et al (2012) Modulation of gamma-secretase for the treatment of Alzheimer's disease. *Int J Alzheimers Dis* 2012: 210756

Terry RD, Masliah E, Salmon DP, Butters N, DeTeresa R, Hill R, Hansen LA, Katzman R (1991) Physical basis of cognitive alterations in Alzheimer's disease: synapse loss is the major correlate of cognitive impairment. *Ann Neurol* 30: 572–580

Thinakaran G, Teplow DB, Siman R, Greenberg B, Sisodia SS (1996) Metabolism of the "Swedish" amyloid precursor protein variant in neuro2a (N2a) cells. Evidence that cleavage at the "beta-secretase" site occurs in the golgi apparatus. *J Biol Chem* 271: 9390–9397

Tomiyama T, Nagata T, Shimada H, Teraoka R, Fukushima A, Kanemitsu H, Takuma H, Kuwano R, Imagawa M, Ataka S et al (2008) A new amyloid beta variant favoring oligomerization in Alzheimer's-type dementia. *Ann Neurol* 63: 377–387

Tsubuki S, Takai Y, Saido TC (2003) Dutch, Flemish, Italian, and Arctic mutations of APP and resistance of Aβ to physiologically relevant proteolytic degradation. *Lancet* 361: 1957–1958

Valensin D, Mancini FM, Łuczkowski M, Janicka A, Wisniewska K, Gaggelli E, Valensin G, Łankiewicz L, Kozlowski H (2004) Identification of a novel high affinity copper binding site in the APP(145-155) fragment of amyloid precursor protein. *Dalton Trans:* 16–22

van den Hurk WH, Bloemen M, Martens GJ (2001) Expression of the gene encoding the β-amyloid precursor protein APP in Xenopus laevis. *Mol Brain Res* 97: 13–20

Vassar R, Bennett BD, Babu-Khan S, Kahn S, Mendiaz EA, Denis P, Teplow DB, Ross S, Amarante P, Loeloff R et al (1999) Beta-secretase cleavage of Alzheimer's amyloid precursor protein by the transmembrane aspartic protease BACE. *Science* 286: 735–741

Vetrivel KS, Cheng H, Lin W, Sakurai T, Li T, Nukina N, Wong PC, Xu H, Thinakaran G (2004) Association of gamma-secretase with lipid rafts in post-Golgi and endosome membranes. *J Biol Chem* 279: 44945–44954

Villemagne VL, Pike KE, Chételat G, Ellis KA, Mulligan RS, Bourgeat P, Ackermann U, Jones G, Szoeke C, Salvado O et al (2011) Longitudinal assessment of Aβ and cognition in aging and Alzheimer disease. *Ann Neurol* 69: 181–192

Wakutani Y, Watanabe K, Adachi Y, Wada-Isoe K, Urakami K, Ninomiya H, Saido TC, Hashimoto T, Iwatsubo T, Nakashima K (2004) Novel amyloid precursor protein gene missense mutation (D678N) in probable familial Alzheimer's disease. *J Neurol Neurosurg Psychiatry* 75: 1039–1042

Walsh DM, Klyubin I, Fadeeva JV, Cullen WK, Anwyl R, Wolfe MS, Rowan MJ, Selkoe DJ (2002) Naturally secreted oligomers of amyloid beta protein potently inhibit hippocampal long-term potentiation in vivo. *Nature* 416: 535–539

Walsh JS, Welch HG, Larson EB (1990) Survival of outpatients with Alzheimer-type dementia. *Ann Intern Med* 113: 429–434

Wang R, Meschia JF, Cotter RJ, Sisodia SS (1991) Secretion of the beta/A4 amyloid precursor protein. Identification of a cleavage site in cultured mammalian cells. *J Biol Chem* 266: 16960–16964

Wang X, Pei G (2018) Visualization of Alzheimer's disease related α-/β-/γ-secretase ternary complex by bimolecular fluorescence complementation based fluorescence resonance energy transfer. *Front Mol Neurosci* 11: 431

Wang Y, Ha Y (2004) The X-ray structure of an antiparallel dimer of the human amyloid precursor protein E2 domain. *Mol Cell* 15: 343–353

Weidemann A, Eggert S, Reinhard FBM, Vogel M, Paliga K, Baier G, Masters CL, Beyreuther K, Evin G (2002) A novel epsilon-cleavage within the transmembrane domain of the Alzheimer amyloid precursor protein demonstrates homology with Notch processing. *Biochemistry* 41: 2825–2835

Weidemann A, König G, Bunke D, Fischer P, Salbaum J, Masters CL, Beyreuther K (1989) Identification, biogenesis, and localization of precursors of Alzheimer's disease A4 amyloid protein. *Cell* 57: 115–126

White JM (2003) ADAMs: modulators of cell-cell and cell-matrix interactions. *Curr Opin Cell Biol* 15: 598–606

Willem M, Garratt AN, Novak B, Citron M, Kaufmann S, Rittger A, DeStrooper B, Saftig P, Birchmeier C, Haass C (2006) Control of peripheral nerve myelination by the beta-secretase BACE1. *Science* 314: 664–666

Wolfe MS (2006) The gamma-secretase complex: membrane-embedded proteolytic ensemble. *Biochemistry* 45: 7931–7939

World Health Organization (WHO) (2021) *Dementia.* https://www.who.int/news-room/fact-sheets/detail/dementia. 12 December 2021

Xu D, Sharma C, Hemler ME (2009) Tetraspanin12 regulates ADAM10-dependent cleavage of amyloid precursor protein. *FASEB J* 23: 3674–3681

Xu P, Liu J, Sakaki-Yumoto M, Derynck R (2012) TACE activation by MAPK-mediated regulation of cell surface dimerization and TIMP3 association. *Sci Signal* 5: ra34

Yamaguchi H, Hirai S, Morimatsu M, Shoji M, Ihara Y (1988) A variety of cerebral amyloid deposits in the brains of the Alzheimer-type dementia demonstrated by beta protein immunostaining. *Acta Neuropathol* 76: 541–549

Yan R, Bienkowski MJ, Shuck ME, Miao H, Tory MC, Pauley AM, Brashier JR, Stratman NC, Mathews WR, Buhl AE et al (1999) Membrane-anchored aspartyl protease with Alzheimer's disease beta-secretase activity. *Nature* 402: 533–537

Yan Y, Xu T-H, Melcher K, Xu HE (2017) Defining the minimum substrate and charge recognition model of gamma-secretase. *Acta Pharmacol Sin* 38: 1412–1424

Yang D-S, Tandon A, Chen F, Yu G, Yu H, Arawaka S, Hasegawa H, Duthie M, Schmidt SD, Ramabhadran TV et al (2002) Mature glycosylation and trafficking of nicastrin modulate its binding to presenilins. *J Biol Chem* 277: 28135–28142

Yoshikai S, Sasaki H, Doh-ura K, Furuya H, Sakaki Y (1990) Genomic organization of the human amyloid beta-protein precursor gene. *Gene* 87: 257–263

Yu C, Rafiq NBM, Cao F, Zhou Y, Krishnasamy A, Biswas KH, Ravasio A, Chen Z, Wang Y-H, Kawauchi K et al (2015) Integrin-beta3 clusters recruit clathrin-mediated endocytic machinery in the absence of traction force. *Nat Commun* 6: 8672

Yu G, Nishimura M, Arawaka S, Levitan D, Zhang L, Tandon A, Song YQ, Rogaeva E, Chen F, Kawarai T et al (2000) Nicastrin modulates presenilin-mediated notch/glp-1 signal transduction and betaAPP processing. *Nature* 407: 48–54

Zhang S, Wang Z, Cai F, Zhang M, Wu Y, Zhang J, Song W (2017) BACE1 cleavage site selection critical for amyloidogenesis and Alzheimer's pathogenesis. *J Neurosci* 37: 6915–6925

Zhang Z, Nadeau P, Song W, Donoviel D, Yuan M, Bernstein A, Yankner BA (2000) Presenilins are required for gamma-secretase cleavage of beta-APP and transmembrane cleavage of Notch-1. *Nat Cell Biol* 2: 463–465

Zhao G, Cui M-Z, Mao G, Dong Y, Tan J, Sun L, Xu X (2005) Gamma-cleavage is dependent on zeta-cleavage during the proteolytic processing of amyloid precursor protein within its transmembrane domain. *J Biol Chem* 280: 37689–37697

Zhao J, Paganini L, Mucke L, Gordon M, Refolo L, Carman M, Sinha S, Oltersdorf T, Lieberburg I, McConlogue L (1996) Beta-secretase processing of the beta-amyloid precursor protein in transgenic mice is efficient in neurons but inefficient in astrocytes. *J Biol Chem* 271: 31407–31411

Zhou L, Brouwers N, Benilova I, Vandersteen A, Mercken M, van Laere K, van Damme P, Demedts D, van Leuven F, Sleegers K et al (2011) Amyloid precursor protein mutation E682K at the alternative β-secretase cleavage β'-site increases Aβ generation. *EMBO Mol Med* 3: 291–302

Zilly FE, Halemani ND, Walrafen D, Spitta L, Schreiber A, Jahn R, Lang T (2011) Ca2+ induces clustering of membrane proteins in the plasma membrane via electrostatic interactions. *EMBO J* 30: 1209–1220

Zou K, Gong J-S, Yanagisawa K, Michikawa M (2002) A novel function of monomeric amyloid β-protein serving as an antioxidant molecule against metal-induced oxidative damage. *J Neurosci* 22: 4833–4841

8 Acknowledgements

First and foremost, I would like to thank my supervisor, Prof. Dr. Thorsten Lang, for giving me the opportunity to work in his research group and on this relevant and very interesting topic. I have greatly benefited from our discussions and his advices regarding my research, his steady support and his supervision.

I also would like to thank Prof. Dr. Ulrich Kubitscheck and his lab for giving me an introduction on FRAP microscopy and for always helping me when questions regarding the method or the operation of the confocal microscope arose
.
I am thankful to the members of my thesis committee Prof. Dr. Thorsten Lang, Prof. Dr. Jochen Walter, Prof. Dr. Eva Kiermaier and Priv.-Doz. Dr. Christiane Dahl for taking the time to evaluate this thesis.

I am further thankful for the funding provided by the DFG that allowed me to conduct the research necessary for this work.

I would like to express my gratitude to all current and former members of the Lang research group, namely Jasmin Mertins, Dominik Sons, Nicholas Reppert, Jerome Finke, Ricarda Sies and Dennis de Coninck for showing me new methods, the lively discussions, advices, help at any time and the great and fun athmosphere in and outside the lab. You really made the time I spent on my PhD special. I would also like to thank all members of the LIMES institute for the support and for sharing common instruments.

I would also like to thank my friends for their years of friendship and support, the fun activities and holidays we spent together. You really helped me through the good and bad times of the PhD.

I owe my deepest gratitude to my family and Torsten Fischer as my extended family for always supporting me, for all their advices, for their help at any time, for always encouraging me and their belief in me.